Title	
Author(s)	Choudhary, Hemant
Citation	
Issue Date	2015-06
Type	Thesis or Dissertation
Text version	ETD
URL	http://hdl.handle.net/10119/12874
Rights	
Description	Supervisor: , ,

Japan Advanced Institute of Science and Technology

Studies on Preparation of Novel Materials as Highly-Pertinent Heterogeneous Catalysts using Solvothermal Method

HEMANT CHOUDHARY

Japan Advanced Institute of Science and Technology

Doctoral Dissertation

Studies on Preparation of Novel Materials as Highly-Pertinent Heterogeneous Catalysts using Solvothermal Method

Hemant Choudhary

Supervisor: Prof. Dr. Kohki Ebitani

School of Materials Science
Japan Advanced Institute of Science and Technology
June 2015

Promoter   :   Prof. Dr. Kohki Ebitani
Referees   :   Prof. Dr. Tetsuya Shishido
                   Prof. Dr. Masayuki Yamaguchi
                   Prof. Dr. Noriyoshi Matsumi
                   Assoc. Prof. Dr. Tatsuo Kaneko

PREFACE

Since Berzelius coined the word "*catalysis*", it have become an integral part of the synthetic organic chemistry. Although, these processes were realized earlier and often termed as contact processes. Excellent works were carried out by eminent scientists of 19th and 20th century and some of them were awarded with the prestigious Noble Prize for their outstanding contributions. Notably, 19% of the Noble Prize winners and 14% of the prizes in chemistry were awarded to the scientists for their achievements related to chemical and enzymatic catalysis. These achievements were more than enough to motivate me to develop catalysts and contribute my role as a researcher in the vast field of science and technology.

"*Studies on Preparation of Novel Materials as Highly-Pertinent Heterogeneous Catalysts using Solvothermal Method*" is a mere first step of my contribution to catalysis and material sciences and symbolizes the determination and enthusiasm. The work included in this dissertation primarily focusses on the development of stable and highly-pertinent heterogeneous catalyst prepared under hydrothermal or solvothermal conditions for useful organic transformations. During the evaluation of these prepared catalysts various interesting mysteries unfolded that are integrated in this thesis. The extent of information derived from the existing literature has been indicated at appropriate places in the text.

Major part of the research work embodied in this doctoral dissertation has been carried out in School of Materials Science, Japan Advanced Institute of Science and Technology (JAIST) under the supervision of Professor Dr. Kohki Ebitani. I owe a deep sense of gratitude and would like to express my sincere thanks to Professor Dr. Kohki Ebitani and

I would also like to acknowledge doctoral graduates (Dr. Duangta and Dr. Son,), doctoral candidates (Mr. Chaiseeda, Ms. Jaya and Mr. Shorotori) and master students (Mr. Ikeda, Mr. Ohmi, Mr. Takahashi, Mr. Jixiang, Mr. Sato, Mr. Shimura, Mr. Fujiwara, Mr. Yoshida, Mr. Mizuhori, Mr. Ozawa, Mr. Matsuzawa, Mr. Umehara, Mr. Yuki, Mr. Miyazaki, Ms. Saumya, Mr. Mujahid, Mr. Jatin, Ms. Kanishka, Mr. Ravi and Ms. Pooja of Ebitani laboratory for their kind help and continuous encouragement during my candidature. I would like to thanks all international communities in JAIST that made life much easier during stressful doctoral research. I want to extend my special thanks to Ashutosh and Jatin for their unprecedented belief in me. Jatin was an excellent student with an excellent grasp over scientific logics; his untimely death was a great loss and I want to dedicate this work to him.

At last but not the least, I take this opportunity to thank my parents, brother sisters and their families for their constant support, understanding and encouragement. I also thank the Almighty for imparting me the patience and strength for accomplishing this thesis.

Hemant Choudhary.

Studies on Preparation of Novel Materials as Highly-Pertinent Heterogeneous Catalysts using Solvothermal Method

Hemant Choudhary

Ebitani Laboratory, School of Materials Science, Japan Advanced Institute of Science and Technology

Introduction

The intelligence of humans understood the phenomena around them partially, which led to the development of society and a gain in living standards at the cost of environmental degradation. These have concerned intellectuals and researchers throughout the globe and alarmed the need to develop technologies for a sustainable future.

Catalysts play an important role in the synthesis of chemicals for various purpose and with sheer knowledge, understanding of science and green chemistry practices; stable and highly-pertinent catalysts can be developed for environmentally benign chemical processes. Also, hydrothermal/solvothermal techniques have tremendously contributed towards development of stable, functionalized materials with excellent reproducibility and high purity.

In this thesis, I have focused on the preparation of stable and functionalized materials under hydrothermal or solvothermal conditions and have studied them to explore their catalyses.

Results and Discussion

In *Part I*, stable catalysts are prepared hydrothermally using inexpensive transition metals for viable applications in bio-refineries. First I have developed a stable magnesia-supported copper catalyst prepared in the presence of cationic surfactant with excellent activity for chemical upgradation of glucose to lactic acid (LA) in the presence of NaOH and formic acid (FA) in the presence of 30% H_2O_2. The catalyst drastically decreased the energy requirement to achieve high yields of LA and FA. Thorough characterization revealed the presence of novel copper oxide species, which inspired my further research. Thereafter, various surfactants were employed for the hydrothermal preparation of supported copper catalyst. I found that the type of supported Cu_xO_y species could be preferentially controlled by the mere control of type of surfactant employed and synthetic parameters, which have been illustrated in detail in the related chapter. The successful control of supported monometallic species, motivated me to extend the synthetic techniques for the bimetallic catalyst. A bimetallic CoPd catalyst was prepared in the presence of three capping agents and investigated for the facile utilization of FA as a hydrogen source. The catalysts were characterized minutely to observe the electronic/geometric changes caused by alloying of Co and Pd in the presence of capping agents. Further, from the viewpoint of bio-refinery the processes developed in this part were clubbed for the direct utilization of inedible-biomass-derived glucose as a hydrogen source.

In *Part II*, the focus have been shifted to design of highly-efficacious catalysts with desirable properties for the industrially exploited petro-refineries based modern organic transformations. I have designed an easily accessible palladium grafted amino-functionalized organozinc coordination polymer as a robust heterogeneous catalyst for Suzuki-Miyaura coupling (TON = 2,106,720), Mizoroki-Heck and hydrogenation reactions under mild conditions. The catalyst characterization revealed the successful implementation of desired properties in the prepared catalyst.

Conclusion

A facile synthetic approach to control and design desired supported catalytic species have been demonstrated in this thesis for efficacious catalysis. This study will contribute to further design of highly-pertinent materials with desirable properties for useful applications in an environmentally-benign manner.

Keywords: Solvothermal synthesis, Heterogeneous catalyst, Biomass, Organic reactions, Catalyst characterization.

TABLE OF CONTENTS

General Introduction

1. Mankind, Environment and the Chemistry: Need for Clean Energy Process

Mother Nature have inspired the mankind to critically think on the various phenomena occurring around them. One of the most basic yet crucial phenomenon is photosynthesis, through which plant harvest sun's energy by fixing carbon dioxide (CO_2) and water (H_2O) in the presence of enzymes into carbohydrates. Also, through respiration, the formed carbohydrates are broken down to produce energy for the metabolic activities and releases CO_2 and H_2O back into the atmosphere. And thus, the energy is consumed and an ecological balance is maintained through photosynthesis and respiration.

The intelligence of mankind understood the importance of energy and followed the process in nature to understand the chemistry involved in these processes. As a result, in few centuries a gain in living standards were observed i.e., from a log of wood to lithium ion batteries (Figure 1). The element that drove this transition is the energy density of various energy types. For instance, fuels high in energy content use less space and are often portable for various uses.

wooden log   *gasoline*   *batteries*
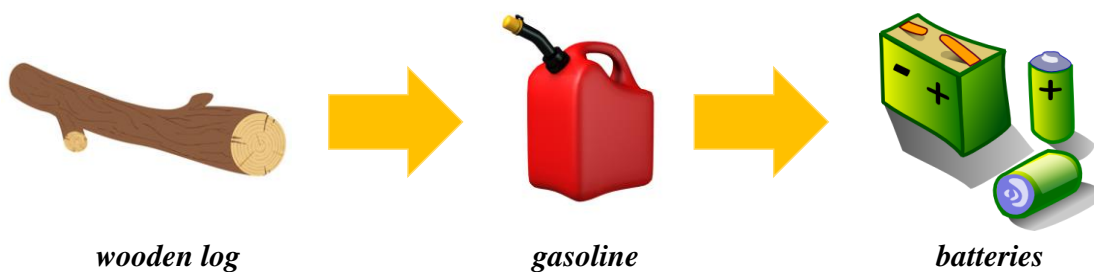
Figure 1. The transition in energy density with the progress of time.

Not only the living standards increased but also the population of mankind on the earth increased, which demanded a high energy output for various applications. The ecological balance is disturbed because of the increased demand of energy by around superior 7 billion inhabitant of earth, humans. According to a survey by United Nations and ExxonMobil (United States), by 2040 the total world population will be 9 billion with a global energy demand of about 700 quadrillion British thermal units (BTUs) (Figure 2).[1]
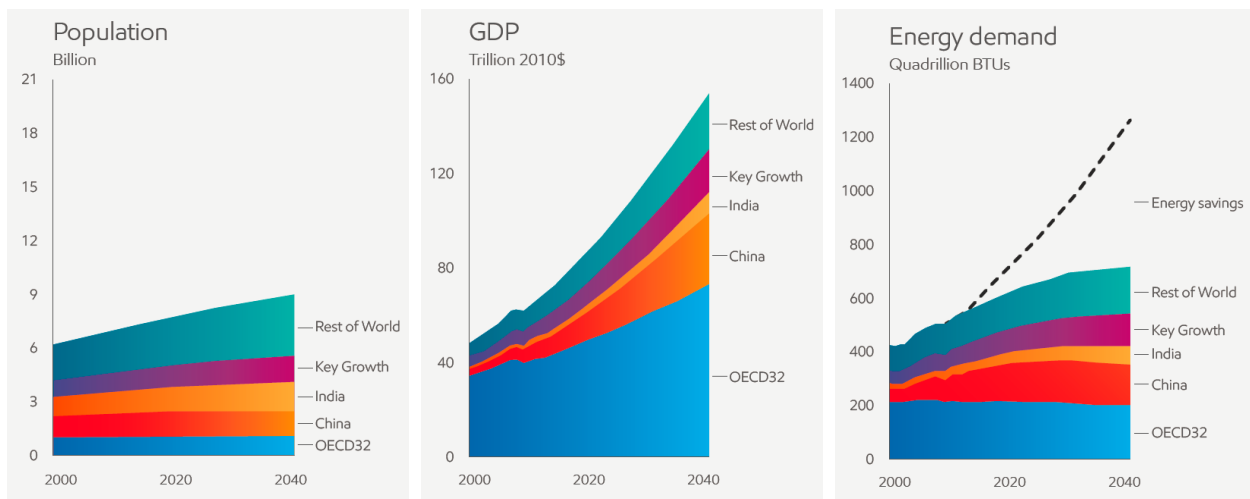
Figure 2. Projected global population, GDP and energy demand by 2040.

Major parts of the energy resources were the non-renewable raw materials like crude oil, and its direct impact was seen as the fluctuations in the oil prices. An extensive use of such raw materials have increased the consumption rate of these fossil resources and it is believed that peak oil (Figure 3) could be somewhere before 2025.[2-5] Not only the depletion of non-renewable resources were observed, but a more serious threat of climate change is the major concern throughout the world these days. Most of the developed countries (like United States and Japan) and some emerging powers (like India and China) have undertook important policy developments to safeguard the earth from the impact of climate change. For instance, Japan considered to restart the nuclear

reactor in new economic growth strategy whereas India assigned a 5% ethanol blend in gasoline and intended to expand the power generation from renewables.
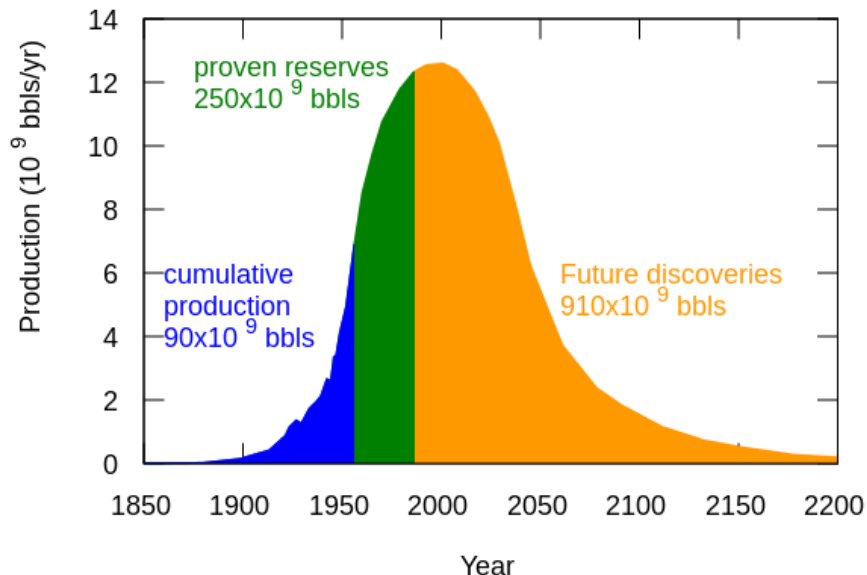
Figure 3. World oil production distribution.[5]

The clean energy processes can be developed by the sheer knowledge and understanding of science and innovation and if handled safely by management and operational excellence, the solution to energy issues can be found easily. Chemistry has a crucial role in maintaining an ecological balance. The issue of global warming and climate change, though, cannot be solved completely but can be controlled following the few basic principles of "*Green Chemistry*".[6] Green chemistry, as the word indicates is not about using green colored chemicals or reagents instead is more diverse. The most accepted definition of green chemistry is, "*Green chemistry efficiently utilizes (preferably renewable) raw materials, eliminates waste and avoids the use of toxic and/or hazardous reagents and solvents in the manufacture and application of chemical products*."[6] As

[4]

per the definition, it can be understood that if the society is willing to be sustainable, the green chemistry is the only possible path to be walked on.

The chemists, thus, have great responsibilities for their society and mankind for a sustainable future. In the process of contributing towards a green and sustainable earth, during the design of the experiments for the doctoral thesis I have adhered to the principles of green chemistry. In this thesis, the three very important elements of green chemistry are applied in all experiments. The three elements are (a) use of renewables or sustainable chemicals (e.g. biomass, etc.), (b) the use of catalysts, (c) use of closed systems (hydro/solvothermal methods), which are described in detail in the following sections.

2. Biomass: Route to sustainability

The depletion of fossil resources or the non-renewable source of energy, as discussed above, raises the issue of sustainability. For a sustainable future it becomes essential to switch the current technologies based on non-renewable sources to renewable sources to ensure a continuous supply of energy. Various forms of renewable energy sources are available which are directly or indirectly dependent on solar energy which have an energy reserve of 23,000 terawatt per year.[7] Solar, wind power, hydropower, biomass and geothermal energies are the forms of renewable energies, among which biomass, wind and solar are the emerging renewable sources as promising candidates (Figure 4).[8-10] Renewable energy sources have the potential to provide about 3050 times the current global energy demand.[10] In this thesis I will be discussing mainly on biomass and its prospects for sustainability.
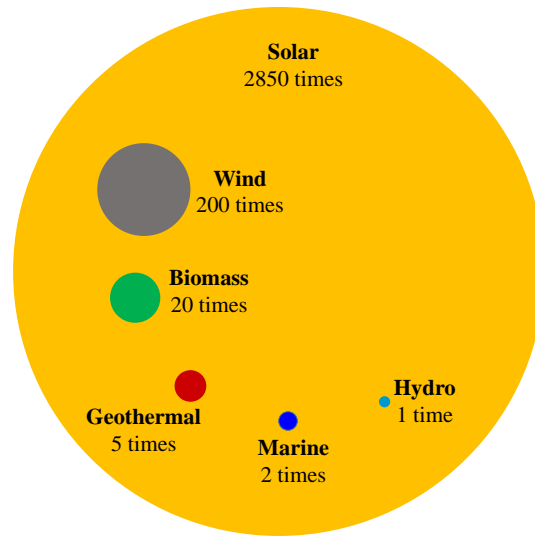
Figure 4. Renewable energy resources of the world and their potential against global energy demand.

All of the earth's living matter in the biosphere derived as a direct or indirect result of photosynthesis can be considered as biomass, but only organic material originating from plants, trees and crops which can be harvested for energy are referred to as biomass.[11-12] Because of the plant origin, the utilization of biomass at larger scale leads to a number of crucial issues, such as competition with food and land, deforestation and thereby global warming. These issues motivated researchers to develop technologies for abundant and cheaper inedible biomass, i.e., lignocellulosic biomass.[13-14]

Lignocellulosic biomasss or lignocellulose are the polymeric material composed of three primary units: cellulose (a glucose polymer), hemicellulose (polymer of five different C_5 and C_6 sugars) and lignin (polymer of propyl-phenol).[12,15-16] A closer look on the structure of plant demonstrates how lignin enwraps and surrounds cellulose and hemicellulose (Figure 5). Cellulose is the major component (comprising anything between 40-80 wt%) in the lignocellulosic biomass. It is a crystalline linear polymer of glucose linked *via* β-1,4-glycosidic bonds that could be hardly

hydrolyzed under natural conditions. Hydrogen bonding maintains the structure of the cellulose. The partial hydrolysis of cellulose yields cellobiose (a dimer of glucose), cellotriose (trimer of glucose), etc. whereas under strongly acidic conditions it can be completely broken down to monomer units i.e, to glucose units.[12] On the other hand, hemicellulose is a polysaccharide composed of different hexoses (such as galactose, glucose and mannose), pentoses (such as xylose and arabinose) and glucoronic acid that makes them more soluble and undergoes hydrolysis easily. About 10-25 wt% of lignocellulose is composed of lignin, a highly branched aromatic polymer, which gives strength to the cell wall along with cellulose.
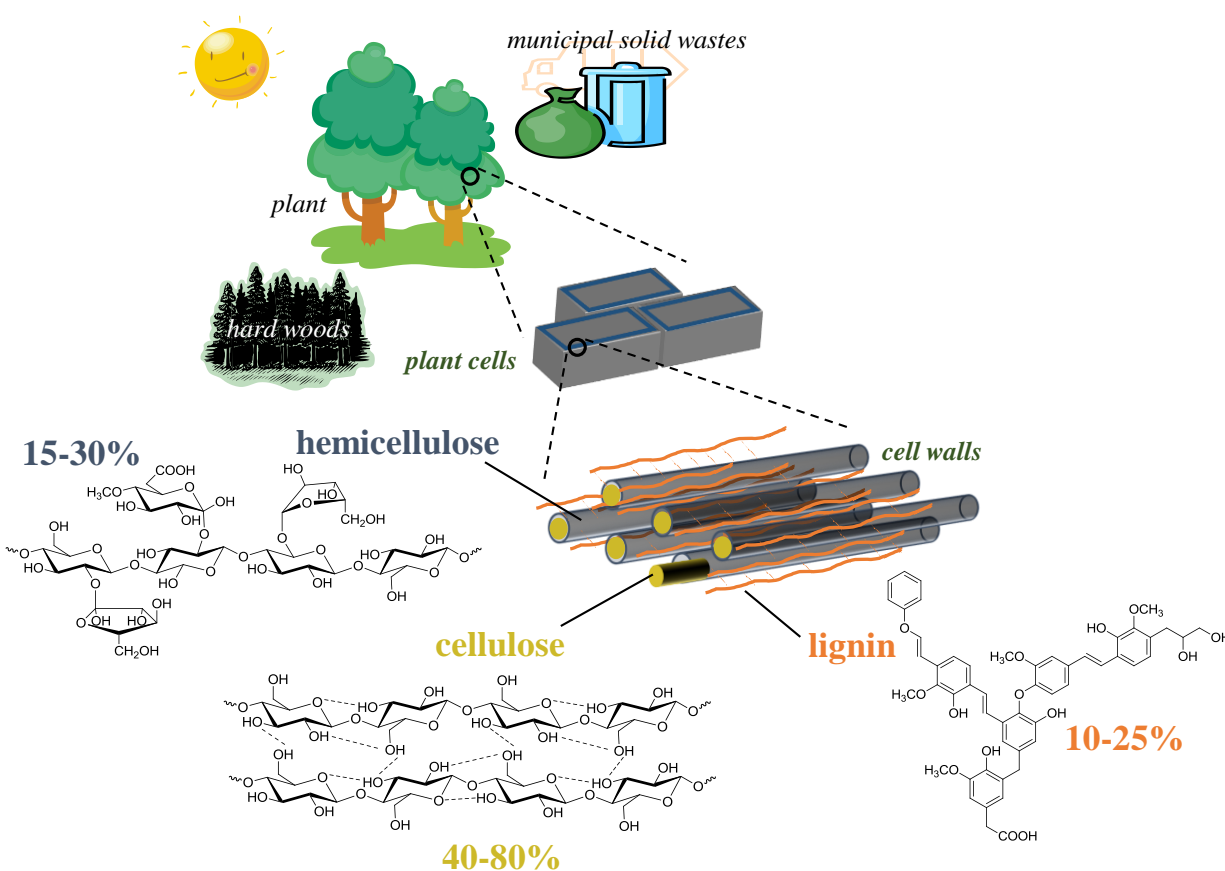
Figure 5. Structures of different lignocellulosic biomass fractions.

Biomass may be utilized in different ways to afford chemicals or materials. The biomass have been utilized traditionally for energy since ages, just after the physical treatment. For instance chopping of wood into logs for cooking or heating. However, for production of chemicals and fuels, the chemical or the bio-chemical processing are essential. The structural and chemical complexity of lignocellulose restricts the direct utilization for energy and chemicals. Figure 6 represents an overview of biomass conversion technologies depending on the water content of the species employed.[17] The three technologies such as gasification, hydrothermolysis and fermentation are key technologies for these conversions. These techniques and tremendous research efforts throughout the globe have developed the bio-refineries, analogous to petroleum refinery, to produce chemicals and energy from biomass. Also, a schematic illustration of bio-refineries and the energy pathways are shown in Figure 7.[18]
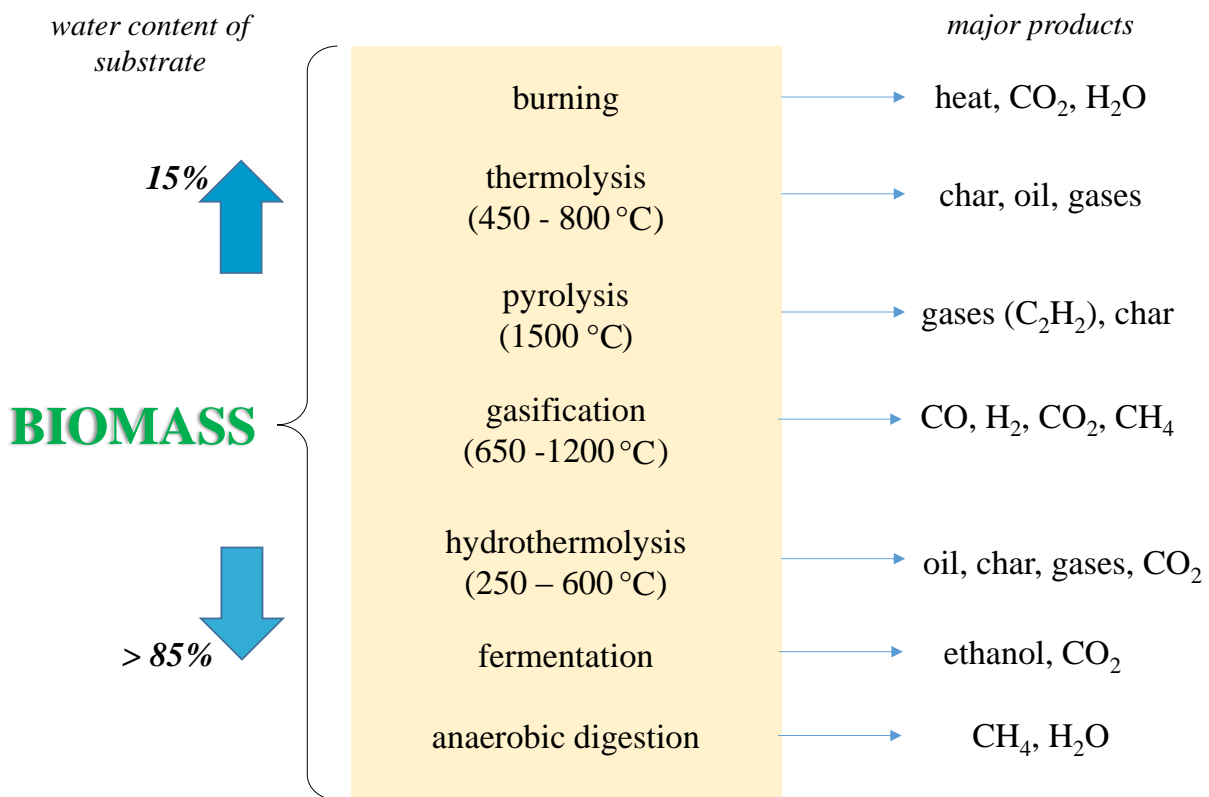
Figure 6. Biomass conversion technologies.
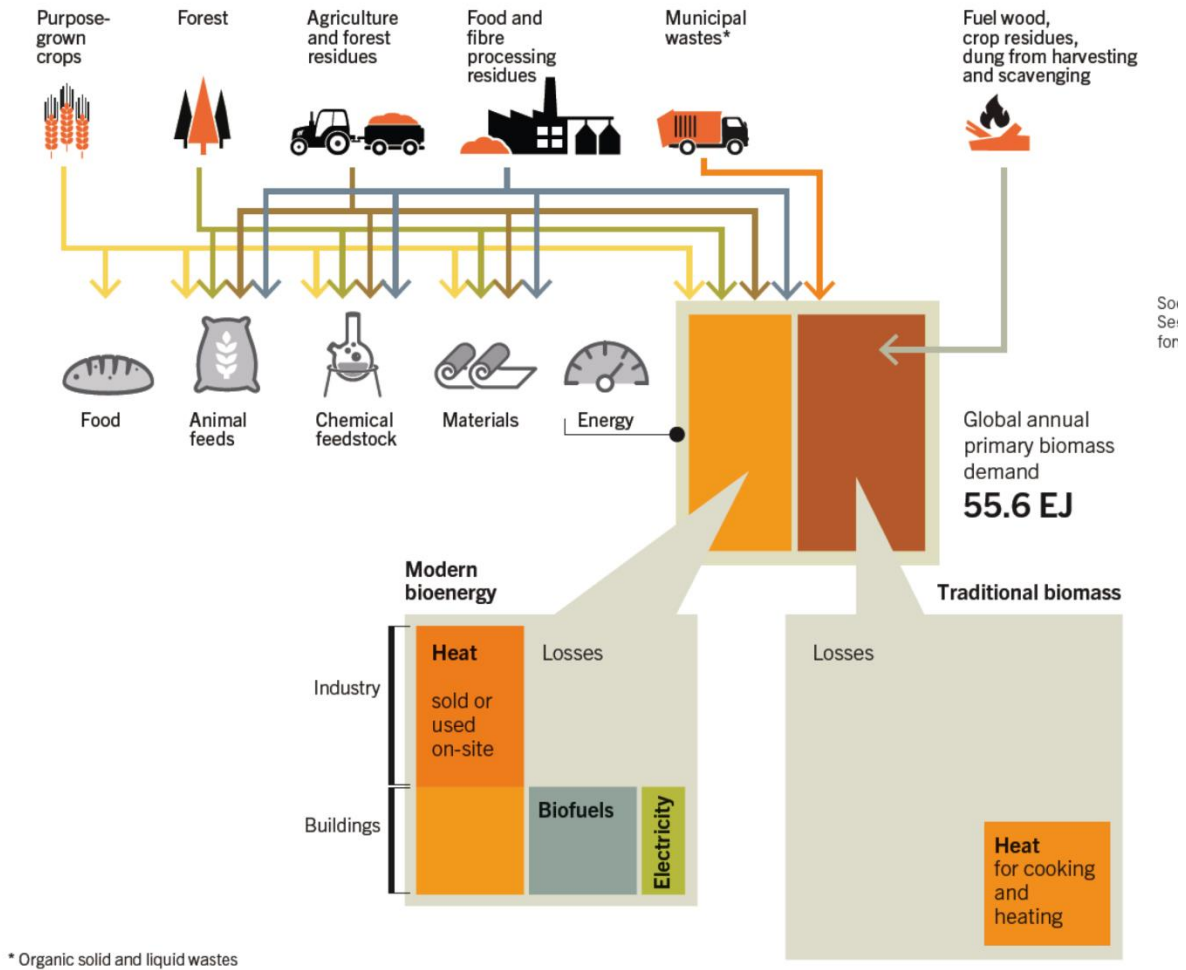
Figure 7. Biomass resources and energy pathways.[18]

3. Hydrothermal or Solvothermal Processes

Hydrothermal processes, although seems as an adolescence in chemistry, but has deeper roots to 19th century in geology. The term hydrothermal was believed to be first used by British geologist, Sir Roderick Murchison, to describe the formation of rocks and minerals in the earth's crust under the action of water at elevated temperature and pressure.[19] It is not too difficult to understand the meaning of the word "*hydrothermal*", where "*hydro*" means water and "*thermal*" means heat;

highlighting the word to be of geological origin. The inspiration by nature and curiosity of chemists, soon motivated chemists to develop minerals in laboratory by mimicking natural conditions. In 1845, K. F. E. Schafhautl for the first time published the successful synthesis of quartz microcrystals in papin's digestor under hydrothermal conditions.[20] This guided to the research for the development and growth of crystals in laboratory and by 1900 more than 150 mineral species were synthesized including diamond.[21] With the advent of the 20th century, hydrothermal strategy was clearly identified as an important tool for material synthesis after Bayer obtained aluminium from bauxite and initiated the commercial applications of hydrothermal strategy.[22-23]

The hydrothermal synthesis was defined by various researchers in their own fashion.[19,21,24-29] However, each of them had few things in common in their definitions, such as elevated temperature, closed reactor and high pressure. But this led to confusion with the regard of very use of the term hydrothermal, for the non-aqueous solvents, that led to various terms such as ammonothermal (for ammonia), glycothermal (for glycols), alcothermal (for alcohols), and so on. G. Demazeau coined a new terminology "*solvothermal*" and defined it as "*a chemical reaction in a closed system in the presence of a solvent (aqueous and non-aqueous solution) at a temperature higher than that of the boiling point of such a solvent*".[30]

Initially because of the poor knowledge of the solubility of chemicals, high temperatures and pressure were utilized in the material synthesis with the upper limit extended over to 1300 K and 500 MPa pressure.[27] Intensive research and knowledge on the physical aspects (PVT relationships) has led to a better understanding of the hydrothermal chemistry and has significantly reduced temperature and pressure values to as low as T<473 K and P<1.5 MPa.[19,27,31-33] These processes have been developed with various objectives: (i) mineral extraction,[34] (ii) synthesis of geological materials,[35-36] (iii) synthesis of novel materials,[30,37-38] (iv) crystal growth,[39] (v) deposition of thin

films,[40] (vi) development of sintering processes under mild conditions,[41] and (vii) preparation of fine particles with well-defined size and morphology[42].

Hydrothermal or solvothermal processes have been carried out in closed reactors, which have been commonly called as autoclaves. However, because of the temperature, pressure and pH conditions, the walls of the autoclaves are often corroded. To avoid corrosion of autoclaves, they are coated with inert material such as teflon from inside, commonly called as liner. Figure 8 shows the Teflon lined autoclaves used for the preparation of catalysts (Figure 8a) and for carrying out the organic transformations (Figure 8b) in this thesis. An ideal hydrothermal autoclave should have the following characteristics:

(a) should be inert to acids, bases and oxidizing agents,

(b) should be easily assemble and dissemble,

(c) should have sufficient length to obtain a desired temperature gradient,

(d) should be leak-proof at desired temperature and pressure.

(e) should bear high pressure and temperature for long duration of time.
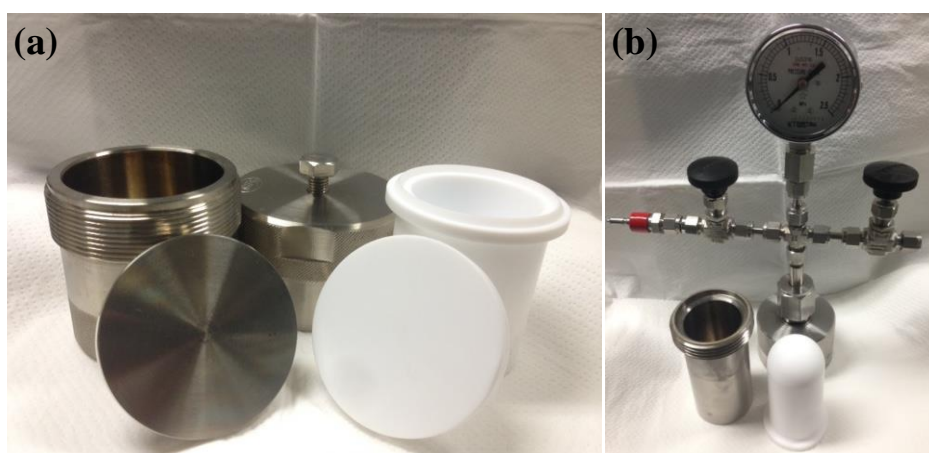
Figure 8. Components of teflon lined autoclave employed for carrying out experiments in this thesis. Autoclave used for (a) catalyst preparation and (b) investigating the catalysis of prepared catalysts.

Solvothermal technology, today, links all important technology like geotechnology, biotechnology, nanotechnology and advanced materials technology and thus is highly interdisciplinary providing a broader prospects. This is because, solvothermal processes are advantageous over the conventional synthetic methods. The advantages can be seen as the creation of compounds with elements in oxidation states that are difficult to attain,[43] or metastable compounds[44] and useful for low-temperature phases[45-46]. Other advantages include (a) environmentally friendly because of closed system, (b) high purity products can be synthesized, (c) crystal size, morphology, composition and polymorphism of the synthesized phases could be easily controlled, (d) unused components can be recycled and the last but not the least (e) high reproducibility of the experiments.

4. Catalysis

A chemical reagent when added to a chemical reaction, if enhances the rate of a chemical reaction then the process is known as catalysis, whereas the substance that enhanced the reaction rate is called as the catalyst. The catalyst can be classically defined as a chemical substance that enhances the rate of a chemical reaction without itself being changed or consumed at the end of the chemical reaction. The catalyst typically lowers the activation energy of the reagents to undergo a chemical reaction (Figure 9). Since, the catalyst lowers the energy requirement of a process and generally decreases the waste produced, the greener aspects of catalytic technology can be realized. However, the three crucial factor measure the extent of greenness of any catalyst, which are as follows:

(a) Selectivity: The ratio of the substrates converted into desired product to the amount of the consumed substrate expressed as percentage. The catalyst would be considered non-effective if it enhances the formation rate of undesired products.

(b) Turnover number (TON): The number of moles of product produced per mole of the catalyst. A high TON generally indicates that a small amount of catalyst is required for the conversion of substrate in large quantity, relating to the catalyst stability and low cost of the process.

(c) Turnover frequency (TOF): It is the number of moles of product per moles of catalyst per second. A high TOF is an indication of enhanced rate of catalysis, which in turn decreases the overall production cost and minimizes waste.
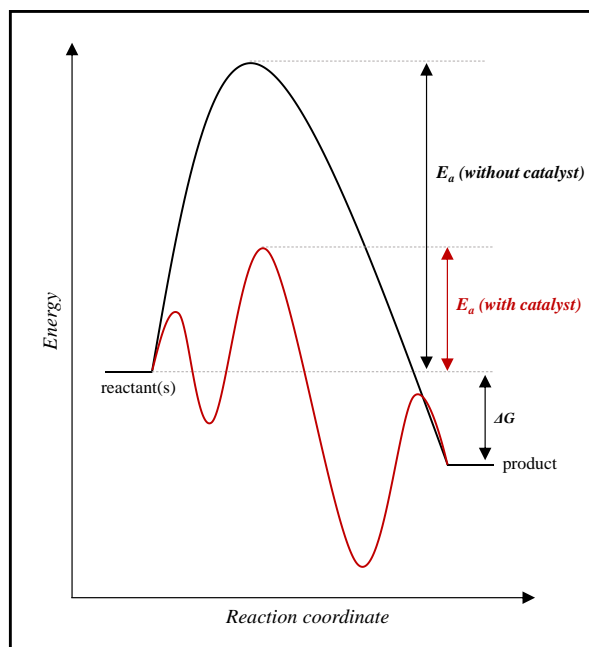
Figure 9. Energy profile of a reaction in the presence and absence of catalyst.

Catalysts, depending on their states with respect to the reaction media are broadly classified into two main types: homogeneous and heterogeneous catalysts. Homogeneous catalysts are in the

same phase as the substrate within the reaction media (generally liquid phase), whereas, heterogeneous catalysts are in a different phase to the reaction media. Owing to the mode of action of the heterogeneous catalysts, they are often known as contact or surface catalysts. Throughout the thesis, I have developed and studied heterogeneous catalyst as they have a range of advantages over homogeneous catalysts such as easily separable, readily generated and recycled, longer service life. But with these advantages, few drawbacks are also accompanied such as often higher energy process, diffusion limited and slower reaction rates. These drawbacks form one of the main aim of this thesis, which is to combine the fast rates, high selectivities of homogeneous catalysts with the ease of recycle and stability of heterogenous catalysts.

The catalytic reaction on a heterogeneous catalyst proceeds on the surface that are generally explained using three mechanisms: Langmuir-Hinshelwood, Rideal-Eley and precursor mechanism. Here, at least one of the substrate is adsorbed on the catalyst surface while the other collides or meet the adsorbed species. These are basically at atomic or molecular scale. Owing to these mechanisms, scientists are rigorously working to develop new synthetic methods of catalyst preparation for precise control of size, structure and location.[47] The collaboration of nanotechnology with the catalysts for the nanocatalysis has been observed as an interesting phenomena in the synthetic organic chemistry.[48-51]

5. Nanotechnology

Dr. Richard Smalley won a Nobel Prize in chemistry in 1996 for his work with carbon nanotubes (known as "Buckyballs") and has been considered as the "Father of Nanotechnology". Nanotechnology is the ability and knowledge to manufacture, observe, measure and manipulate

things at the nanometer scale that is the size of atoms and molecules. To observe/realize nanometer scale, a human hair strand can be considered which is about 75,000 to 100,000 nanometers in diameter. Also, Figure 10 illustrates the object at various scale for easy understanding of nanometer scale.
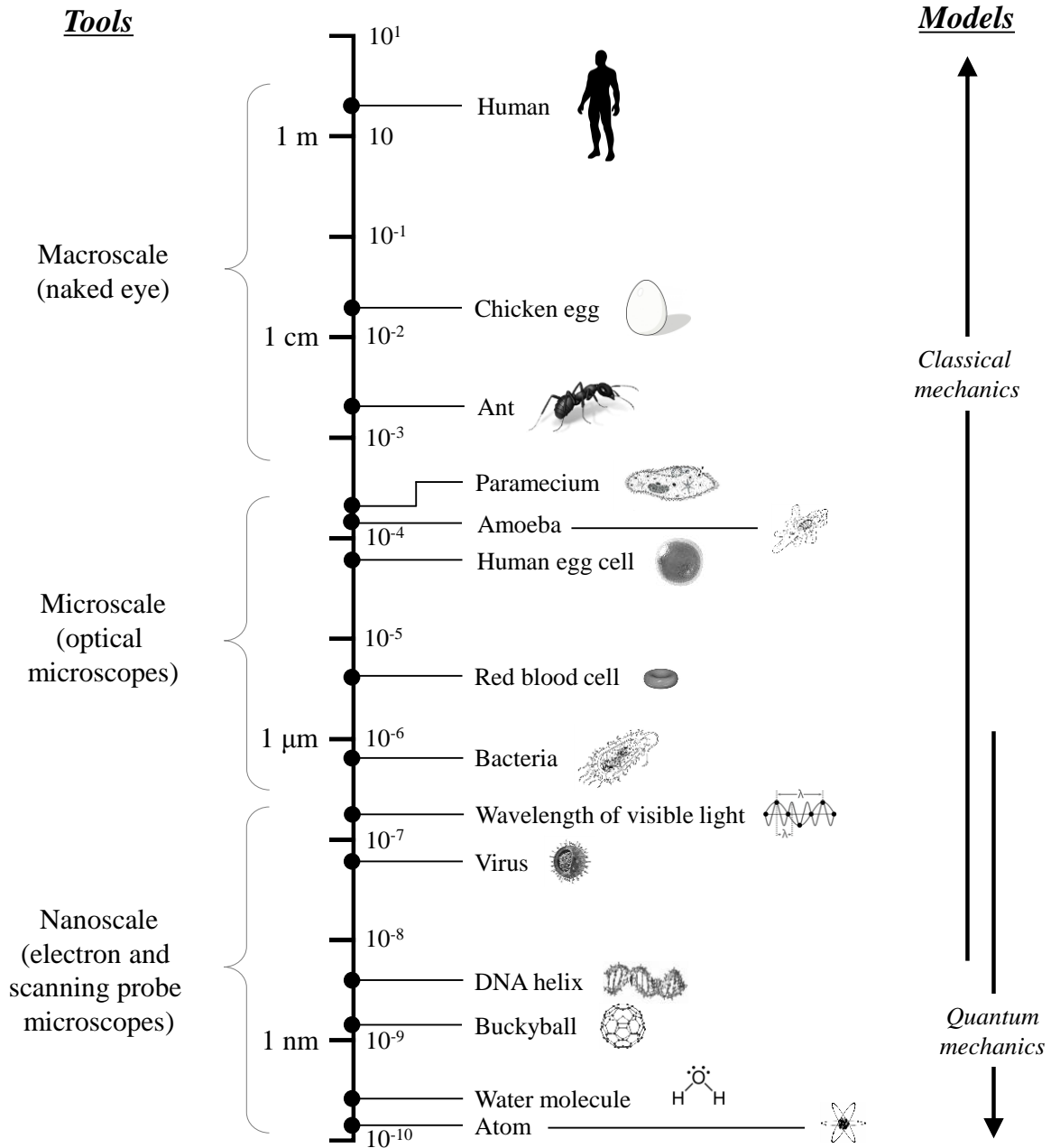
Figure 10. Tools, dominant objects and models at various different scales.

The nanoparticles (NPs) have been reported to acquire new properties (in comparison to the bulk material) at this scale, and these properties were observed as a function of size and shape.[52] Since nanoparticles show surface plasmon resonance, electronic and magnetic proeprties; they find interesting applications in the fields of optics,[53] chemical and bio sensing,[54-56] catalysis,[57] electronics,[58] and many others[59-60]. The decrease in the size of transition metal NPs, increases the surface-to-volume ratio. The change in surface-to-volume ratio and the ability to make them in different sizes and shapes, strongly contribute to the potential catalytic applications. Excellent work have been carried out using NPs to achieve remarkable results for various catalytic transformations.[57,61]

The simple synthesis of metal NPs involves complicated chemistry of nucleation and particle growth, which the scientists have understood of late. The typical mechanism of NPs formation can be divided into stages: a) generation of atoms, b) self-nucleation and c) growth, as shown in Figure 11. Here, as the time increases the precursor decomposes to increase the concentration of the metal atoms. After the attainment of supersaturation (of the metal atoms), the atoms aggregates into small clusters, often termed as nuclei *via* self-nucleation and these nuclei then grow tremendously fast that decreases the concentration of metal atoms. When the concentration falls too fast below the supersaturation, nucleation does not occur any further. Else, the nuclei grows into NPs of large size until the equilibrium is reached. In the case of the synthesis of reduced NPs, the precursor are in higher oxidation states. The generation of atoms and nuclei formation are still not clear; that is if the precursors decompose into zero valent atoms, which aggregate to form nuclei or if the precursors decompose and forms nuclei which are reduced thereafter.
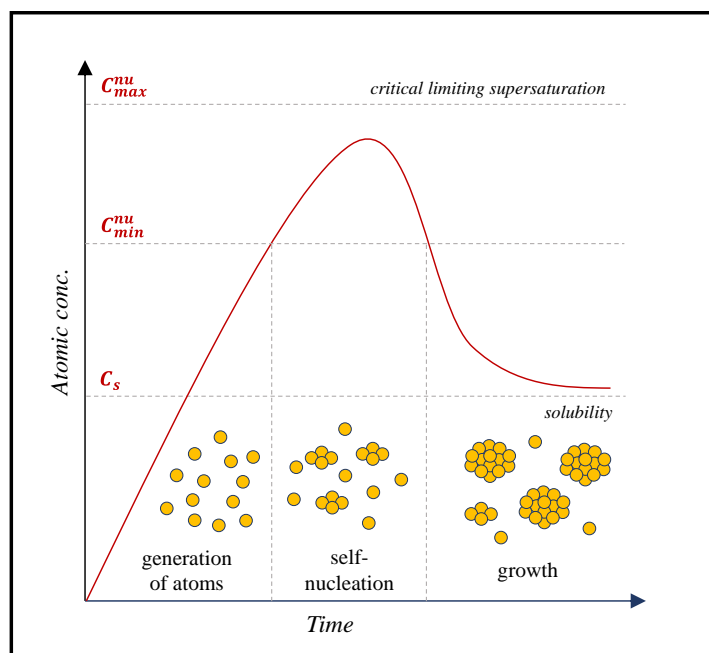
Figure 11. Schematic illustration of formation mechanism of NPs.

Various methods have been reported for the synthesis of colloidal homogeneous NPs or supported NPs for their fruitful applications in catalysis.[62] The simple wet-chemical reduction method involving the metal precursor, stabilizer and reducing agent is widely utilized for the synthesis of highly dispersed NPs. In 1951, colloidal Au NPs were synthesized using citrate as both stabilizer and reducing agent.[63] Motivated by this research report, various other researchers tried to prepare colloidal NPs using a range of organic compounds such as ascorbic acid, glucose, poly(*N*-vinyl-2-pyrrolidone), etc.[64-67] Not only the preparation of monometallic metal NPs, but also the synthesis of multi-metallic NPs have been reported in various excellent works for a range of applications.[68-71] In this thesis, in contribution towards synthesis of metal NPs, I have prepared supported bimetallic NPs using a surfactant in the absence of a reducing agent under hydrothermal conditions to observe remarkable catalysis under mild conditions.

6. Objectives of the thesis

The main objective of this thesis is to develop stable and highly-active heterogeneous materials by hydro- or solvothermal methodology for efficient and practical catalysis. Thus, studies in this thesis will focus on:

(i)   combining the advantages of homogeneous and heterogeneous catalysts,

(ii)   engineering of cost-effective chemical profiles for top value-added chemicals,

(iii)   adhering to the principles of green and sustainable chemistry by minimizing the energy usage, waste production and use of safer reagents,

(iv)   design and synthesis of stable, highly-efficacious and reusable heterogeneous catalyst to minimize cost,

(v)   substitution of non-renewable or expensive petroleum feedstock by renewable and ample sources like inedible-biomass as far as possible.

7. Outline of the thesis

In **general introduction** section, various issues related to the chemical, material and sustainable sciences have been raised. The need for sustainable development of chemical technologies for materials and energy have been commented first followed by remarks on biomass, hydro- or solvothermal strategy, catalysis and nanotechnology. Lastly, the objectives for this work has also been included.

The thesis thereafter has been divided into two parts namely Part I and Part II. **Part I** of the thesis introduces the novel catalysis of hydrothermally synthesized transition metal catalyst for

utilization of inedible-biomass, and **Part II** focusses on the design of stable heterogeneous catalyst for efficient applications in industrially important organic transformations.

In **Chapter 1** of **Part I**, the current challenges involved and their possible solutions for the efficient alkaline conversion of glucose to lactic acid (LA) and formic acid (FA) has been discussed. The synthesis, catalysis for glucose upgradation to LA & FA and characterization of supported copper catalyst is mentioned in this part. The hydrothermally synthesized magnesia-supported copper catalyst in the presence of cetyltrimethyl ammonium bromide (CTAB) as the capping agent (denoted as Cu-CTAB/MgO) not only boosted the yields for such organic acids in comparison to recent literature but also minimized the energy demand of the process. I found that hydrothermally-synthesized copper on magnesia in the presence of surfactant possessed excellent catalytic activity for the conversion of various biomass-derived sugars (glucose, cellobiose, etc) into LA (in the presence of NaOH) and FA (in the presence of 30% H_2O_2) at 393 K in high yields (30-70%). The catalyst could be recycled without any loss of high activity. The supported catalyst was characterized thoroughly to identify the active species and propose a suitable mechanism responsible for enhanced selective catalysis.

formic acid (FA)   biomass-derived saccharides   lactic acid (LA)
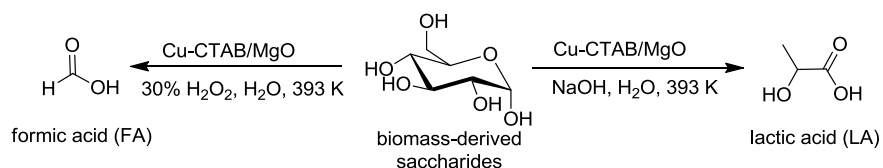
Inspired by the effect of CTAB in the catalysis and novel species, in **Chapter 2** of **Part I** a more detailed investigation of influences due to the nature of surfactants were carried out. Various surfactants (cationic, non-ionic and anionic) were employed during the hydrothermal synthesis of Cu-surfactant/MgO catalysts. Although it was found that the cationic type surfactant possessed the highest catalytic activity for LA synthesis from glucose in comparison to the anionic or non-ionic

surfactant, but an interesting impact on the copper oxide (CuO, Cu_4O_3 and Cu_2O) species was observed as a function of surfactant and preparation methodology. The rare copper oxide phase (Cu_4O_3) were preferably formed in the presence of quaternary ammonium salts containing surfactants under controlled synthesis. In this chapter, a simple surfactant-mediated hydrothermal strategy to control the supported species has been illustrated.

glucose → Cu-surfactant/MgO, NaOH, H_2O, 393 K → lactic acid (LA)
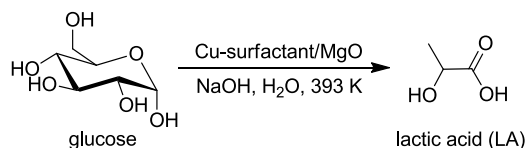
Chapter 3 of **Part I**, in continuity of applications of biomass, focusses on the design of potential catalytic surface for maximizing the direct applications of inedible-biomass. A CoPd catalyst was synthesized hydrothermally in the presence of different capping agents and studied for hydrogenation of maleic anhydride (MAn) into succinic acid (SA, C4 building block) using FA as hydrogen source under mild conditions. Among compared capped bimetallic CoPd catalysts, *N,N*-dimethyldodecylamine *N*-oxide (DDAO) capped bimetallic CoPd NPs supported on AlOOH (CoPd-DDAO/AlOOH) exhibited higher efficiency and remarkable reusability for the hydrogenation reaction as an advantage over commercial Pd catalyst. The hydrogenation activity was optimized and the catalyst was carefully characterized using advanced instrumental techniques to reveal the favorable electronic/geometric changes for adsorption of substrates caused by alloying of Co with Pd in the presence of DDAO capping agent. For the viable applications in the bio-refinery, a two-step one-pot reaction strategy using glucose as hydrogen source for the hydrogenation of MAn was also successfully studied.

maleic anhydride (MAn) + formic acid (FA) (from biomass) → CoPd-DDAO/AlOOH, 353 K, H_2O → succinic acid (SA)
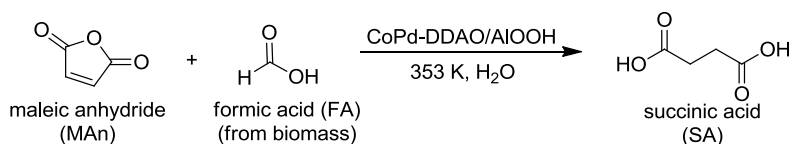
In Suzuki-Miyaura coupling (SMC) reaction, the stability and catalytic activity of a traditional heterogeneous catalysts are inversely related. In the literature, the catalytic activities were observed as a function of easy access of the substrates and reagents to active species. As **Chapter 1** of **Part II**, with a view of preparation of stable and easily accessible active sites for enhanced activity palladium grafted on amino functionalized organozinc coordination polymer (denoted as Pd/AZC) was synthesized solvothermally and their catalysis for the SMC reaction was explored. An efficient activity was noticed with sub-ppm levels of Pd to afford >99% product yield reaching turnover number (TON) as high as 2,106,720 for the reaction with bromobenzene with excellent reusability. Pd/AZC also possessed remarkable catalytic activity for the conversion of activated chlorobenzenes. A possible structure around ionic Zn and Pd species were proposed based on spectroscopic characterizations. The characterization of the catalyst after the SM reaction revealed that the catalyst retained the original structural features. The amino functionality in AZC was supposed to prevent active Pd(II) species from leaching into the reaction medium. The Mizoroki-Heck coupling, hydrogenation of nitro and C=C functional groups were also efficaciously catalyzed by Pd/AZC.
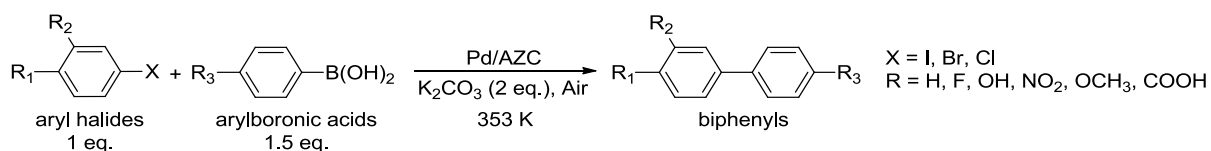
A **general conclusion** comparing the expectations with achievements was summarized at the end. The scope for the further design of heterogeneous catalysts and their catalysis has been also integrated in the same section.

REFERENCES

1. *"The Outlook for Energy: A View to 2040"*, Exxon Mobil Corporation, United States, **2015**. http://cdn.exxonmobil.com/~/media/Reports/Outlook%20For%20Energy/2015/2015-Outlook-for-Energy_print-resolution.pdf. (Latest retrieved on 6th February, 2015).

2. J. Cheng, (ed) *Biomass to Renewable Energy Processes*, CRC Press, Boca Raton, **2010**.

3. Energy Information Administration (EIA), International Energy Outlook, 2007.

4. M. K. Hubbert, "Nuclear Energy and the Fossil Fuels 'Drilling and Production Practice'". Spring Meeting of the Southern District. Division of Production. American Petroleum Institute. San Antonio, Texas: Shell Development Company. **1956**, pp. 22–27. (Latest retrieved on 6th February, 2015).

5. Peak oil, http://en.wikipedia.org/wiki/Peak_oil#cite_note-10. (Latest retrieved on 6th February, 2015).

6. P. Anastas, J. C. Warner, *Green Chemistry: Theory and Practice*, Oxford Science publications, Oxford, **1998**.

7. R. Perez, M. Perez, "A fundamental look at energy reserves for the planet", IEA/SHC Task 36 solar resource knowledge management data.

8. http://www.treia.org (Latest retrieved on 6th February, 2015).

9. A. Brown, S. Muller, Z. Dobrotkova, "Renewable energy: markets and prospects by technology", International Energy Agency Information paper, 2011.

10. O. Ellabban, H. Abu-Rub, F. Blabjerg, *Renew. Sustainable Energy Rev.* **2014**, *39*, 748.

11. D. L. Klass, "Biomass for renewable energy, fuels and chemicals", Academia press, San Diego, **1998**.

12. A. J. Ragauskas, C. K. Williams, B. H. Davison, G. Britovsek, J. Cairney, C. A. Eckert, W. J. Frederick, J. P. Hallett, D. J. Leak, C. L. Liotta, J. R. Mielenz, R. Murphy, R. Templer, T. Tschaplinski, *Science* **2006**, *311*, 484.

13. P. Gallezot, *Chem. Soc. Rev.* **2012**, *41*, 1538.

14. A. Takagaki, S. Nishimura, K. Ebitani, *Catal. Surv. Asia* **2012**, *16*, 164.

15. G. W. Huber, S. Iborra, A. Corma, *Chem. Rev.* **2006**, *106*, 4044.

16. J. C. Serrano-Ruiz, R. Luque, A. Sepulveda-Escribano, *Chem. Soc. Rev.* **2011**, *40*, 5266.

17. C. Okkerse, H. van Bekkum, *Green Chem.* **1999**, *1*, 107.

18. E. K. Ackon, D. Alemagi, N. B. Ackom, P. A. Minang, Z. Tchoundjeu, *Energy Policy* **2013**, *63*, 101.

19. K. Byrappa, M. Yoshimura, "*Handbook of Hydrothermal Technology*", Noyes Publications/William Andrew Publishing LLC, USA, **2001**.

20. K. F. E. Schafhautl, *Gelehrte Anzeigen Bayer. Akad.* **1845**, *20*, 557.

21. G. W. Morey, P. Niggli, *J. Am. Chem. Soc.* **1913**, *35*, 1086.

22. K. J. Bayer, **1887**; cited by F. Habashi in a textbook of hydrometallurgy, Canada, **1993**.

23. M. Yoshimura, K. Byrappa, *J. Mater. Sci.* **2008**, *43*, 2085.

24. R. A. Laudise, "*The Growth of Single Crystals*", Prentice-Hall, Englwood Cliffs, New Jersey, **1970**, pp. 278-281.

25. A. Rabenau, *Angew. Chem. Int. Ed.* **1985**, *24*, 1026.

26. A. N. Lobachev, (ed.), "*Crystallization Processes under Hydrothermal Conditions*", Consultants Bureau, New York, **1973**, pp. 1-255.

27. R. Roy, *J. Solid State Chem.* **1994**, *111*, 11.

28. "*Hydrothermal Growth of Crystals*", K. Byrappa, (ed.), Pergamon press, Oxford, **1992**, pp. 1-365.

29. M. Yoshimura, H. Suda, "*Hydrothermal Processing of Hydroxyapatite: Past, Present, and Future, in: Hydroxyapatite and Related Materials*", P. W. Brown, B. Constanz, (eds.), CRC Press, Inc, **1994**, pp. 45-72.

30. G. Demazeau, *J. Mater. Chem.* **1999**, *9*, 15.

31. S. Somiya, "*Hydrothermal Reactions for Materials Science and Engineering. An Overview of Research in Japan*", Elsevier Science publishers Ltd., U.K., **1989**.

32. M. Yoshimura, W. L. Suchanek, K. Byrappa, *MRS Bull.* **2000**, *25*, 17.

33. B. Gersten, M. Lencka, R. E. Riman, *Chem. Mater.* **2002**, *14*, 1950.

34. F. Habashi, *Hydrometallurgy* **2005**, *79*, 15.

35. R. W. Goranson, *Am. J. Sci.* **1931**, *22*, 481.

36. M. Hosaka, *Prog. Cryst. Growth Charact. Mater.* **1991**, *21*, 71.

37. S. Feng, R. Xu, *Acc. Chem. Res.* **2001**, *34*, 239.

38. L. N. Demianets, *Prog. Cryst. Growth Charact. Mater.* **1991**, *21*, 299.

39. A. Rabenau, H. Rau, *Philips Tech. rev.* **1969**, *30*, 89.

40. Y. G. Gogotsi, M. Yoshimura, *Nature* **1994**, *367*, 628.

41. N. Yamasaki, K. Yanagisawa, M. Nishioka, S. Nakahara, *J. Mater. Sci. Lett.* **1986**, *5*, 355.

42. M. Rajamathi, R. Seshadri, *Curr. Opin. Solid State Mater. Sci.* **2002**, *6*, 337.

43. H. Y. Chen, D. M. hiller, J. E. Hudson, C. J. A. Westenbroek, *IEEE Trans. Magn.* **1984**, *20*, 24.

44. R. Kniep, A. Rabenau, *Top. Curr. Chem.* **1983**, *111*, 145.

45. H. Rau, A. Rabenau, *Solid State Cammun.* **1967**, *5*, 331.

46. V. A. Nikitcnko, V. I. Popolitov, S. G. Stoyukhin, A. Y. Shapiro, A. N. Lohachev, A. I. Tereshchenko, V. G. Kolotilova, *Sou. Tech. Phvs. Lett. Engl. Transl.* **1979**, *5*, 493.

47. G. A. Somorjai, K. McCrea, *Appl. Catal. A* **2001**, *222*, 3.

48. "*Nanopartcles and Catalysis*", D. Astruc, (ed.), Wiley-VCH, Weinheim, **2008**.

49. "*Nanomaterials in Catalysis*", P. Serp, K. Philippot, (eds.), Wiley-VCH, Weinheim, **2013**.

50. R. Schlgl, S. B. A. Hamid, *Angew. Chem. Int. Ed.* **2004**, *43*, 1628.

51. Y. Mikami, A. Dhakshinamoorthy, M. Alvaro, H. Garcia, *Catal. Sci. Technol.* **2013**, *3*, 58.

52. C. Burda, X. Chen, R. Narayanan, M. A. El-Sayed, *Chem. Rev.* **2005**, *105*, 1025.

53. P. Zijlstra, J. W. M. Chon, M. Gu, *Nature* **2009**, *459*, 410.

54. R. Elghanian, J. J. Storhoff, R. C. Mucic, R. L. Letsinger, C. A. Mirkin, *Science* **1997**, *277*, 1078.

55. J. N. Anker, W. P. Hall, O. Lyandres, N. C. Shah, J. Zhao, R. P. Van Duyne, *Nat. Mater.* **2008**, *7*, 442.

56. J. Burgin, M. Liu, P. Guyot-Sionnest, *J. Phys. Chem. C* **2008**, *112*, 19279

57. D. Astruc, F. Lu, J. R. Aranzaes, *Angew. Chem. Int. Ed.* **2005**, *44*, 7852.

58. O. Crespo-Biel, B. J. Ravoo, J. Huskens, D. N. Reinhoudt, *Dalton Trans.* **2006**, 2737

59. S. E. Skrabalak, J. Chen, L. Au, X. Lu, X. Li, Y. Xia, *Adv. Mater.* **2007**, *19*, 3177.

60. Y. Xia, Y. Xiong, B. Lim, S. E. Skrabalak, *Angew. Chem. Int. Ed.* **2008**, *48*, 60.

61. M. Besson, P. Gallezot, C. Pinel, *Chem. Rev.* **2014**, *114*, 1827.

62. J. M. Campelo, D. Luna, R. Luque, J. M. Marinas, A. A. Romero, *ChemSusChem* **2009**, *2*, 18.

63. J. Turkevich, P. C. Stevenson, J. Hiller, *Discuss. Faraday Soc.* **1951**, *11*, 55.

64. G. Frens, *Nature* **1973**, *241*, 20.

65. J. Turkevich, *Gold Bull.* **1985**, *18*, 86.

66. S. Link, Z. L. Wang, M. A. El-Sayed, *J. Phys. Chem. B* **1999**, *103*, 3529.

67. B. Lim, M. Jiang, J. Tao, P. H. C. Camargo, Y. Zhu, Y. Xia, *Adv. Funct. Mater.* **2009**, *19*, 189.

68. N. Toshima, T. Yonezawa, *New J. Chem.* **1998**, 1179.

69. R. Ferrando, J. Jellinek, R. L. Johnston, *Chem. Rev.* **2008**, *108*, 845.

70. C. J. Serpell, J. Cookson, D. Ozkaya, P. D. Beer, *Nat. Chem.* **2011**, *3*, 478.

71. P. Bushwalter, J. Rose, P. Braunstein, *Chem. Rev.* **2015**, *115*, 28.

Part I

Hydrothermal preparation of novel catalysts for efficient utilizations of biomass-resources

Chapter 1

Conversion of sugars into organic acids using novel hydrothermally prepared copper catalyst

ABSTRACT

Design of a suitable catalyst for the conversion of inedible-biomass, a renewable resource, into high-value chemicals is an immense and important area of research in an era of energy crisis. This paper demonstrates batch conversion of sugars into lactic acid (LA) and formic acid (FA) employing a supported copper catalyst. A magnesia-supported copper catalyst was synthesized by a hydrothermal methodology using CTAB as the capping agent (denoted as Cu-CTAB/MgO). I found that the Cu-CTAB/MgO not only dramatically boosted the yields of LA and FA from sugars but also decreased the energy demand of the process by decreasing the reaction temperature from 523 K to 393 K. The high yields of LA (70%) in the presence of NaOH and of FA (65%) in the presence of H_2O_2 were achieved from glucose at 393 K in water using a Cu-CTAB/MgO catalyst, which could be recycled without any significant loss of activity. The copper catalyst was also found to exhibit excellent activity for the transformation of other sugars. The catalyst was characterized using PXRD, H_2-TPR, N_2 adsorption-desorption, and other analytical techniques to investigate the active Cu species and propose a plausible mechanistic pathway to LA.

1. INTRODUCTION

The demanding consumption of non-renewable fossil fuels has increased CO_2 concentrations in the environment. The depleting resources and increasing environmental concerns are inspiring researchers to develop renewable sources for a sustainable and stable future. The potential to use biomass as a substitute for the conventional petroleum feedstock has been known and realized in the past few years.[1-7] In principle, the uses of biomass could be more diverse than for crude oil; however, realization of this is challenging. Currently, both academic and industrial professionals are striving to convert the cellulosic or lignocellulosic biomass into commodity chemicals at higher efficiencies. A variety of chemicals, such as 5-hydroxymethyl-2-furaldehyde[8-13], 2-furaldehyde[8-13], 2,5-dimethylfuran[14-16], 2,5-diformylfuran[17-19], succinic acid[20-22], levulinic acid[23-24], fatty acids and alcohols[25-27], and lactic acid (LA)[28-32] can be produced from biomass by engineering suitable catalysts and reaction conditions. Among these commodity chemicals, LA has attracted the most attention, and the direct conversion of sugars into LA is highly desired. Formic acid (FA) is another organic acid of high interest to the researchers of this era, who are trying to harvest it in higher yields from renewable feedstock. LA is used extensively in detergents, antibacterial agents, cosmetics, food additives, and biodegradable plastics, whereas FA is used as a potential hydrogen donor and hydrogen storehouse.[33-39] This increasing global demand of high value and energy chemicals emphasizes the importance of research on cellulosic biomass transformation.

The fermentation of sugars is the key process as a potential candidate for syntheses of LA[40-41] and FA[42]. The industrial synthesis of LA is dominated by fermentation method because of increasing market demand of *bio*-LA.[43] The hydrolysis of methyl formate is the current state of art for FA with an approximately 49% of total production capacity.[44] The fermentation processes are,

[30]

however, expensive due to product purification, strict control of reaction conditions, and restricted large scale operations. Water at higher temperatures has a unique property which eases the reaction pathway to an extent that even the use of catalyst is not needed. Inspired from this, many researchers have successfully converted carbohydrates into chemicals; mainly LA and FA, with or without additives as discussed later. The employment of drastic conditions of high temperatures and pressures to produce LA and FA in moderate yields opens up new researches to decrease energy demand for such severe processes. Moreover, the hydrothermal condition at higher temperatures often decreases the selectivity and varieties of products are obtained like 5-hydroxymethyl-2-furaldehyde, organic acids, and char[45]. Herein, I have focused on the development of process technologies for selective conversion of sugars to LA and FA under milder conditions using catalyst.

Various research groups have reported the synthesis of LA from biomass under alkaline hydrothermal conditions or with acidic catalysts[28-32] producing LA in low to moderate yields. Although LA was known as alkaline degradation product of sugars since long ago,[46] extensive research for the improvement in the yields have been carried out in recent years. Enomoto's group studied glycoaldehyde and glucose as substrates to afford LA in lower yields at higher temperature.[47] As an improvement, they also reported that uses of sodium hydroxide (NaOH) and calcium hydroxide ($Ca(OH)_2$) can afford LA with 27% yield (from glucose) for shorter reaction time at 573 K.[48] Most of the report in literatures focused on NaOH or $Ca(OH)_2$ for the alkaline hydrolysis of biomass. These encouraged Esposito and Antonietti to investigate the effect of other bases; an impressive LA yield of 53% with homogeneous barium hydroxide ($Ba(OH)_2$) at 493 K for longer reaction time was reported.[49] In contrast to the reports on LA production from biomass, very few researchers have published the direct formation of FA from biomass. Gao et al.

successfully afforded FA in 22% yield from pretreated cellulose at 483 K for 30 h.[50] A high yield of 75% FA was introduced by Jin et al. at 523 K utilizing 120% H_2O_2 from glucose.[51] Other reports exhibits the formation of FA in traces as a side product during LA synthesis.

The major drawback in previous reports is the operations at high temperature (493-623 K), or low to moderate yields of desired organic acids. This kindles the need for development of suitable catalyst or process for decreasing the energy demand involved in the alkaline hydrolysis of carbohydrates. Many researchers have focused on the role of earlier transition metal for improving the LA yields under alkaline hydrothermal conditions.[52-55] Onda et al. introduced the calcined hydrotalcite as a heterogeneous base catalyst to obtain 20% LA yield from glucose.[52] Zhang et al. reported the increment in the yields of LA to 42% using Zn and Ni as co-catalyst from cellulose.[53] In another recent work, the role of copper oxide was explored in the alkaline hydrothermal conversion in improving the yields from 37-42% to 59% at 573 K.[56] It was reported that copper clusters synthesized under hydrothermal conditions exhibited a superior activity for oxidation reaction as compared to previous literatures.[57-59] These achievements inspired us to synthesize hydrothermally loaded copper catalysts for high yields of organic acids *via* alkaline hydrolysis of saccharides.

In this study, I have demonstrated the promotional effect of hydrothermally loaded copper oxide species on magnesia catalyst using capping agent (cetyltrimethylammonium bromide; CTAB), Cu-CTAB/MgO, for the batch conversions of biomass-derived sugar into LA or FA in high yields under milder conditions (Scheme 1). In addition, the copper catalyst was found to be reusable with a simple reactivation by calcination, as an advantage over the non-recyclable conventional methodologies involved for LA and/or FA synthesis from sugars. Moreover, not only glucose, but also other sugars including mono and disaccharides were successfully converted into LA and FA

using the supported copper catalyst. Finally, plausible reaction pathway to LA is proposed based on the characterization results which identify the active Cu species.
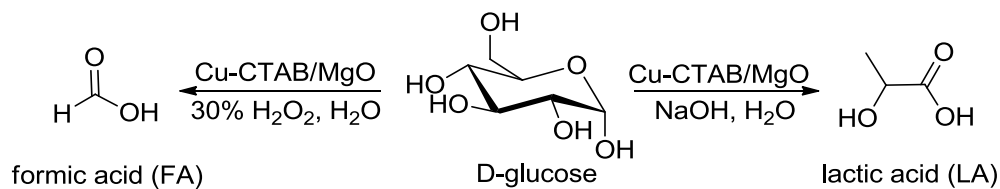
Scheme 1. Glucose conversions into LA and FA

2. EXPERIMENTAL SECTION

Chemicals. D(+)-glucose, starch (soluble), lactose monohydrate, sucrose, D(+)-raffinose pentahydrate, cetyltrimethylammonium bromide (CTAB), formic acid (FA), DL-glyceraldehyde, copper(I) oxide (Cu_2O), copper nitrate hexahydrate ($Cu(NO_3)_2 \cdot 6H_2O$), and 30% hydrogen peroxide (H_2O_2) were purchased from Wako Pure Chemical Industries, Ltd. D(-)-fructose, D(+)-xylose, D(+)-cellobiose, acetic acid, magnesium oxide (MgO), sulfuric acid (H_2SO_4), and sodium hydroxide (NaOH) were procured from Kanto Chemical Co., Inc. Tokyo Chemical Industry Co., Ltd. supplied D(+)-galactose and glycolic acid whereas DL-glyceric acid (GlycA) was bought from Nacalai Tesque, Inc. L(+)-Lactic acid (LA) and pyruvaldehyde (PAL) were obtained from Sigma-Aldrich, Co. LLC. Merck KGaA provided dihydroxyacetone (DHA) and microcrystalline cellulose. Strem Chemicals Inc. was the source for a high purity (99.999%) of copper(II) oxide (CuO).
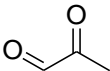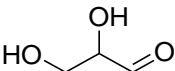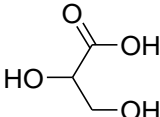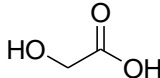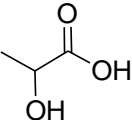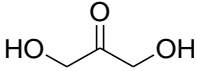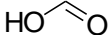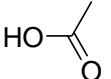
Catalyst preparation. CTAB capped copper supported on magnesia (Cu-CTAB/MgO) have been synthesized by a hydrothermal method as described by Sarkar et al. with some modifications.[58]

CTAB, a cationic surfactant, was selected as the capping agent and dissolved in deionized water. In a typical synthesis methodology, MgO was dispersed in deionized water, and then an aqueous solution of $Cu(NO_3)_2 \cdot 6H_2O$ containing requisite amount of copper was added dropwise into the solution under vigorous stirring. To this mixture, an aqueous solution of CTAB was added, and vigorously stirred for 3 h. The obtained mixture was sealed in a 100 mL Teflon lined autoclave, and heated to 453 K at a heating rate of 6 K min^{-1} in an oven, and maintained at the same temperature for 24 h. The oven was allowed to cool slowly to room temperature. The obtained solid was washed with deionized water till the pH of filtrate became neutral, followed by washing with ethanol before drying *in vacuo* overnight at room temperature. The dried materials were further calcined at 383, 573, 773, 973 or 1173 K with a ramp-rate of 10 K min^{-1} for 6 h in air. Various copper loaded magnesia catalysts were denoted as xCu-CTAB/MgO; where the x is Cu content in mmol per gram of catalyst (mmol g^{-1}) in theory.

Catalytic testing. All experiments to test the catalytic activity were performed in a 50 mL Teflon lined autoclave. The catalytic activity was evaluated for glucose conversion into LA or FA in aqueous media. In a general reaction procedure, glucose (or sugar) was dissolved in 5 mL deionized water. Catalyst was added to the solution followed by the addition of NaOH solution or 30% H_2O_2 solution. The autoclave was sealed and purged with an Ar (0.4 MPa), and mounted on a preheated oil bath at 373-413 K. The mixture was allowed to react for various time intervals with continuous magnetic stirring. After the reaction, a part of the resultant solution was diluted 20 times with deionized water (or 10 mM H_2SO_4 for the samples containing alkali), and the catalyst was filtered off using a Milex®-LG 0.20 μm. The obtained filtrate was analyzed by high performance liquid chromatography (HPLC, WATERS 600) using an Aminex HPX-87H column (Bio-Rad Laboratories, Inc.) attached to a refractive index detector. An aqueous 10 mM H_2SO_4 (as

mobile phase) was run through the column (maintained at 323 K) at a flow rate of 0.5 mL min^{-1}. The conversion and yield(s) were determined with a calibration curve method by the equations shown below. The chemical name and structure for expected/detected products were listed in Table 1. A typical HPLC chromatogram is shown in Figure 1.

Table 1. Chemical name and structure for expected/detected products.

Entry	Abbreviation	Chemical Name	Chemical Structure
1	PAL	pyruvaldehyde	
2	GlycAld	glyceraldehyde	
3	GlycA	glyceric acid	
4	GlcoA	glycolic acid	
5	LA	lactic acid	
6	DHA	dihydroxyacetone	
7	FA	formic acid	
8	AA	acetic acid	

Recycling tests were performed to check stability of the synthesized catalysts during the reaction. The catalyst was separated from the reaction mixture by centrifugation. The supernatant liquid was

[35]

stored, and then analysis of products and leaching test of catalysts were performed. The residual catalyst was washed by centrifugation with deionized water. Finally, the catalyst was dried *in vacuo* overnight, and heated at 773 K for 6 h at a heating rate of 10 K min^{-1}. Fresh substrates and reagents were added to the catalyst, and then the reaction was performed again.
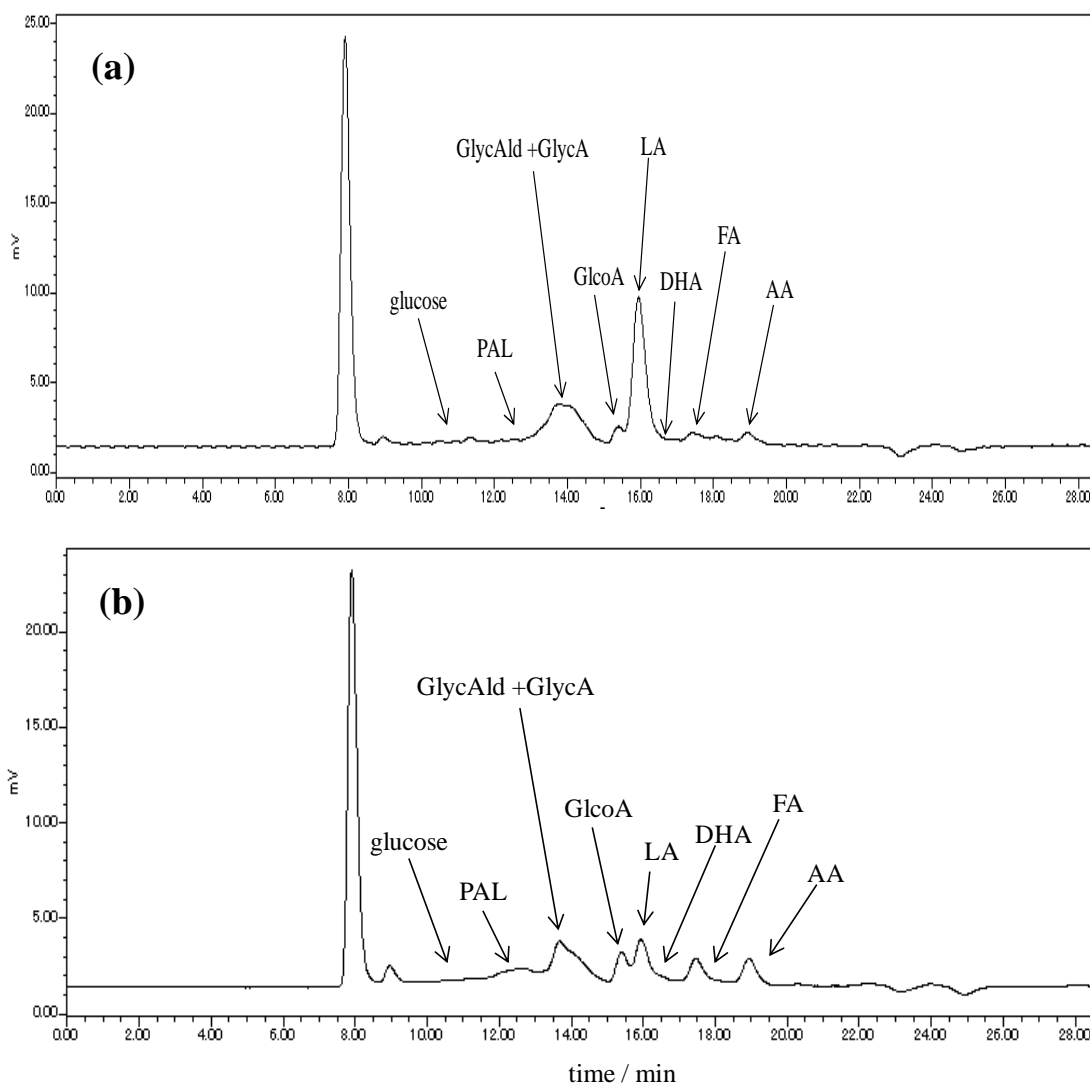
Figure 1. HPLC chromatogram for glucose degradation to LA (a) in the presence of or (b) in the absence of Cu catalyst (1Cu-CTAB/MgO, 60 mg) under alkaline hydrothermal conditions. PAL and DHA were not observed under the reaction conditions. *Reaction conditions*: Glucose (0.5 mmol), 1M NaOH (1 mL), Water (5 mL), Autoclave, Ar (0.4 MPa), 393 K, 1 h, Stirring.

Calculation. The substrate conversion, product yields and carbon mass balance were calculated using the equations shown.

$$\% \text{ Conversion} = 100 - \left\{ \left(\frac{Amount\ of\ saccharide\ detected\ (in\ mmol)}{Amount\ of\ saccharide\ used\ (in\ mmol)} \right) \times 100 \right) \right\}$$

$$\% \text{ Product Yield} = \left(\frac{Number\ of\ carbon\ in\ product\ \times\ Amount\ of\ product\ detected\ (in\ mmol)}{Number\ of\ carbon\ in\ saccharide\ \times\ Amount\ of\ saccharide\ used\ (in\ mmol)} \right) \times 100$$

$$\% \text{ Carbon balance} = \left(\frac{\sum (Yield\ of\ each\ product\ \times\ Number\ of\ carbon\ in\ each\ product)}{(Conversion\ of\ saccharide\ \times\ Number\ of\ carbon\ in\ saccharide)} \right) \times 100$$

For xylose, since one molecule of xylose produces one molecule of LA, the calculation formulae were modified as shown. Such calculation formula is believed to be one of the reason for high activity of xylose in comparison to other monosaccharides.

$$\% \text{ LA Yield} = \left(\frac{Amount\ of\ LA\ detected\ (in\ mmol)}{Amount\ of\ xylose\ used\ (in\ mmol)} \right) \times 100$$

Characterization. Crystal structure was analyzed by powder X-ray diffraction (PXRD) with a SmartLab (Rigaku Co.) using a Cu Kα radiation (λ= 0.154 nm) at 40 kV and 30 mA in the range of 2θ = 10-80°. The diffraction patterns were analyzed with the database in the joint committee of powder diffraction standards (JCPDS). Porosity and surface area were determined by a nitrogen adsorption-desorption method using a Brunauer-Emmett-Teller (BET) model in a BELSORP-max (BEL Jpn., Inc.). Sorption experiments were performed at liquid nitrogen temperature (77 K), and equilibration was allowed for each data point. All samples were pretreated at 373 K for 3 h under vacuum prior to the measurement. For inductively coupled plasma atomic emission spectroscopy (ICP-AES) analysis, an ICPS-7000 ver. 2 (Shimadzu Co.) was employed to quantify the real Cu

amount loaded over MgO and to evaluate the Cu leaching, if any, during the reaction. Contents of Cu in the catalyst and/or the reaction medium were estimated by a calibration curve method. A H-7100 (Hitachi, Ltd.) operating at 100 kV was utilized to acquire the morphology of catalyst by a transmission electron microscopy (TEM) image. The samples for TEM measurements were dispersed in water, and the supernatant liquid was dropped onto a copper grid before drying *in vacuo* overnight. The electronic state of Cu on MgO was analyzed by X-ray photoelectron spectroscopy (XPS). The experiments were conducted on an AXIS-ULTRA DLD spectrometer system (Shimadzu Co. and Kratos Analytical Ltd.) using an Al target at 15 kV and 10 mA in an energy range of 0-1200 eV. The binding energies were calibrated with the C 1s level (284.5 eV) as an internal standard reference. Temperature-programmed reduction (TPR) was performed with an Ohkura BP-2 instrument interfaced with a TCD. The TCD results were normalized to the mass of the used samples, and the rate of H_2 consumption was estimated based on the calibration curve of pure CuO (99.999%) reduction. The TPR profile was recorded from 323 K under a H_2/Ar (5/95) flow at a ramping rate of 10 K min^{-1}. X-ray absorption spectroscopy (XAS) was performed with a transmission mode at a BL-9C in KEK-PF under the approval of the Photon Factory Program Advisory Committee (Proposal No. 2013G586). All samples were grained and pressed to pellets with a diameter of 10 mm. The amount of the Brønsted basic sites in MgO or Cu-CTAB/MgO was calculated by the titration method using benzoic acid. For instance, in an Erlenmeyer flask, 0.025 g of catalyst were dispersed in a 5 mL of mixed solution (H_2O:EtOH (4:1; v/v)), and phenolphthalein was added as an indicator. 0.05 M benzoic acid was added dropwise to the solution containing sample, and whirled until the discharge of pink color of the solution. The procedure was repeated to obtain concordant readings for each catalyst. The amount of the basic sites (mmol g^{-1}) was calculated as the ratio of consumed benzoic acid to the mass of the catalyst

[38]

used. The IR measurements of samples were carried out on a PerkinElmer Spectrum 100 FT-IR spectrometer at room temperature.

3. RESULTS AND DISCUSSION

Catalytic activity. The catalytic activity of the synthesized catalyst was evaluated, and the reaction condition was optimized to achieve higher efficiencies for sugars transformation with glucose as model compound. In this section, the catalytic activity for glucose transformation to LA and FA is described. Potential of the catalyst was further established by reusability experiments, and testing with various other sugars.

Glucose conversion to LA. For a sustainable future, the conversion of sugars into LA in higher yields is an attractive topic to various researchers. I chose glucose as the model compound for optimization of reaction conditions to achieve LA in high yields under milder conditions. In the glucose conversion to LA, glyceric acid (GlycA) and glyceraldehyde (GlycAld) were the general by-products along with traces of acetic acid (AA), FA, and glycolic acid (GlcoA) in some cases. In 2008, Onda et al. published the effect of calcination temperature on the activity of hydrotalcite as solid base catalyst in the presence of alkali. The group reported a glucose conversion of 57% and a LA yield of 20%, employing 0.6 g of catalyst for 25 mmol L^{-1} of glucose in a 50 mmol L^{-1} NaOH solution. They found that the catalytic activity for LA depended linearly on the calcination temperature of hydrotalcite with increasing numbers of Brønsted basic sites.[52]

I investigated the activity of Cu-CTAB/MgO calcined at various temperatures (383-1173 K) for glucose conversion to LA. As shown in Figure 2, the activity for LA increased spontaneously for

[39]

calcination temperature of 383 K, 573 K and 773 K, and decreased thereafter. Additionally, the amount of Brønsted basic site increased with the increase in the calcination temperature, and then the amount of basic site gradually decreased above at 773 K as also plotted in Figure 2. MgO support alone possessed some activities; however, these were lower than Cu-CTAB/MgO. The amount of basic sites was found to be lower for MgO in comparison to Cu-CTAB/MgO. Thus, the calcination temperature seemed to influence the basic sites[52] and/or the oxidation states of Cu-CTAB/MgO; thereby, improving the yields of LA from glucose. Cu-CTAB/MgO calcined at 773 K exhibited the maximum amount of Brønsted basic site and yield for LA (53.4%).
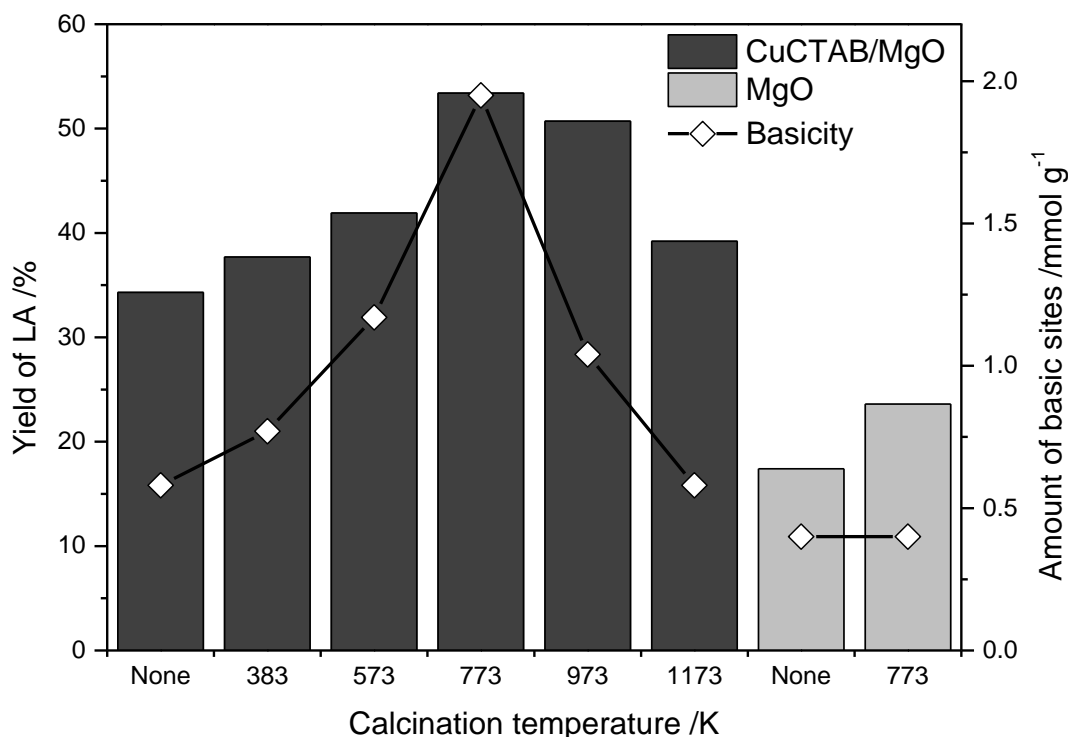
Figure 2. Effect of the calcination temperature of Cu-CTAB/MgO on LA yields. Yields of LA for Cu-CTAB/MgO (dark gray columns) and MgO (light gray columns). Amount of basicity ($\diamondsuit$). *Reaction conditions*: glucose (0.5 mmol, 90 mg), Catalyst (1Cu-CTAB/MgO, 60 mg), Water (5 mL), 1M NaOH (1 mL), Autoclave, Ar (0.4 MPa), 393 K, 1 h, Stirring.

Table 2. Screening of optimum conditions for LA synthesis from glucose[a]

Entry	Catalyst[b]	Cu cont.[c] /mmol g^{-1}	NaOH /mL	React. Temp./K	React. Time/h	Conv. of glucose[d]/%	Yield[d]/%						Carbon mass balance[e]/%*
							LA	GlycAld	GlycA	GlcoA	FA	AA	
1	1Cu-CTAB/MgO	0.998	1.0M/0.5	**373**	3	>99	14.1	14.2	13.8	3.9	15.3	5.6	28.6
2				**383**		>99	20.3	13.5	12	5.5	18.5	17	33.5
3				**393**		>99	29.6	10.6	11.9	8.9	13.8	15	36.4
4				**403**		>99	31.1	1.8	3.7	12.1	14.6	13	29.1
5				**413**		>99	35.6	0.4	1.9	10.5	20.7	15.6	31.1
6	1Cu-CTAB/MgO	0.998	1.0M/0.5	393	**0.5**	94.2	18.8	20.1	15	3.9	0.6	0.9	38.4
7					**1**	>99	44.7	14.1	16.6	5.4	8.3	9.9	44.2
8					**2**	>99	36.4	12.8	11.2	14.7	5.6	11.6	39.9
9					**3**	>99	29.6	10.6	11.9	8.9	13.8	15	36.4
10	MgO	**0**	1.0M/0.5	393	3	>99	10.8	16.6	9.2	2.8	16.7	18.5	28.2
11	0.3Cu-CTAB/MgO	**0.306**				95.6	12.4	19.2	15.8	10.1	11.3	13.7	41.6
12	0.5Cu-CTAB/MgO	**0.497**				98.9	16.9	17.6	19.4	8.1	14.9	20.7	39.8
13	1Cu-CTAB/MgO	**0.998**				>99	29.6	10.6	11.9	8.9	13.8	15	36.4
14	2Cu-CTAB/MgO	**1.856**				>99	35.8	24.9	12.2	2.3	16.3	19.0	45.8
15	1Cu-CTAB/MgO	0.998	**None**	393	1	88.7	21.1	15.8	18.4	5	15.2	16.2	68.6
16			**1.0M/0.5**			>99	29.6	10.6	11.9	8.9	13.8	15	36.4
17			**1.0M/1.0**			>99	53.4	13.1	14.7	6.8	6.7	7.4	46.3
18			**2.5M/1.0**			>99	69.9	34.1	16.6	2.5	3.7	5.7	63.7
19	**1Cu/MgO**	0.368	1.0M/1.0	393	1	>99	37.2	11	5.9	3.3	5.2	4	30.4
20	**CuO^f (non-calcined)**	1.081^g	2.5M/1.0	393	1	>99	32.3	6.3	1.6	2.1	6.3	23.5	29.7
21	**MgO (non-calcined)**	0	1.0M/0.5	393	3	>99	8.6	5.8	3.2	0.9	0	0.3	23.9
22	**Blank**	0	2.5M/1.0	393	1	97.3	18.9	12.1	8.4	7.3	2.6	4.8	27.8
23	**Blank**	0	None	393	1	0.8	0	0	0	0	0	0	-

[a]*Reaction conditions*: Glucose (0.5 mmol, 90 mg), Catalyst (60 mg), Water (5 mL), Autoclave, Ar (0.4 MPa), Stirring. [b]Calcined at 773 K. [c]Determined by ICP-AES. [d]Calculated by HPLC analysis using calibration curve method. [e]Determined on the basis of observed products. [f]99.999% CuO, (0.06 mmol, 4.8 mg). [g]Theoretically calculated to match copper content in active catalyst.

Table 2 describes the results of screening the conditions for LA synthesis from glucose over Cu-CTAB/MgO catalyst calcined at 773 K. A positive effect in the yield of LA was noticed with increase in reaction temperature from 373 K to 413 K (entries 1-5) as reported earlier.[47-48] However, with the increase in reaction temperature above 393 K, the yields for smaller carbon-containing acids (GlcoA, FA and AA) increased with a decrease in carbon mass balance. Some researchers have concluded that the highest LA yields *via* alkaline sugar degradation were obtained within a few seconds at higher temperatures[46-49,53,56], whereas other scientists reported the deconstruction process at lower temperatures need longer reaction time in micro-reactors, or with small scale of glucose or more complex cellulosic material[49-50,52]. In the present study, comparatively longer reaction time for high LA yields was essential due to the lower reaction temperatures. It has been suggested that the rate of LA formation is greater than the rate of decomposition for LA from glucose below 623 K.[48,60] The rate of decomposition of LA also has been increased significantly at temperatures above 600 K.[48] In this study, the yields of LA increased gradually with advancement of reaction time and decreased after 1 h at 393 K (entries 6-9), which depend on the further breakdown of LA to lower carbon containing compounds like GlcoA and AA (observed in the HPLC chart). Over-reaction of LA to GlcoA or AA was also detected in previous reports.[50,56,60] In addition, at shorter reaction time (within 1 h), the LA yields were low even though glucose conversion reached 94.2%. GlycAld and GlycA dominated as the by-products in the reaction mixture at shorter intervals, whereas mixture of GlcoA, AA, and FA were the major by-products at longer time reaction. Such results also indicated the decomposition of LA into smaller carbon containing compounds at longer reaction time under the reaction condition. Surprisingly, neither

dihydroxyacetone (DHA) nor pyruvaldehyde (PAL) were detected at any stage of the reaction using Cu-CTAB/MgO catalyst.

The catalysts with copper loadings in the range of 0.3 to 2 mmol g^{-1} were synthesized, and the catalytic efficiency was screened (entries 11-14). It was found that on increasing metal content from 0 to 2 mmol g^{-1}, the yield of LA correspondingly increased from 10.8% to 35.8% (entries 10-14); however, these effects became little at higher concentration of copper; *i.e.* increasing the copper loading from 0.998 to 1.856 mmol g^{-1} only induced an elevation of 6.2% on LA yield. Moreover, the ICP-AES analysis of the reaction mixture indicated the leaching of copper species occurred in the case of 2Cu-CTAB/MgO calcined at 773 K (0.063 mmol L^{-1}). While, no ionic copper (or leached copper) were observed for copper loading below 2 mmol g^{-1} in *x*Cu-CTAB/MgO
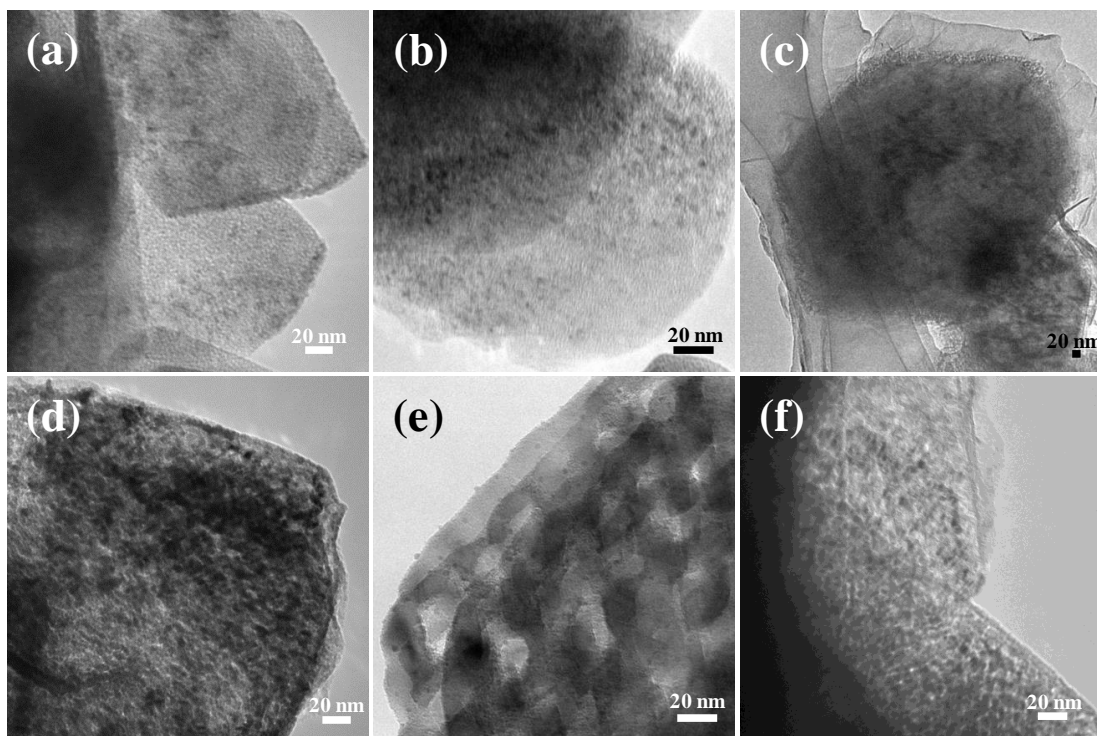
Figure 3. TEM images of (a) non-calcined Cu-CTAB/MgO; Cu-CTAB/MgO calcined at (b) 383 K, (c) 573 K, (d) 773 K, and (e) 973 K; (f) Cu-CTAB/MgO calcined at 773 K after reactivation.

[43]

after the reaction of glucose. Furthermore, 1Cu/MgO catalyst without capping agent calcined at 773 K (0.368 mmol g^{-1} Cu) possessed the catalytic activity (37.2% LA yield from glucose) (entry 19), but leaching of metal species in the reaction medium was also observed by ICP-AES. Thus, the Cu species seemed to be easily and strongly stabilized onto MgO in the presence of CTAB. CTAB has been known to favor high dispersion of metals such as Cu when it was used with metal oxides. Well distributed copper clusters on magnesia were observed throughout the Cu-CTAB/MgO catalyst calcined at 773 K in comparison to uncalcined catalysts (Figure 3). The effect of copper on the increment of yields of LA from sugars was discussed in the report as due to the *in-situ* ionic copper formation.[56] The copper(II) ions were proposed to make stable coordination with hydroxyl groups in glucose that eases the transfer of electron from oxygen to copper to reduce it to copper(0). This electron donation would cleave glucose to LA and consequently produce LA to AA.[56]

The importance of alkali amount and concentration is also depicted from Table 2 (entries 16-18), where LA yield maximizes with 2.5 M NaOH, in accordance to the previous reports using NaOH.[47-50,52-53,56] The mechanistic study for the alkaline degradation of sugars have portrayed aldol condensation, isomerization, keto-enol tautomerization and benzilic acid rearrangement as the crucial steps involved in the reaction path.[47,60] The basicity of the reaction medium hastens the rate of above reactions, confirming the formation of LA as a function of base concentration. A similar trend and requirement of basic sites was also observed in Figure 2, establishing the role of basicity in the present glucose conversion. The precise analysis of the reaction mixture using HPLC (Figure 1) and NMR indicated that no polymerization occurred under our reaction conditions. The carbon mass balance was low in spite of high conversions of sugars. The HPLC chromatogram demonstrated no extra peak corresponding to any other organic carbon product.

Thereby, the reaction mixture was analyzed by NMR (^{1}H and ^{13}C) to understand that no new carbon based material other than expected products/intermediates formed under our reaction conditions. Additionally, the absence of any signal for carbon based material in the XRD patterns of the catalyst after reaction, too, encouraged us to conclude that no polymerization occurred. It was assumed that the left over carbons are transformed into char as indicated by increased mass and changed color of the catalyst after reaction.

A synergistic effect of catalyst and alkali existed under the reaction conditions. In the absence of either base or catalyst lower activity for LA synthesis could be observed, 21.1% or 18.9% yield of LA for each, which is enhanced 3 folds on the co-existence of both catalyst and base in the reaction (69.9% yield of LA). In these cases, the use of only catalyst converted 88.7% glucose in comparison to >97.3% for only base (Table 2, entries 15 and 22). The CuO (commercial) was used as co-catalyst with NaOH (2.5 M, 1.0 ml) to verify the effect of bulk CuO on the yields of LA; nevertheless, the bulk CuO exhibited lower activity (32.3% yield) than the synthesized 1Cu-CTAB/MgO (69.9%) under the same condition (entry 20). These results establish the enhanced promotional effect of synthesized copper clusters over bulk copper.[56,61] Reaction of glucose at 393 K in water for 1 h afforded no products, which in turn reflects the potential of this catalytic system employed for LA synthesis (entry 23). Unlike the report by Wang et al.[56] the CTAB capped copper catalyst was selective for LA synthesis rather than AA. The experiments at lower temperatures in addition to nano-sized copper (*vide infra*; earlier reports utilized bulk copper as catalyst) could be one of the reasons for such observed differences. The use of copper in the reaction decreased the by-products as usually found for alkaline degradation of sugars under hydrothermal conditions. The possible metal-substrate interaction could account for such high selectivity as discussed later.

Glucose oxidation to FA. In the past, few researchers have reported the formation of FA by hydrothermal treatment of biomass.[50-51,62] Enomoto's group reported the difficulties in the synthesis of FA from sugars under hydrothermal conditions.[51,63] They utilized 120% H_2O_2 for FA production at 523 K for shorter reaction time to achieve 24% FA yield. Other research group reported the easy decomposition of FA under hydrothermal conditions or in the presence of excess H_2O_2, thereby suggested that suppression of the oxidative decomposition of FA significantly enhances the FA yield.[63-65] This motivated me to investigate new catalytic system for controlling the oxidative decomposition of FA and thereby increase FA yields using less concentrated H_2O_2. For typical glucose oxidation to FA; GlcoA and GlycA were observed as the only by-products.

Table 3. Effect of Cu loading on yields of FA[a]

Entry	Catalyst[b]	Cu cont.[c] /mmol g^{-1}	Time/h	Conv.[d]/%	Yield[d]/% FA	GlycA	GlcoA	Carbon mass balance[e]/%
1	0.1Cu-CTAB/MgO	0.103	3	97.4	22.8	16.8	10.1	16
2	0.3Cu-CTAB/MgO	0.306	3	>99	34.1	12.1	15.5	17
3	0.5Cu-CTAB/MgO	0.497	3	>99	30.6	15.2	16	18.2
4	1Cu-CTAB/MgO	0.998	3	>99	15.4	20.7	18.2	19.1
5	2Cu-CTAB/MgO	1.726	3	>99	8.5	29.3	22.1	23.5
6	0.3-CuCTAB/MgO	0.306	12	>99	51.2	16.3	13.3	21.3
7[f,g]			12	>99	16.6	15.8	33.2	21.8
8[f,h]			12	>99	65	29	16.6	30.9
9	MgO (non-calcined)	0	3	82.9	4.7	4.4	12.5	8.6
10	Blank	0	12	20.6	4.9	7.1	2.3	25
11[i]	Blank	0	12	0.6	0	0	0	-

[a]*Reaction conditions*: Glucose (0.5 mmol, 90 mg), Catalyst (60 mg), 30% H_2O_2 (2 mmol, 250 μL), Water (5 mL), Autoclave, Ar (0.4 MPa), 393 K, Stirring. [b]Calcined at 773 K. [c]Determined by ICP-AES. [d]Calculated by HPLC analysis using calibration curve method. [e]Determined on the basis of observed products. [f]30% H_2O_2 (4 mmol). [g]Catalyst (30 mg). [h]Catalyst (90 mg). [i]No 30% H_2O_2.

The effect of copper loading on the FA yield from glucose was summarized in Table 3. The increase in copper loading over MgO from 0.1 to 0.3 mmol g^{-1} increased the FA yield (entries 1-2). However, further increase of copper loading resulted in decrease of FA yield. (entries 3-5). The Cu species with high loading may catalyze the FA decomposition. FA decomposition was confirmed by monitoring time course of FA yield (Figure 4). An increment in the FA yield was
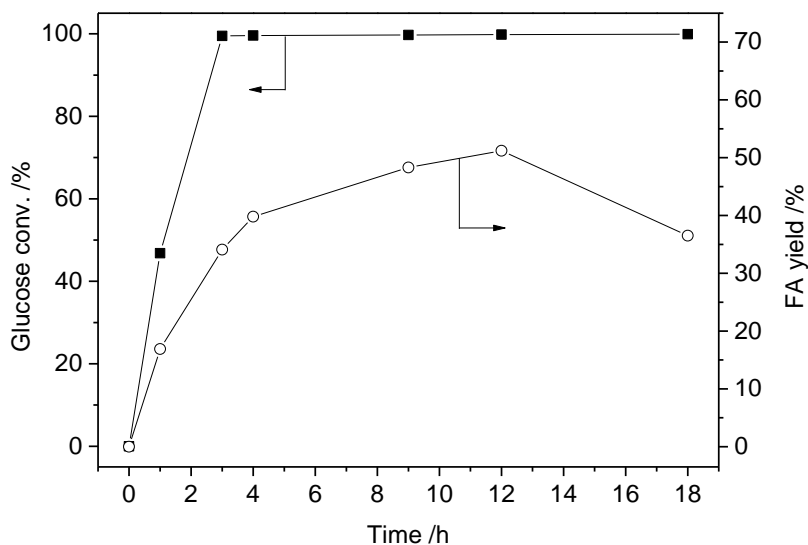
Figure 4. Time course profile of FA formation. Glucose conversion (■), FA yield (○). *Reaction conditions*: Glucose (0.5 mmol, 90 mg), Catalyst (0.3Cu-CTAB/MgO calcined at 773 K, 60 mg), 30% H_2O_2 (2 mmol, 250 μL), Water (5 mL), Autoclave, Ar (0.4 MPa), 393 K, Stirring.

found with the reaction progress, and the FA yield maximized at 12 h. The GC analysis of the gaseous products declined the presence of both H_2 and CO_2 (dissociation products of FA), indicating the transformation of FA to carbonates or bicarbonates under longer reaction time. Ideally complete oxidation of glucose to FA requires six equivalents of oxygen.[63] Therefore, increased amount of H_2O_2 with lower catalyst amount were utilized, however, the yields were found to decrease (Table 3, entry 7). Finally, it was found that highest FA yield of 65% was achieved with increased amount of low copper loaded catalyst and high amount of H_2O_2 (entry 8).

The potential role of the catalyst was ascertained by the blank reactions under similar reaction conditions with glucose; all of them showed low or no activity (entries 10-11).

Reusability and viability of the catalyst. For any heterogeneous catalyst, recyclability of the catalyst is one of the most important factor as a measure of its catalytic efficiency and stability. The retention of active site or the prevention of metal from leaching forms the challenging task for reactions. The reports utilizing Lewis acid catalyst for sugars degradation have demonstrated the efficient reusability of catalysts in organic solvents whereas the activity is compromised in aqueous media.[30]
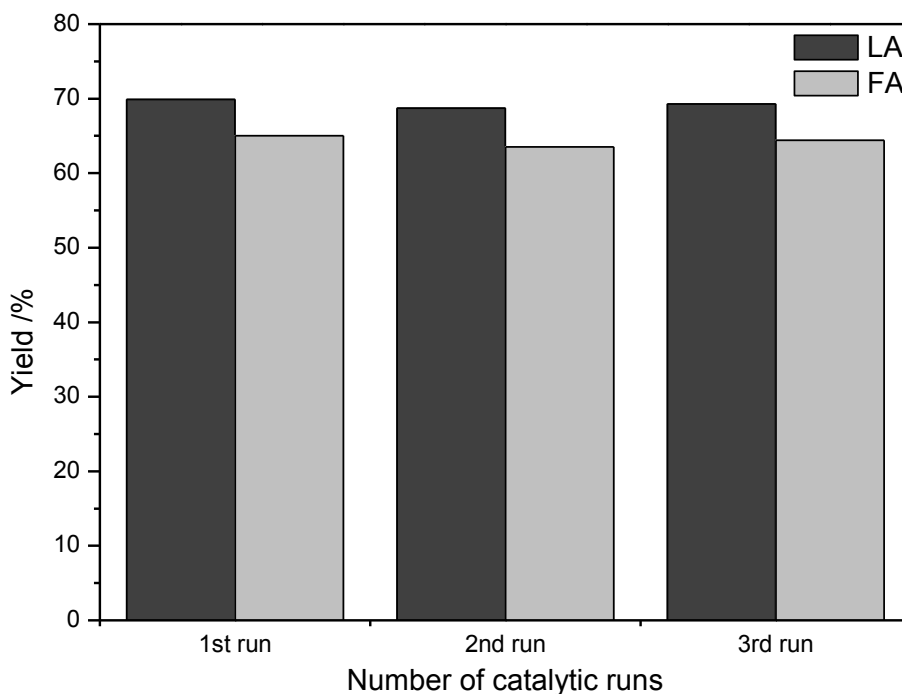
Figure 5. Reusability of the catalyst for glucose conversion. Yields of LA (dark gray bars) and FA (light gray bars). *Reaction conditions for LA synthesis:* Glucose (90 mg), Catalyst (1Cu-CTAB/MgO calcined at 773 K, 60 mg), 2.5M NaOH (1 mL), Water (5 mL), Autoclave, Ar (0.4 MPa), 393 K, 1 h, Stirring. *Reaction conditions for FA synthesis:* Glucose (90 mg), Catalyst (0.3Cu-CTAB/MgO calcined at 773 K, 90 mg), 30% H_2O_2 (4 mmol, 500 µL), Water (5 mL), Autoclave, Ar (0.4 MPa), 393 K, 12 h, Stirring.

The catalyst after the reaction was washed with water and recalcined at 773 K. The recalcined catalyst was found to be effectively reused for the conversion of glucose into LA and FA as shown in Figure 5. Moreover, ICP-AES analysis of the supernatant liquid of the reaction mixture after centrifugation, confirmed that the active catalyst did not leached into the solution under the reaction conditions, implying the heterogeneous nature of the Cu-CTAB/MgO catalyst.

An ideal catalytic system for sugars conversion along with efficient recyclability should also have a wide scope of substrates with high activity. Various saccharides including monosaccharides (xylose, galactose, etc.), disaccharides (cellobiose, etc.), trisaccharides (raffinose), and polysaccharides (cellulose, starch, etc.) were examined as substrates under the same reaction conditions as shown in Figure 6. Interestingly, xylose (monosaccharide containing five carbons) exhibited the highest yields for LA and FA among other saccharides. In general, the activity of catalyst for organic acids syntheses from saccharides decreased with increase in complexity in structure of the substrates; *i.e.*, the catalytic activity decreased from monosaccharide to disaccharide to polysaccharide even under the optimized conditions for each. The polysaccharides were stable under the present catalytic system with no yields of LA and FA. Some activity of the catalyst were observed for soluble starch (90 mg) to afford 11.4 mg of LA (in the presence of 1M NaOH) and 40.7 mg of FA (in the presence of 2 mmol 30% H_2O_2). Because of the uncertainty in the molecular mass of starch, the yields of LA and FA could not be calculated. Based on the above results, I suppose that the present catalytic system could rupture the $\beta 1 \rightarrow 4$ type bonds present in the disaccharides (as in lactose). The $\alpha 1 \rightarrow 6$ bonding in raffinose or the $\alpha 1 \rightarrow 2$ bonding in sucrose may restrict the performance of the present catalyst, and thus no products were obtained.
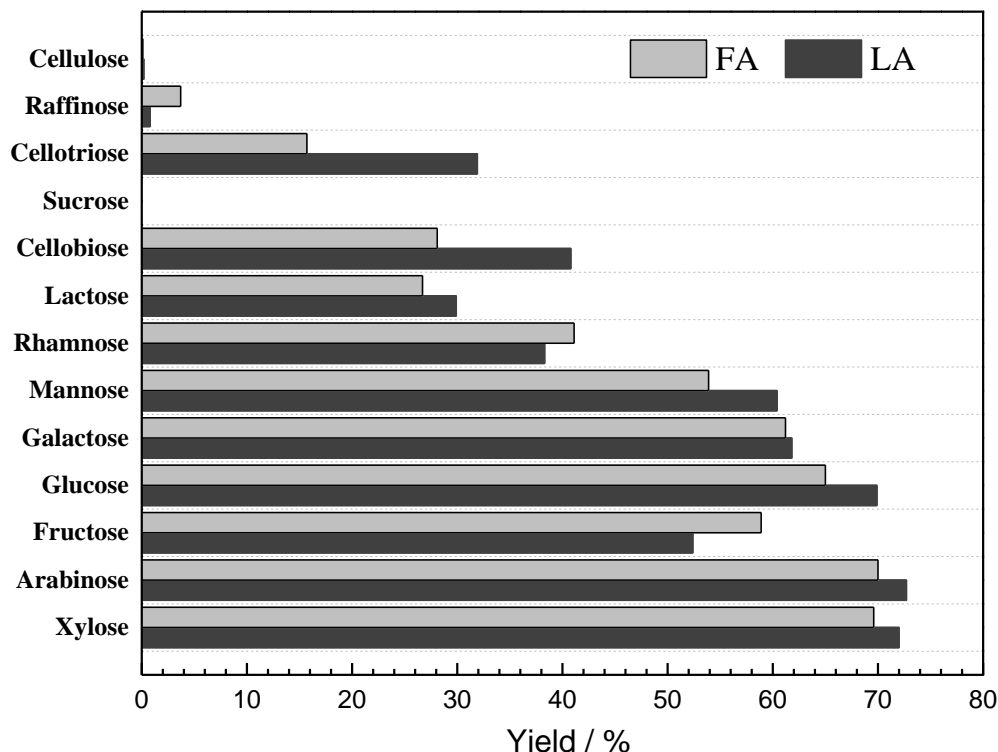
Figure 6. Viability of the catalytic process for various saccharides. Yields of LA (dark gray columns) and FA (light gray columns). *Reaction conditions for LA synthesis*: Saccharide (90 mg), Catalyst (1Cu-CTAB/MgO calcined at 773 K, 60 mg), 2.5M NaOH (1 mL), Water (5 mL), Autoclave, Ar (0.4 MPa), 393 K, 1 h, Stirring. *Reaction conditions for FA synthesis*: Saccharide (90 mg), Catalyst (0.3Cu-CTAB/MgO calcined at 773 K, 90 mg), 30% H_2O_2 (4 mmol), Water (5 mL), Autoclave, Ar (0.4 MPa), 393 K, 12 h, Stirring.

Catalyst characterization. In order to identify the actual phase of the catalyst and nature of copper species, PXRD patterns of the catalysts were measured (Figure 7). To understand the correlation of copper and MgO influenced by calcination temperature, the PXRD patterns for the Cu-CTAB/MgO catalyst calcined at various temperatures were obtained as in Figures 7a-f. The PXRD of CuO, Cu_2O, MgO and the surfactant CTAB are compacted as Figure 8. No reflections of the crystalline MgO was observed for the non-calcined Cu-CTAB/MgO or the Cu-CTAB/MgO
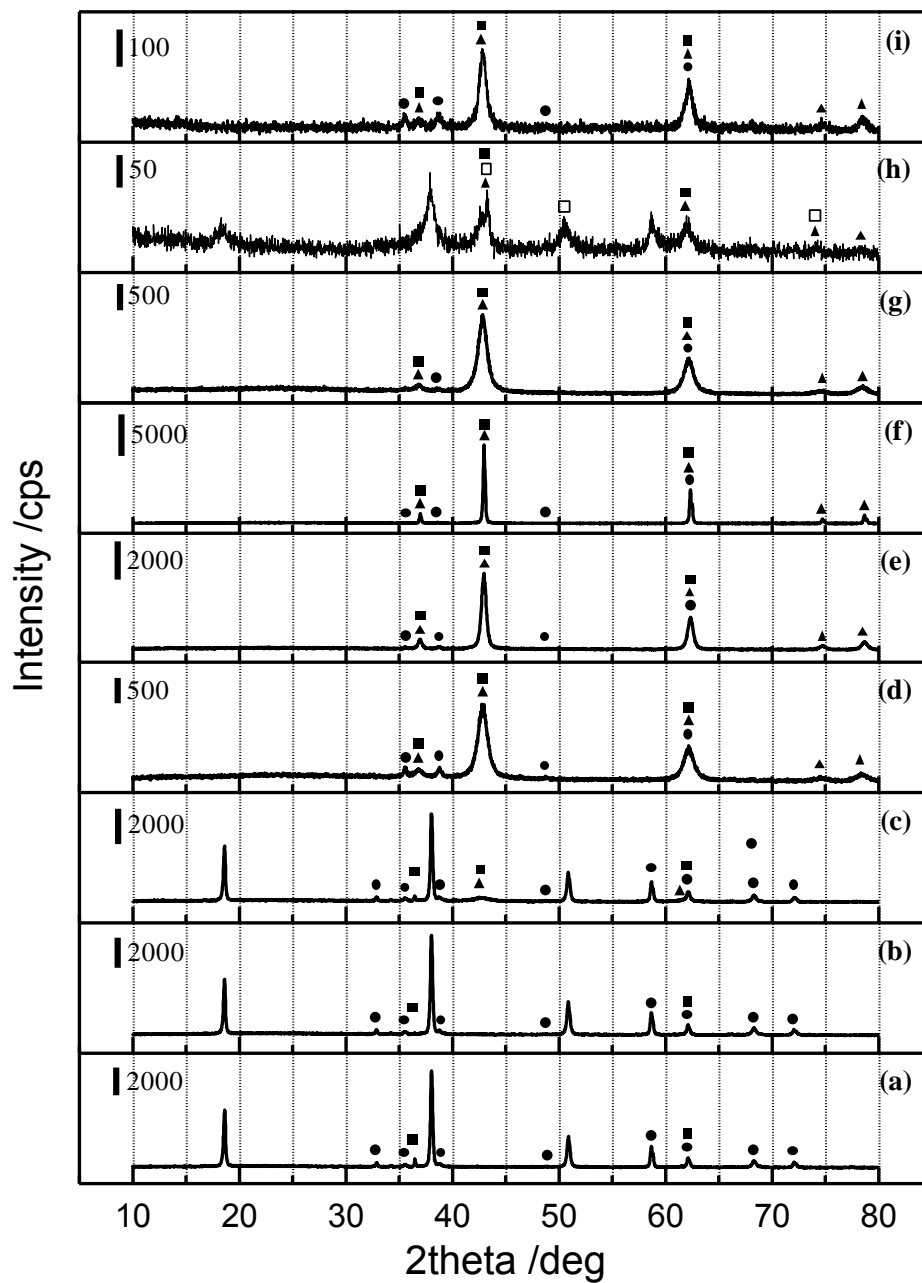
Figure 7. PXRD patterns of 1Cu-CTAB/MgO catalyst. The different species are shown as; CuO (closed circle, ●); Cu_2O (closed square, ■); Cu (open square, □); and MgO (closed triangle, ▲). (a) non-calcined Cu-CTAB/MgO; Cu-CTAB/MgO calcined at (b) 383 K, (c) 573 K, (d) 773 K, (e) 973 K and (f) 1173 K; (g) Cu/MgO calcined at 773 K; Cu-CTAB/MgO calcined at 773 K after (h) 1st use for LA synthesis from glucose, and (i) reactivation.

[51]
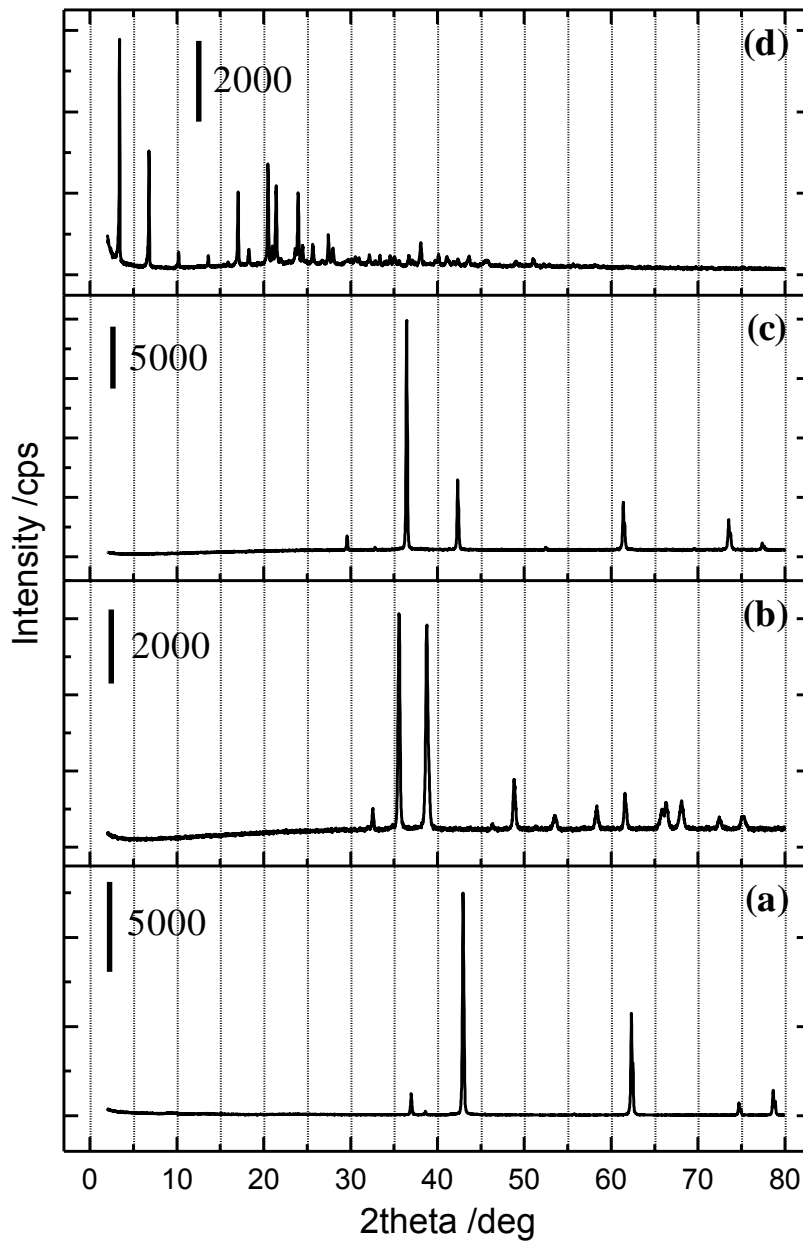
Figure 8. PXRD patterns of references. (a) MgO; (b) CuO; (c) Cu_2O; (d) CTAB.

calcined at lower temperatures of 383-573 K (Figure 7a-c); however, the crystalline MgO phase

becomes prominent with the increase in calcination temperature (Figure 7d-f). The oxide species

of copper forms the active constituent of the synthesized catalyst with a variable concentration of

both Cu_2O and CuO. Some unknown peaks at 2θ values of 19.1, 38.4, and 51.3 were observed for

low calcination temperatures which subsequently disappeared at higher temperatures. These peaks are assigned to the highly crystalline Cu-Mg spinel type (or mixed oxide) formed during the catalyst synthesis as obtained in a report by Nagaraja et al.[66] This could be the other reason for the absence of crystalline MgO in the PXRD patterns for the catalyst treated at lower temperatures. The peaks at 36.4° and 39.5° corresponding to the (002) and (200) plane of CuO revealed the presence of CuO crystallites for the catalyst calcined at 773 K (Figure 7d). Although some CTAB were decomposed at high calcination temperatures and formed copper clusters as observed by TEM images (Figure 3), XRD patterns of catalyst synthesized without CTAB (Cu/MgO) marked the absence of any signals corresponding to oxide phase of copper responsible for glucose conversion (Figure 7d,g). The absence of activity for such catalyst (37.2% yield for LA synthesis; see Table 2) and absence or low concentration of copper oxide species observed in the PXRD patterns establishes the crucial role of copper oxide species as the active species in the Cu-CTAB/MgO catalyst for organic acid productions from sugars. The copper catalysts were found to be durable and retain the active site on recalcination as revealed by PXRD patterns of fresh and used catalyst in LA synthesis (Figure 7d,h-i). The observed patterns were interesting as it was found that the catalyst after sugar conversion (Figure 7h) formed similar structural sites (spinel type or mixed oxide phase) as those observed for the non-calcined catalyst (Figure 7a) along with MgO phase. The peaks at 43.24° (111), 50.38° (200) and 74.28° (220), which were assigned to metallic copper (JCPDS; Cu: 04-0836), were observed after the reaction (Figure 7h). The active species were regenerated on recalcination of the catalyst (Figure 7i).

Studies by X-ray absorption spectroscopy also indicated that the oxidized state of copper was present on the fresh Cu-CTAB/MgO catalyst and which contributed to the catalytic activity for the

[53]
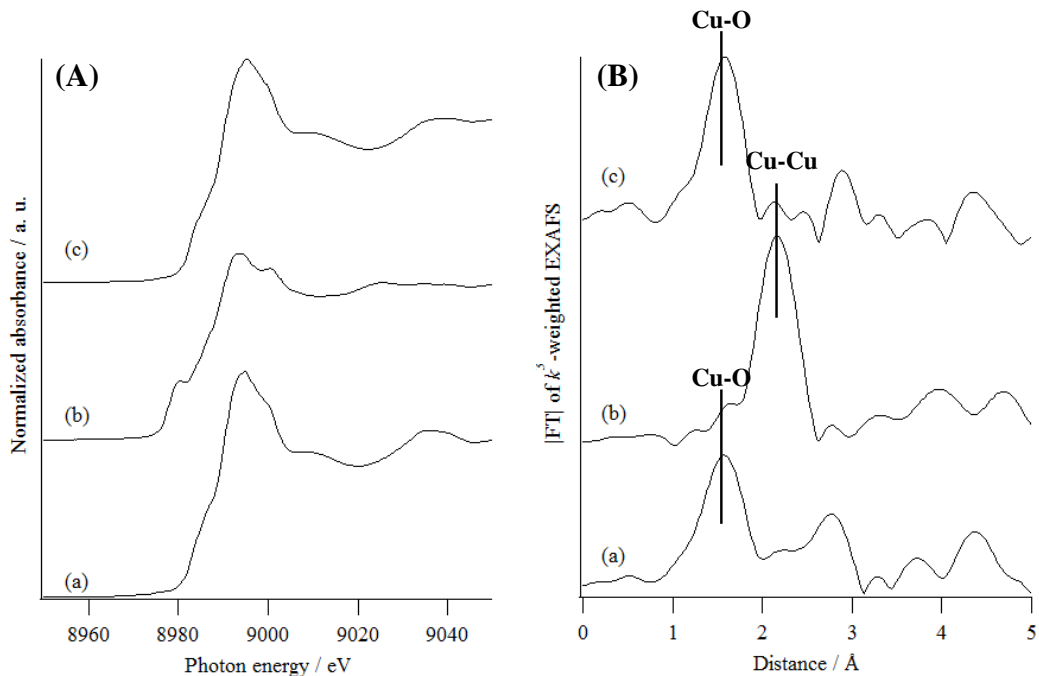
Figure 9. (A) X-ray absorption near edge structures and (B) Fourier transform (FT) of k^3-weighted extended X-ray absorption fine structure of 1Cu-CTAB/MgO after (a) calcination at 773 K, (b) 1st use for LA synthesis from glucose and (c) reactivation by calcination.
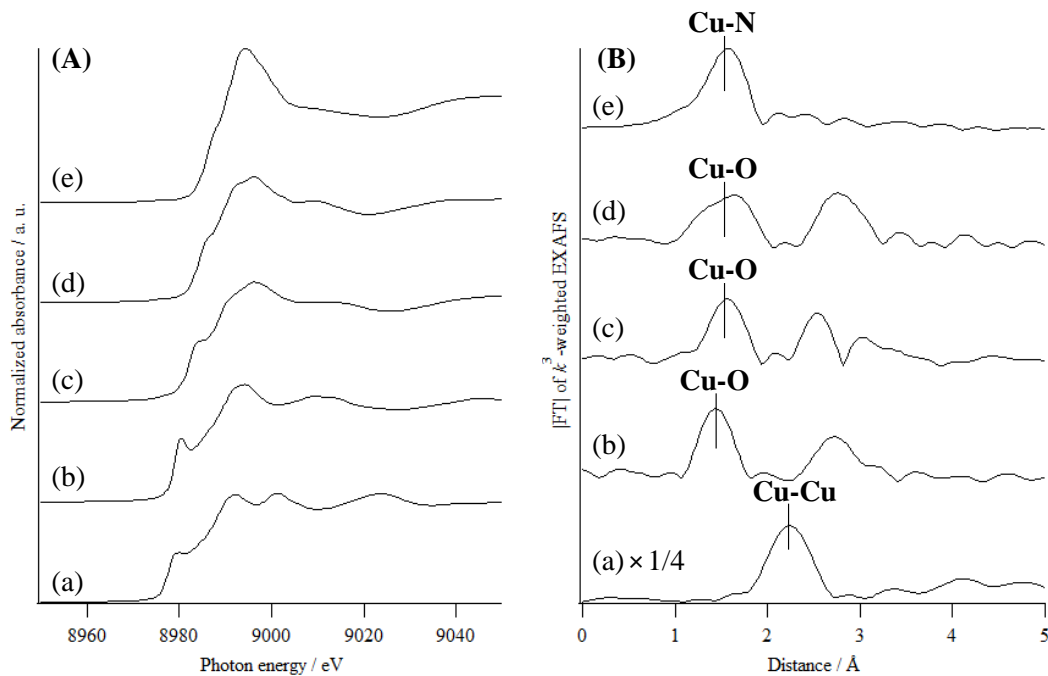
Figure 10. (A) X-ray absorption near edge structures and (B) Fourier transform (FT) of k^3-weighted extended X-ray absorption fine structure of references. (a) Cu foil, (b) Cu_2O, (c) CuO, (d) $Cu(OH)_2$ (e) $Cu(NO_3)_2$.

conversion of glucose, and reactivation treatment was effective for reproduction of such active Cu species (see Figures 9 and 10). It was supposed that CTAB strongly influenced the generation/regeneration of such active Cu species during calcination; that was still retained within the structure even after repeated treatment at 773 K (Figure 11).
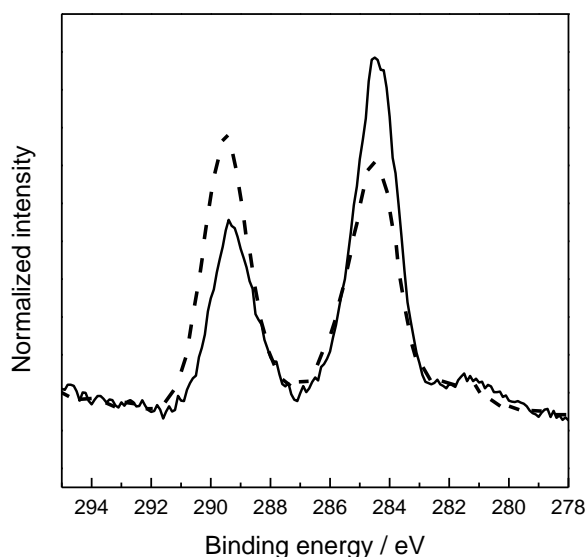
Figure 11. C1s XP spectra of 1Cu-CTAB/MgO calcined at 773 K (solid line) and reactivated at 773 K (dashed line). The peak at 284.5 was observed for carbon tape (used as reference).

The temperature programmed reduction using hydrogen gas (H_2-TPR) is a common tool adopted by various researchers to investigate the dispersion and/or redox behavior of copper catalyst.[67-70] For better understanding of the type of copper phase over MgO, H_2-TPR profiles were recorded for fresh catalysts (non-calcined 1Cu-CTAB/MgO, 1Cu-CTAB/MgO calcined at 573 K, 773 K and 973 K) and the used catalysts (1Cu-CTAB/MgO calcined at 773 K after 1st use for glucose to LA and Cu-CTAB/MgO calcined at 773 K after reactivation) for comparison of type of species and interactions in the catalyst. The presence of oxide species of copper on the catalyst was reflected in Figure 12. Most of the profiles exhibited at least two peaks, indicating the different

redox behavior of the present copper oxide species. Non-calcined Cu-CTAB/MgO had two peaks at 540 K with a shoulder at 570 K and 685 K. Cu-CTAB/MgO calcined at 573 K had a humped peak at similar position with a broader peak around at 540 K. Cu-CTAB/MgO calcined at 773 K displayed a different spectrum with two peaks at 585 K and 660 K. Similar trend was observed for catalyst calcined at 973 K which had a peak at 575 K and a shoulder at 620 K. This has been understood in general that the signals at lower temperatures are due to the easily reducible species in the sample whereas the signals at higher temperature values are hard to be reduced. According
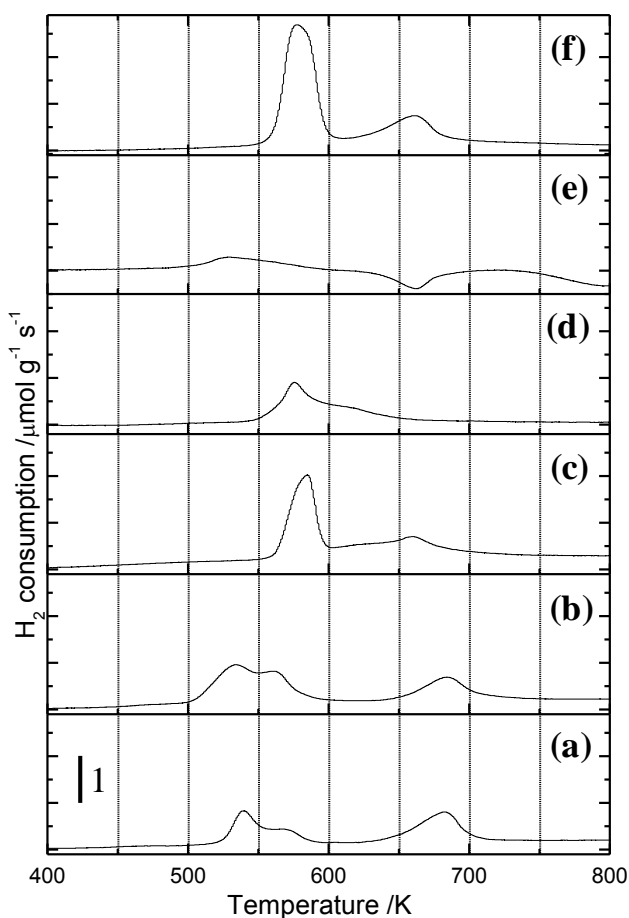
Figure 12. H_2-TPR profiles of fresh and used 1Cu-CTAB/MgO catalysts. (a) non-calcined Cu-CTAB/MgO; Cu-CTAB/MgO calcined at (b) 573 K, (c) 773 K and (d) 973 K; (e) Cu-CTAB/MgO calcined at 773 K after 1st use of glucose to LA; (f) Cu-CTAB/MgO calcined at 773 K after reactivation.

to the trend in Figure 12, it was concluded that with the increase of calcination temperature, the Cu species in the sample gradually transforms into a stable and single species which demands high temperature to be reduced. The peaks observed at 680 K were attributed to the spinel (or mixed oxide) type species, and could not be traced after calcination at higher temperatures as described by Nagaraja et al. for Cu/MgO-SSW type catalyst.[66] Such species are considered to be responsible for the unknown peaks in PXRD and TPR profiles at lower calcination temperatures.

From the TEM images of copper catalyst (Figure 3), I can identify the well dispersion of copper in non-calcined form, and thus they can be easily reduced. On the other hand, thecalcination at higher temperature induces strong interaction between metal and support making them hard to be reduced at lower temperatures. Some literatures suggested that the small CuO clusters and/or isolated ionic type copper can be reduced at lower temperatures than the larger CuO particles.[71] Thus, the peak above 550 K could be related to the reduction of the larger CuO particles. Various research groups have reported similar TPR profiles for different supported copper catalysts, and had demonstrated the effect of interaction between supports on the redox properties of copper oxide.[68-72] Interestingly, the H_2-TPR profile for the spent catalyst failed to notice any peak, that is spent catalyst did not consumed any H_2 gas (Figure 12e). Such observations suggested that the Cu oxide species present in the fresh catalyst was reduced into metal species during sugar transformation, indicating the reducing nature of the saccharides under the reaction conditions for LA synthesis. The result of H_2-TPR for Cu-CTAB/MgO calcined at 773 K after reactivation was more interesting as it unveiled the hidden Cu species in the catalyst (Figure 12f). Since the reduction of this reactivated catalyst required a higher H_2 consumption as compared to the fresh catalyst (Figure 12c). This in turn indicates that the fresh catalyst along with copper oxide species contained some copper metal species. After the reaction when the catalyst was reactivated at 773

[57]

K, all copper species turned into oxide species which needed increased amount of H_2 to be reduced to metallic state.

The PXRD and H_2-TPR studies portrayed the presence of unstable phases for the non-calcined and the catalyst calcined at 383 K and 573 K. The presence of unstable species in such catalyst (non-calcined and the catalyst calcined at 383 K and 573 K) is considered to be the reason of low activity. With further increase in calcination temperature (higher than 700 K), the MgO phase becomes more prominent and also crystallinity of the catalyst is increased, diminishing the catalytic activity. The H_2-TPR studies as discussed above, hints about the presence of easily reducible Cu species in the non-calcined or the catalyst calcined at lower temperatures. Also, the loaded metal species was reduced after the reaction, in accordance with the report by other research groups.[56,61] In general, easily reducible Cu species should be more active for such glucose transformation; however, in the present case due to the presence of both oxide and spinel type (or mixed oxide) phase diminishes the amount of easily accessible copper species for the substrate leading to a low activity for non-calcined Cu-CTAB/MgO (Figure 2). Cu-CTAB/MgO calcined at 773 K was found to be the most active catalyst with copper oxide interacting strongly with MgO as depicted from N_2 adsorption isotherm. Table 4 enlists the specific surface area (S_{BET}), pore volume (V_p), and pore radius (r_p) of copper catalyst utilized for the saccharide conversion. The adsorption-desorption isotherm for the various synthesized catalysts are given in Figure 13. A general trend of low surface area was observed for calcined support to that of non-calcined support, for example, the S_{BET} for MgO was 18.7 $m^2\,g^{-1}$ as compared to 13.4 $m^2\,g^{-1}$ for the calcined MgO. Among all catalyst, it was observed that relatively strong interaction (type VI) between the support and the N_2 exists for the catalyst calcined at 773 K and 973 K. After the hydrothermal synthesis of catalyst, the surface area of the sample decreases from its parent source (MgO) which gradually

increases with calcining temperature reaching maxima at 773 K. The maximum surface area of 134.6 m² g⁻¹ was found for Cu-CTAB/MgO catalyst calcined at 773 K.

Table 4. N$_2$ adsorption data of support and catalyst

Entry	Catalysts	Cal. Temp. /K	S_{BET}/m^2 g^{-1a}	V_p/cm^3 g^{-1b}	r_p/nm^b	Isotherm
1	1Cu-CTAB/MgO	None	2.3	0.07	14.1	III
2		383	5.6	0.06	14.1	III
3		573	22.1	0.11	1.2	II, III
4		773	134.6	0.36	2.1	VI
5		973	45.1	0.27	8.1	VI
6		1173	7.6	0.11	22.1	III
7	MgO	None	18.7	0.16	2.1	III
8		773	13.4	0.01	53.0	III

[a]Analyzed by BET method. [b]Calculated by BJH method.
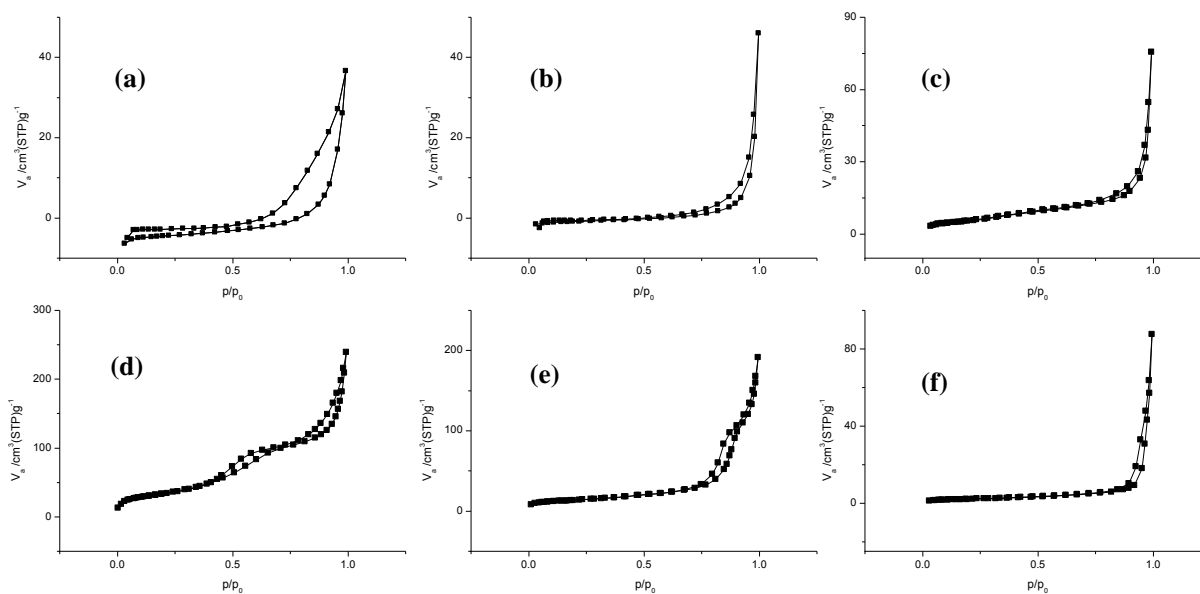
Figure 13. The adsorption–desorption isotherm of 1Cu-CTAB/MgO catalyst. (a) non-calcined Cu-CTAB/MgO; Cu-CTAB/MgO calcined at (b) 383 K, (c) 573 K, (d) 773 K, (e) 973 K and (f) 1173 K.

Mechanistic considerations. Various research group have proposed the mechanistic pathways for organic acids production from sugars under hydrothermal conditions.[47,54,56,60,63] Recently, the role of copper has also been studied for the deconstruction of sugars by Mariani et al.[61] A general reaction progress of LA synthesis affords various intermediates or by-products like GlycAld, GlycA, AA, GlcoA, DHA, PAL, and FA (see Table 1). A careful and minute analysis of experimental evidences, helped in proposing a plausible mechanistic pathway as Scheme 2 for glucose conversion to LA.

At the initial stages, the alkali and/or the catalyst dissect the sugars to GlycAld and DHA. An equilibrium exists between GlycAld and DHA *via* 1,2,3-propenetriol. Under the present reaction conditions, I could not detect DHA at any stage of the reaction, indicating the shift of keto-enol tautomerism towards GlycAld, which was observed along with GlycA. The next intermediate candidate is PAL by dehydration and rearrangement of GlycAld, which thereafter undergoes a methyl shift to generate LA.[60] However, no PAL was observed in the presence of copper catalyst under our reaction conditions. Additionally, HPLC chromatogram of reactions in the absence of copper catalyst shows trace amount of PAL. The minimal amount of PAL hints about the conversion of GlycAld to PAL as rate-determining step.[30,73]

Combined experiments were conducted to account for the absence of PAL under the reaction conditions. Cu-CTAB/MgO catalyst calcined at 773 K was stirred with an aqueous solution of PAL in D_2O at room temperature for 1 h (set A). As a control experiment, an aqueous solution of PAL in D_2O (set B) and Cu-CTAB/MgO catalyst calcined at 773 K in D_2O (set C) were also stirred in two separate vials at room temperature for 1 h. After the stipulated time, catalyst was isolated from set A and C by centrifugation and dried at room temperature. The NMR spectra was recorded for the filtrates (obtained from set A and C) and reaction mixture of set B. The signals in ^{1}H-NMR
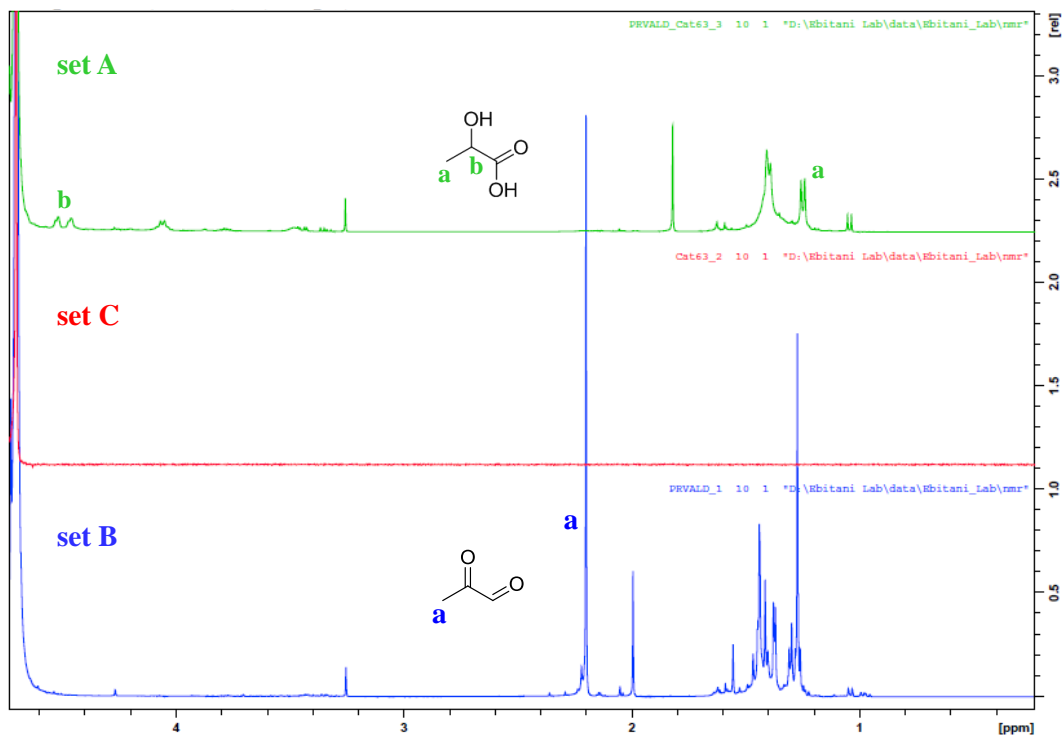
Figure 14. ^{1}H-NMR spectra of set B and filtrates from set A and C.
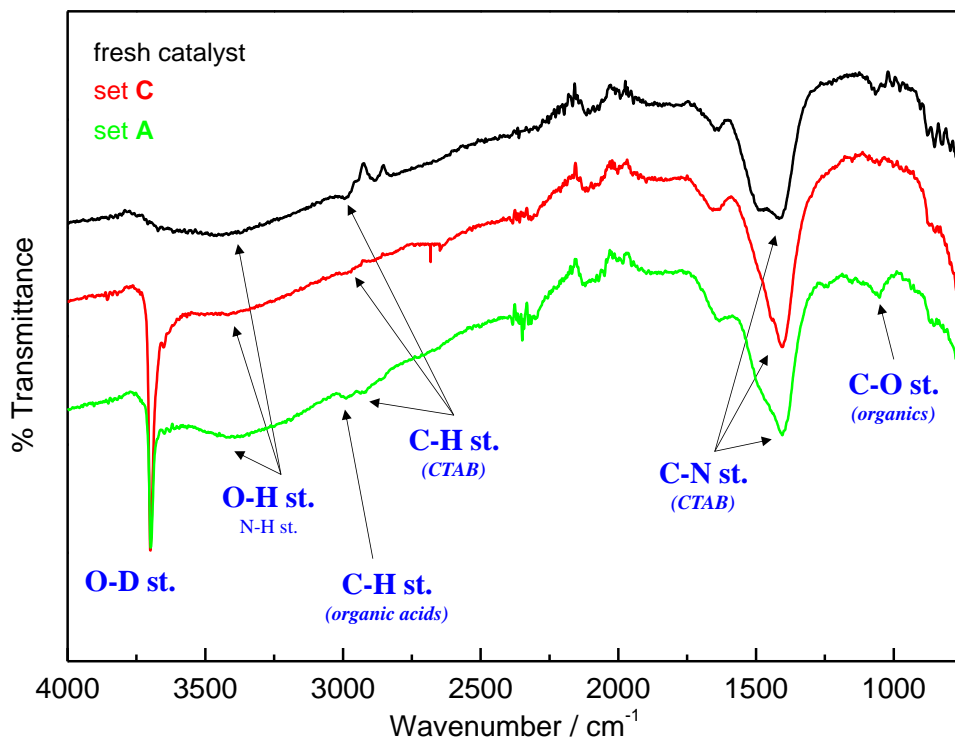
Figure 15. Infrared spectra of fresh catalyst and catalysts isolated from set A and C.
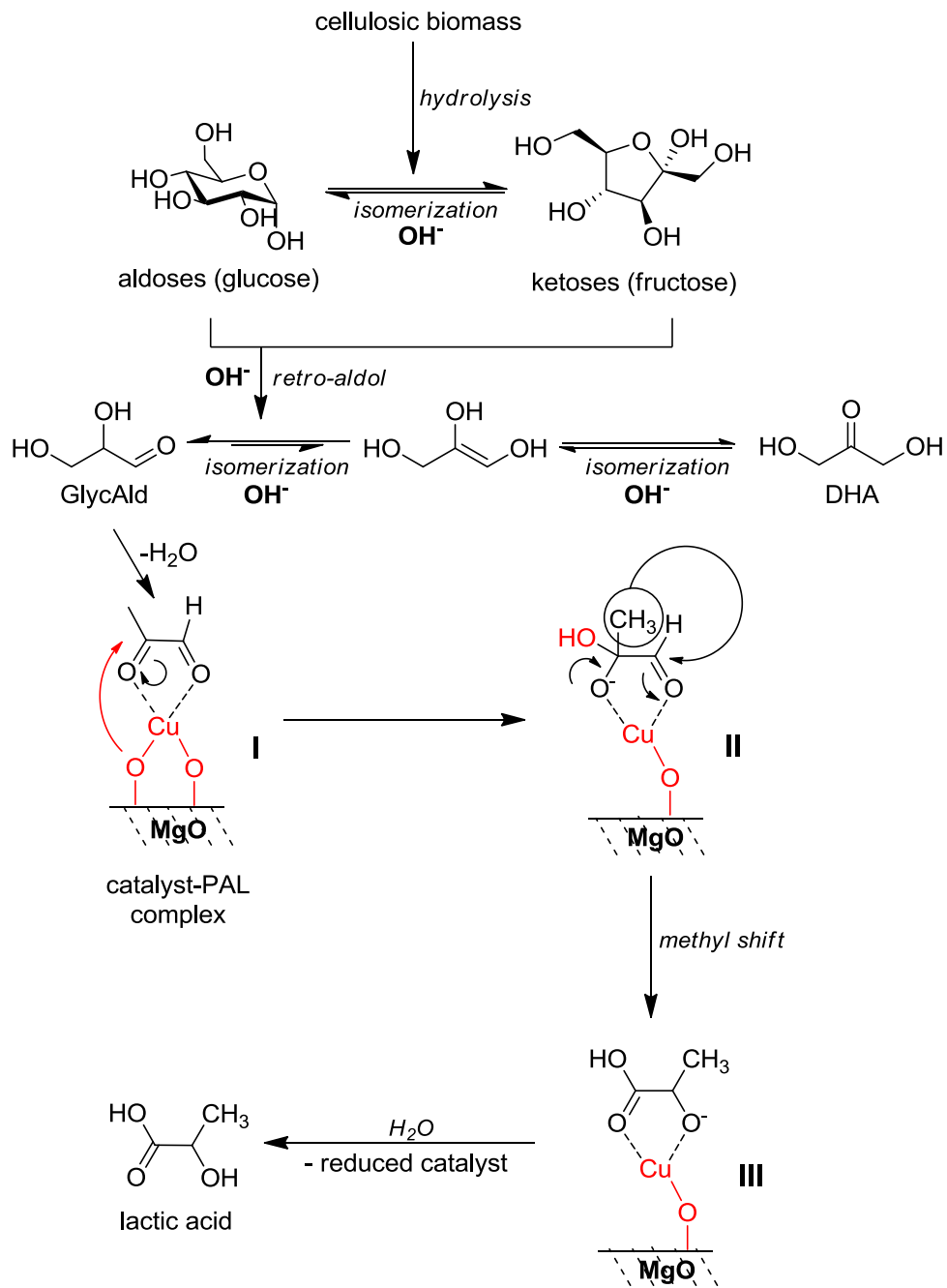
Scheme 2. Proposed Cu-catalyzed pathway for glucose conversion to LA in the presence of alkali.

spectra (Figure 14) demonstrated the absence of PAL in the filtrate of set A and marked the presence of LA. On contrary, the PAL could be clearly observed in the reaction mixture of set B. No signals other than residual solvent were observed for the filtrate of set C. Also, the IR spectra

were recorded for the fresh catalyst (Cu-CTAB/MgO calcined at 773 K) and catalyst isolated from set A and set C. The IR spectra hinted the presence of adsorbed organics on the catalyst from set A (Figure 15). The adsorption of PAL onto the catalyst surface and formation of a catalyst-PAL complex (**I**, Scheme 2) might be responsible for such observations. Further, the HPLC analysis of experiments conducted using PAL and DHA as substrate with Cu-CTAB/MgO catalyst calcined at 773 K in aqueous media at room temperature verified the formation of LA (44% yield) exclusively from PAL.

The hydrothermally loaded copper oxide species has strong interaction with support (concluded from H_2-TPR) which prevents the formation of free cationic copper as reported by Wang et al.[56] The attack of the bind oxygen atom of Cu-O-Mg from catalyst (indicated by red arrow) on the carbonyl carbon may generate **II**. The formation step of **II** generates a reduced Cu species as found by characterization data for the spent catalyst. Following this step, the back donation of electrons from oxygen atom forces methyl group to migrate to nearest carbon to produce **III**. The hydrolysis of such complexes yields free LA, representing the role of water as solvent. Since no free cationic species is generated, the reason of no leaching of catalyst was addressed.

The oxidative mechanism for FA formation from sugars are proposed in accordance to the report by Jin et al. assuming a direct oxidation pathway; where six moles of FA are produced per mole of glucose.[74] This mechanism supports the formation of FA in higher yields with increasing amount of 30% H_2O_2 as discussed above.[75] The copper loaded catalyst not only influences the FA yield but also has substantial effect in activation of 30% H_2O_2 for the oxidation of sugars. Therefore, the use of large amount of catalyst increases the dissociation of H_2O_2 that increases the FA yield (Table 3, entry 8).

4. CONCLUSIONS

In conclusion, hydrothermally loaded copper oxide species on magnesia with CTAB agent (Cu-CTAB/MgO) acts as stable heterogeneous catalyst which could afford high yields of LA and FA under milder reaction conditions. Use of 1Cu-CTAB/MgO along with NaOH (2.5M, 1 mL) sustained 70% LA yield from glucose at 393 K for 1 h in water solvent. I also found that 0.3Cu-CATB/MgO catalyst in the presence of aqueous 30% H_2O_2 furnished 65% FA yields from glucose at 393 K after 12 h. Such catalytic system possessed advantages of high yields, lower energy input, recyclability of the catalyst and wide scope for various sugars. The characterization of prepared catalyst revealed the effect of calcination on the nature of species on the catalyst. The high selectivity of LA in the presence of copper catalyst was accounted by proposing a plausible mechanism.

These advantages of the above discussed process seem to have promising potential for bio-refinery and future sustainability. In future the catalyst will be finely adapted to ensure conversion of polysaccharides and real biomass like municipal wastes with high carbon balance. Further investigation of the catalyst and the reaction analysis are also needed to propose a suitable mechanism for FA formation. To my belief, such high efficiencies for alkaline sugar conversion under milder conditions into LA and FA are reported for the first time.

REFERENCES

1. A. Corma, S. Iborra, A. Velty, *Chem. Rev.* **2007**, *107*, 2411.

2. D. M. Alonso, S. G. Wettstein, J. A. Dumesic, *Chem. Soc. Rev.* **2012**, *41*, 8075.

3. H. Kobayashi, A. Fukuoka, *Green Chem.* **2013**, *15*, 1740.

4. Y. Nakagawa, M. Tamura, K. Tomishige, *ACS Catal.* **2013**, *3*, 2655.

5. J. C. Serrano-Ruiz, R. Luque, A. Sepulveda-Escribano, *Chem. Soc. Rev.* **2011**, *40*, 5266.

6. P. Y. Dapsens, C. Mondelli, J. Perez-Ramirez, *ACS Catal.* **2012**, *2*, 1487.

7. A. Takagaki, S. Nishimura, K. Ebitani, *Catal. Surv. Asia* **2012**, *16*, 164.

8. M. Bicker, J. Hirth, H. Vogel, *Green Chem.* **2003**, *5*, 280.

9. A. Takagaki, M. Ohara, S. Nishimura, K. Ebitani, *Chem. Commun.* **2009**, *45*, 6276.

10. T. Stahlberg, W. Fu, J.M. Woodley, A. Riisager, *ChemSusChem* **2011**, *4*, 451.

11. J. Tuteja, S. Nishimura, K. Ebitani, *Bull. Chem. Soc. Jpn.* **2012**, *85*, 275.

12. I. -J. Kuo, N. Suzuki, Y. Yamauchi, K. C-W. Wu, *RSC Adv.* **2013**, *3*, 2028.

13. I. Jimenez-Morales, A. Teckchandani-Ortiz, J. Santamaria-Gonzalez, P. Maireles-Torres, A. Jimenez-Lopez, *Appl. Catal. B* **2014**, *144*, 22.

14. M. Chidambaram, A.T. Bell, *Green Chem.* **2010**, *12*, 1253.

15. Y. Zu, P. Yang, J. Wang, X. Liu, J. Ren, G. Lu, Y. Wang, *Appl. Catal. B* **2014**, *146*, 244.

16. S. Nishimura, N. Ikeda, K. Ebitani, *Catal. Today* **2014**, *232*, 89.

17. G. A. Halliday, R. J. Young Jr., V. V. Grushin, *Org. Lett.* **2003**, *5*, 2003.

18. A. Takagaki, M. Takahashi, S. Nishimura, K. Ebitani, *ACS Catal.* **2011**, *1*, 1562.

19. G. D. Yadav, R. V. Sharma, *Appl. Catal. B* **2014**, *147*, 293.

20. C. Delhomme, D. Weuster-Botz, F. E. Kühn, *Green Chem.* **2009**, *11*, 13.

21. H. Choudhary, S. Nishimura, K. Ebitani, *Chem. Lett.* **2012**, *41*, 409.

22. H. Choudhary, S. Nishimura, K. Ebitani, *Appl. Catal. A* **2013**, *458*, 55.

23. R. Weingarten, J. Cho, R. Xing, W. C. Corner Jr., G. W. Huber, *ChemSusChem* **2012**, *5*, 1280.

24. P. A. Son, S. Nishimura, K. Ebitani, *React. Kinet. Mech. Catal.* **2012**, *106*, 185.

25. M. J. Climent, A. Corma, S. B. A. Hamid, S. Iborra, M. Mifsud, *Green Chem.* **2006**, *8*, 524.

26. T. Miyake, T. Makino, S. Taniguchi, H. Watanuki, T. Niki, S. Shimizu, Y. Kojima, M. Sano, *Appl. Catal. A* **2009**, *364*, 108.

27. E. J. Steen, Y. Kang, G. Bokinsky, Z. Hu, A. Schirmer, A. McClure, S. B. del Cardayre, J. D. Keasling, *Nature* **2010**, *463*, 559.

28. M. S. Holm, S. Saravanamurugan, E. Taarning, *Science* **2010**, *328*, 602.

29. F. Chambon, F. Rataboul, C. Pinel, A. Cabiac, E. Guillon, N. Essayem, *Appl. Catal. B* **2011**, *105*, 171.

30. F. Clippel, M. Dusselier, R. V. Rompaey, P. Vanelderen, J. Dijkmans, E. Makshina, L. Giebeler, S. Oswald, G. V. Baron, J. F. M. Denayer, P. P. Pescarmona, P. A. Jacobs, B. F. Sels, *J. Am. Chem. Soc.* **2012**, *134*, 10089.

31. D. Tongsakul, S. Nishimura, K. Ebitani, *ACS Catal.* **2013**, *3*, 2199.

32. R. K. P. Purushothaman, J. van Haveren, D. D. van Es, I. Melian-Cabrera, J. D. Meeldijk, H. J. Heeres, *Appl. Catal. B* **2014**, *147*, 92.

33. G. -Q. Chen, M. K. Patel, *Chem. Rev.* **2012**, *112*, 2082.

34. F. A. C. Martinez, E. M. Balciunas, J. M. Salgado, J. M. D. Gonzalez, A. Converti, R. P. S. Oliveira, *Trends Food Sci. Tech.* **2013**, *30*, 70.

35. A. Boddien, D. Mellmann, F. Gartner, R. Jackstell, H. Junge, P. Dyson, G. Laurenczy, R. Ludwig, M. Beller, *Science* **2011**, *333*, 1733.

36. Q. -Y. Bi, X. -L. Du, Y. -M. Liu, Y. Cao, K. -N. He, K. -N. Fan, *J. Am. Chem. Soc.* **2012**, *134*, 8926.

37. M. Grasemann, G. Laurenczy, *Energy Environ. Sci.* **2012**, *5*, 8171.

38. J. Tuteja, H. Choudhary, S. Nishimura, K. Ebitani, *ChemSusChem* **2014**, *7*, 96.

39. P. A. Son, S. Nishimura, K. Ebitani, *RSC Adv.* **2014**, *4*, 10525.

40. R. P. John, K. M. Nampoothiri, A. Pandey, *Appl. Microbiol. Biotechnol.* **2007**, *74*, 524.

41. K. Okano, T. Tanaka, C. Ogino, H. Fukuda, A. Kondo, *Appl. Microbiol. Biotechnol.* **2010**, *85*, 413.

42. E. J. Ordal, H. O. Halvorson, *J. Bacteriol.* **1939**, *38*, 199.

43. S. P. Chahal, Lactic Acid in Ullmann's Encyclopedia of Industrial Chemistry, Wiley-VCH Verlag GmbH & Co, Germany, **2000**, pp. 11-19.

44. W. Reutemann, H. Kieczka, Formic Acid in Ullmann's Encyclopedia of Industrial Chemistry, Wiley-VCH Verlag GmbH & Co, Germany, **2011**, pp. 49-70.

45. S. K. Hoekman, A. Broch, C. Robbins, *Energy Fuels* **2011**, *25*, 1802.

46. P. A. Shaffer, T. E. Friedemann, *J. Biol. Chem.* **1930**, *86*, 345.

47. H. Kishida, F. Jin, X. Yan, T. Moriya, H. Enomoto, *Carbohydr. Res.* **2006**, *341*, 2619.

48. X. Yan, F. Jin, K. Tohji, A. Kishita, H. Enomoto, *AIChE J.* **2010**, *56*, 2727.

49. D. Esposito, M. Antonietti, *ChemSusChem* **2013**, *6*, 989.

50. P. Gao, G. Li, F. Yang, X. -N. Lv, H. Fan, L. Meng, X. -Q. Yu, *Ind. Crops Prod.* **2013**, *48*, 61.

51. F. Jin, J. Yun, G. Li, A. Kishita, K. Tohji, H. Enomoto, *Green Chem.* **2008**, *10*, 612.

52. A. Onda, T. Ochi, K. Kajiyoshi, K. Yanagisawa, *Catal. Commun.* **2008**, *9*, 1050.

53. S. Zhang, F. Jin, J. Hu, Z. Huo, *Bioresour. Technol.* **2011**, *102*, 1998.

54. M. Bicker, S. Endres, L. Ott, H. Vogel, *J. Mol. Catal. A* **2005**, *239*, 151.

55. L. Kong, G. Li, H. Wang, W. He, F. Ling, *J. Chem. Technol. Biotechnol.* **2008**, *83*, 383.

56. Y. Wang, F. Jin, M. Sasaki, Wahyudiono, F. Wang, Z. Jing, M. Goto, *AIChE J.* **2013**, *59*, 2096.

57. M. Tada, R. Bal, X. Mu, R. Coquet, S. Namba, Y. Iwasawa, *Chem. Commun.* **2007**, *44*, 4689.

58. B. Sarkar, P. Prajapati, R. Tiwari, R. Tiwari, S. Ghosh, S.S. Acharyya, C. Pendem, R.K. Singha, L.N.S. Konathala, J. Kumar, T. Sasaki, R. Bal, *Green Chem.* **2012**, *14*, 2600.

59. S. S. Acharyya, S. Ghosh, R. Bal, *ACS Sustainable Chem. Eng.* **2014**, *2*, 584.

60. A. V. Ellis, M. A. Wilson, *J. Org. Chem.* **2002**, *67*, 8469.

61. M. Mariani, F. Zaccheria, R. Psaro, N. Ravasio, *Catal. Commun.* **2014**, *44*, 19.

62. A. T. Quitain, M. Faisal, K. Kang, H. Daimon, K. Fujie, J. Hazard. Mater. **2002**, 93, 209.

63. F. Jin, H. Enomoto, *Energy Environ. Sci.* **2011**, *4*, 382.

64. N. Akiya, P. E. Savage, *AIChE J.* **1998**, *44*, 405.

65. J. Yu, P. E. Savage, *Ind. Eng. Chem. Res.* **1998**, *37*, 2.

66. B. M. Nagaraja, V. S. Kumar, V. Shashikala, A. H. Padmasri, S. S. Reddy, B. D. Raju, K. S. R. Rao, *J. Mol. Catal. A* **2004**, *223*, 339.

67. H. -P. Wang, C. -T. Yeh, *J. Chinese Chem. Soc.* **1983**, *30*, 139.

68. L. Kundakovic, M. -F. Stephanopoulos, *Appl. Catal. A* **1998**, *171*, 13.

69. M. Vijayaraj, C. S. Gopinath, *J. Catal.* **2006**, *241*, 83.

70. S. Nishimura, T. Shishido, J. Ohyama, K. Teramura, A. Takagaki, T. Tanaka, K. Ebitani, *Catal. Sci. Technol.* **2012**, *2*, 1685.

71. R. Rajeev, K. A. Devi, A. Abraham, K. Krishnan, T. E. Krishnan, K. N. Ninan, C. G. R. Nair, *Thermochim. Acta.* **1995**, *254*, 235.

72. E. Moretti, M. Lenarda, L. Storaro, A. Talon, T. Montanari, G. Busca, E. Rodriguez, A. Jimeenez, M. Turco, G. Bagnasco, *Appl. Catal. A* **2008**, *335*, 46.

73. C. B. Rasendra, B. A. Fachri, I. Gusti, B. N. Makertihartha, S. Adisasmito, H. J. Heeres, *ChemSusChem* **2011**, 4, 768.

74. F. Jin, Z. Zhou, T. Moriya, H. Kishida, H. Higashijima, H. Enomoto, *Environ. Sci. Technol.* **2005**, *39*, 1893.

75. For FA production mechanism from glucose in the presence of H_2O_2, see; H.S. Isbell, R.G. Naves, *Carbohydr. Res.* **1974**, *36*, C1.

Chapter 2

Controlled growth of various species of copper oxides on magnesia using surfactants under hydrothermal conditions

ABSTRACT

In the event of designing advanced materials and devices, the controlled synthesis of materials in a facile way is gaining interest. Herein, I developed a convenient surfactant-mediated hydrothermal approach to control supported copper oxide species in a reproducible way. The catalytic activity for the upgradation of glucose to lactic acid (LA) were investigated to afforded 70% LA yield. The careful characterization using XRD, Raman and TPR studies revealed the paramelaconite (or Cu_4O_3) phase on MgO as the catalytically active species. Also, I found that cuprite phase can be prepared in the presence of DDAO while the tenorite phase was obtained as the dominant phase in the absence of surfactant after the hydrothermal treatment. The use of CTAB selectively afforded paramelaconite phase as the supported species. The systematic approach to control the supported species, in this chapter, demonstrates that a substantial improvement in the catalytic activity (or other properties) can be achieved by careful control of the surface species through a simple and inexpensive preparation route.

1. INTRODUCTION

The recent research interest in the synthesis and characterization of advanced materials for a wide variety of applications has resulted in the development of various new potent materials, for instance organic-inorganic hybrid molecules for methane storage or the inorganic mixed oxides as photocatalyst for the oxidation of water.[1-2] Inorganic nanocrystals has gained interest because of their potential applications in biology, electronics and other.[3] Also, the use of nanoscale building units were fruitful in achieving the advanced materials,[4] with control of size and shapes of colloidal inorganic nanocrystals. The properties of these inorganic crystals were observed to vary with their size, shape and crystallinity and thereby it becomes essential to control them. In recent years, rigorous and excellent studies have been carried out to control the morphology of the materials at nanoscale using wet chemical synthetic route.[5-6] Organic ligands such as polymers or surfactants were used as capping agents to effectively control the shape and size of these nanocrystals. For instance, the preparation of wide range of shapes were simply achieved by the mere variation of synthetic parameters such as surfactant composition, etc.[7] The surface atoms such as capping agents not only control the growth of nanocrystals in specified geometry, but also contribute to the thermodynamic characteristics and determine the structural transitions.[8-9] The surface energies of the capped particles are lower than that of the bare particles, which prevent them from agglomeration.

One of the most important transition metal oxides, considering the wide applicability and environmental friendliness, is the oxides of copper. The oxides of copper has been explored for wider applications in superconductors,[10] gas sensors,[11] and as catalysts for water-gas shift reaction,[12] steam reforming[13] or CO oxidation[14]. The three kinds of copper oxides are known to
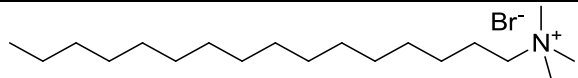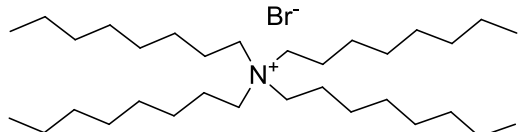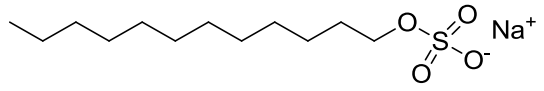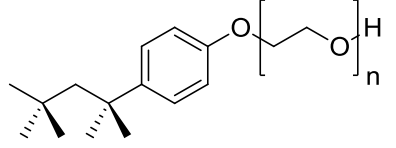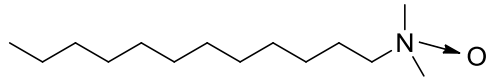
exist naturally; CuO (tenorite), Cu_2O (cuprite) and Cu_4O_3 (paramelaconite) with monoclinic, cubic and tetragonal crystal structures.[15-18] Paramelaconite (Cu_4O_3) is an intermediate oxide of copper between Cu_2O and CuO (the two typically known oxides of copper), and is commonly written as $Cu^+_2Cu^{2+}_2O_3$.[18-20] According to the thermodynamics, the oxidation states of copper are known to vary as a function of temperature and oxygen partial pressure.[21-22]

The catalysis over copper oxide have been suggested to be significantly influenced by the surface states and defects.[23] Consequently, a range of successful reports exist for the successful formation of supported or unsupported copper oxides with different morphologies.[24-26] Since the composition of oxides can affect the surface states and defects and there by the catalytic properties, methods for manipulating these factors should be found. However, to the best of my knowledge, till date there has been no successful attempt for a controlled synthesis of supported copper oxide species. In this chapter, I have developed a facile surfactant-mediated method to control the surface copper oxide species under hydrothermal conditions. The copper catalysts were prepared in the presence of different surfactants to investigate their catalytic activities for the chemical upgradation of glucose to lactic acid (LA). This study is believed to open up new pathways for the controlled synthesis of desired phases of various metal oxide nanocrystals.

2. EXPERIMENTAL SECTION

Catalyst preparation. All reagents were used as obtained from the respective manufacturers. All surfactant treated/non-treated copper supported on magnesia catalysts (denoted as Cu-surfactant/MgO) have been synthesized by a hydrothermal method as described by me previously[27]. Various surfactants (see Table 1) such as cetyltrimethylammonium bromide (CTAB, cationic

Table 1. Surfactants and their structures

Entry	Surfactant	Nature	Structure
1	Cetyltrimethylammonium bromide (CTAB)	Cationic	
2	Tetraoctylammonium bromide (TOAB)	Cationic	
3	Sodium dodecyl sulphate (SDS)	Anionic	
4	Triton X 100 (TX100)	Non-ionic	
5	*N,N*-dimethyldodecylamine *N*-oxide (DDAO)	Non-ionic	

surfactant, Wako), tetraoctylammonium bromide (TOAB, cationic surfactant, Wako), sodium dodecyl sulfate (SDS, anionic surfactant, Sigma-Aldrich), *N,N*-dimethyldodecylamine *N*-oxide (DDAO, non-ionic surfactant, Sigma-Aldrich) and Triton X-100 (TX-100, non-ionic surfactant, TCI) were employed in the current study. In general, magnesium oxide (MgO, Kanto; 1 g) was dispersed in deionized water (20 mL), and then copper nitrate (Cu(NO$_3$)$_2$·6H$_2$O, Wako, 1 mmol) in 5 mL deionized water was added drop-wise into the solution under vigorous stirring. To this mixture, surfactant (0.5 mmol) was added, and vigorously stirred for 3 h. The obtained mixture was sealed in a 100 mL Teflon lined autoclave, and heated to 453 K at a heating rate of 6 K min^{-1} in an oven, and maintained at the same temperature for 24 h. The oven was allowed to cool slowly to room temperature. The obtained solid was washed with deionized water till the pH of filtrate became neutral, followed by washing with ethanol before drying *in vacuo* overnight at room temperature. The dried materials were grained and calcined at 773 K (ramp-rate of 10 K min^{-1}) for 6 h in air. Similarly, copper catalyst were also synthesized in the absence of surfactant (denoted as Cu-None/MgO).

Catalytic testing. All experiments to test the catalytic activity were performed in a 50 mL Teflon lined autoclave. The catalytic activity was evaluated for glucose conversion into lactic acid (LA, Sigma-Aldrich) in aqueous media. In a general reaction procedure, D-(+)-glucose (Wako, 0.5 mmol) was dissolved in 5 mL deionized water and copper catalyst was added to the solution followed by the addition of 1 mL of 2.5 M sodium hydroxide (NaOH, Kanto) solution. The reaction mixture purged with Ar (0.4 MPa) in a sealed autoclave were allowed to react at 413 K for 1 h with continuous magnetic stirring. After the reaction, a part of the resultant solution was diluted up to 20 times with 10 mM H$_2$SO$_4$ (Kanto) and was filtered using a Milex®-LG 0.20 μm. The obtained filtrate was analyzed by high performance liquid chromatography (HPLC, WATERS

[75]

600) using an Aminex HPX-87H column (Bio-Rad Laboratories, Inc.) attached to a refractive index detector. An aqueous 10 mM H_2SO_4 (as mobile phase) was run through the column (maintained at 323 K) at a flow rate of 0.5 mL min^{-1}. The conversion and yield(s) were determined with a calibration curve method by the equations shown below.

Calculation. The substrate conversion, product yields and carbon mass balance were calculated using the equations shown here.

$$\% \text{ Conversion} = 100 - \left\{ \left(\frac{Amount\ of\ glucose\ detected\ (in\ mmol)}{Amount\ of\ glucose\ used\ (in\ mmol)} \right) \times 100 \right\}$$

$$\% \text{ Yield} = \left\{ \left(\frac{Amount\ of\ product\ detected\ (in\ mmol) \times Number\ of\ carbon\ n\ the\ product}{Amount\ of\ glucose\ used\ (in\ mmol) \times 6} \right) \times 100 \right\}$$

$$\% \text{ Carbon balance} = \left\{ \left(\frac{\sum (Yield\ of\ each\ product \times Number\ of\ carbon\ in\ each\ product)}{Conversion\ of\ glucose \times 6} \right) \times 100 \right\}$$

Characterization. Crystal structure was analyzed by powder X-ray diffraction (PXRD) with a SmartLab (Rigaku Co.) using a Cu Kα radiation (λ= 0.154 nm) at 40 kV and 30 mA in the range of 2θ = 10-80°. The diffraction patterns were analyzed with the database in the joint committee of powder diffraction standards (JCPDS). For inductively coupled plasma atomic emission spectroscopy (ICP-AES) analysis, an ICPS-7000 ver. 2 (Shimadzu Co.) was employed to quantify the real Cu amount loaded over MgO in the presence of various surfactants. Contents of Cu in the catalyst was estimated by a calibration curve method. A H-7100 (Hitachi, Ltd.) operating at 100 kV was utilized to acquire the morphology of catalyst by a transmission electron microscopy (TEM) image. The samples for TEM measurements were dispersed in water, and the supernatant liquid was dropped onto a copper grid before drying *in vacuo* overnight. Temperature-programmed reduction (TPR) was performed with an Ohkura BP-2 instrument interfaced with a TCD. The TCD

results were normalized to the mass of the used samples, and the rate of H_2 consumption was estimated based on the calibration curve of pure CuO (Strem, 99.999%) reduction. The TPR profile was recorded from 323 K under a H_2/Ar (5/95) flow at a ramping rate of 10 K min^{-1}. X-ray absorption spectroscopy (XAS) was performed with a transmission mode at a BL-9C in KEK-PF under the approval of the Photon Factory Program Advisory Committee (Proposal No. 2013G586). All samples were grained and pressed to pellets with a diameter of 10 mm. Raman spectra were recorded on a T64000 (HORIBA, Ltd.) to clearly demonstrate the particular type of oxide species present in the catalyst. The amount of the Brønsted basic sites in Cu-surfactant/MgO was calculated by the titration method using benzoic acid. For instance, in an Erlenmeyer flask, 0.025 g of catalyst were dispersed in a 5 mL of mixed solution (H_2O:EtOH (4:1; v/v)), and phenolphthalein was added as an indicator. 0.05 M Benzoic acid was added dropwise to the solution containing sample, and whirled until the discharge of pink color of the solution. The procedure was repeated to obtain concordant readings for each catalyst. The amount of the basic sites (mmol g^{-1}) was calculated as the ratio of consumed benzoic acid to the mass of the catalyst used.

3. RESULTS AND DISCUSSION

Catalytic activity. Recently, I have reported Cu-CTAB/MgO calcined at 773 K as an efficient catalyst for the synthesis of LA from glucose at 393 K in high yields. In my previous report, I found that the use of CTAB affords stable copper oxide species that also enhanced the catalytic activity for LA.[27] Continuing with the research efforts, I utilized various surfactants (Table 1) to synthesize the Cu-surfactant/MgO catalysts and explore their catalytic activity for the conversion

Table 2. Catalytic activity of Cu-surfactant/MgO catalysts for LA synthesis from glucose.[a]

Entry	Catalyst	Cu loading / mmol g^{-1}[b]	Yield / %[c]						Carbon balance / %[d]
			LA	GlycAld	GlycA	GlcoA	FA	AA	
1	Cu-TOAB/MgO	1.014	70.8	37.6	16.8	2.4	3.3	5	65.7
2	Cu-CTAB/MgO	0.998	69.9	34.1	16.6	2.5	3.7	5.7	63.7
3	Cu-SDS/MgO	0.937	61.6	34.9	15.2	2.1	3.7	2.4	58.1
4	Cu-TX100/MgO	0.996	48.3	21.8	7.8	1.2	1.4	4.4	41.1
5	Cu-DDAO/MgO	1.030	48	26.4	12.7	0.4	1	3.4	44.8
6	Cu-None/MgO	0.368	45.9	19.4	9.9	1.5	6.1	4.2	40.8

[a]*Reaction conditions:* Glucose (0.5 mmol), Catalyst (60 mg), Water (5 mL), 2.5M NaOH (1 mL), Teflon lined autoclave, Ar (0.4 MPa), 393 K, 1 h. The conversion for glucose was >99% in all cases. [b]The copper content in catalyst was determined by ICP-AES. [c]The conversion of glucose and yields of LA were calculated by HPLC analysis using calibration curve method. [d]Determined based on the observed products. LA; lactic acid. GlycAld; glyceraldehyde. GlycA; glyceric acid. GlcoA; glycolic acid. FA; formic acid. AA; acetic acid.

of glucose to LA. The yields for all product and the carbon balance are shown in Table 2 for various Cu-surfactant/MgO catalysts. Both Cu-TOAB/MgO and Cu-CTAB/MgO demonstrated high LA selectivity with *ca.* 70% LA yield. The catalyst synthesized using non-ionic surfactants like DDAO (Cu-DDAO/MgO) and TX100 (Cu-TX100/MgO) or the catalyst prepared without surfactant (Cu-None/MgO) had similar activities producing LA in yields less than 50% with a low carbon balance values. Cu-SDS/MgO had an intermediate activity. The activities of these catalysts were found to be independent of the amount of the copper (Table 2). Also, a very low copper loading was detected in the absence of any surfactant; while other surfactant effectively promoted copper loading on magnesia.

Various research reports, including my own, highlighted the importance of basicity of the catalysts or the reaction media for the successful conversion of glucose to LA.[27-30] Thus, the basicity of the Cu-surfactant/MgO were determined and plotted together with the catalytic activities in Figure 1. Cu-SDS/MgO having a moderate catalytic activity, but possessed highest basicity among all the catalysts employed in this study. The basicity decreased from Cu-SDS/MgO to Cu-CTAB/MgO to Cu-TOAB/MgO, while the catalytic activity increased and was almost constant for Cu-CTAB/MgO and Cu-TOAB/MgO. A further decrease in the basicity was observed for Cu-DDAO/MgO and Cu-TX100/MgO catalysts, and LA yields were lower using these catalysts. The Cu-None/MgO catalyst possessed lowest basicity to give lowest LA yield from glucose. Based on Figure 1, an intermediate basicity of the catalyst is expected to favor the optimum catalytic activity. An increase in the catalytic basic sites enhances the over reaction of LA, whereas, the lower basicity of the catalyst was insufficient to drive the reaction forward. However, the distribution profile of other products and the carbon balance did not complemented

[79]

the above expectations (Table 2). To explain these anomalies, the prepared catalysts were thoroughly characterized using various spectroscopic techniques.
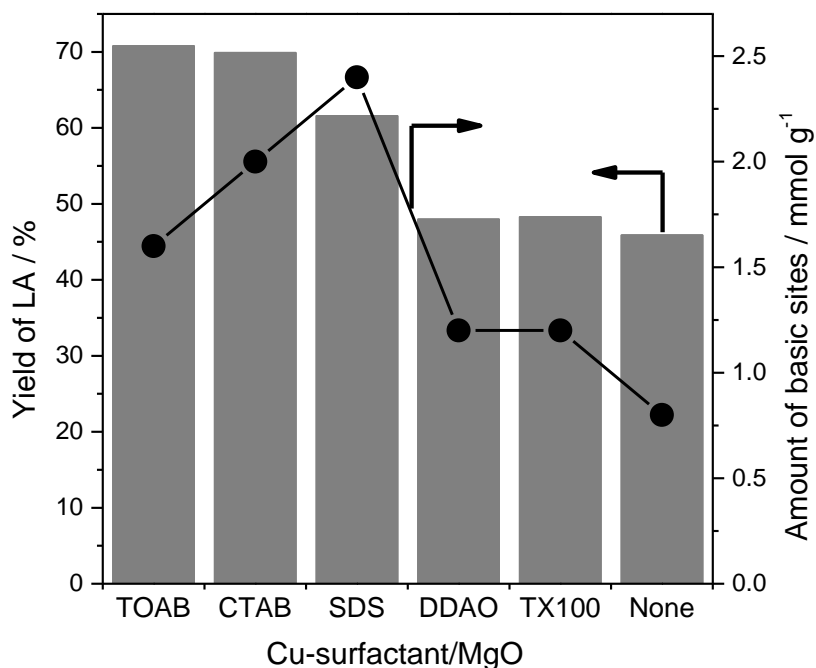
Figure 1. LA yield and basicity profile of various Cu-surfactant/MgO. Yields of LA (gray bars) and basicity (●). *Reaction conditions*: glucose (0.5 mmol), catalyst (60 mg), water (5 mL), 2.5M NaOH (1 mL), Teflon lined autoclave, Ar (0.4 MPa), 393 K, 1 h.

Catalyst characterization. In order to understand the structure-activity relationship of Cu-surfactant/MgO, diverse techniques like XRD, Raman, H_2-TPR, etc. were employed. The differences in the phases of the Cu-surfactant/MgO catalysts were revealed by XRD patterns as shown in Figure 2. The crystalline MgO phase along with the oxide species of copper were observed in the XRD patterns. The diffraction patterns for MgO appeared at 36.98°, 42.94°, 62.34°, 74.72° and 78.64° in all catalysts. The peaks at 36.4° and 39.5° were assigned to the (002) and (200) planes of CuO crystallites. The diffraction patterns for Cu_2O (2θ= 36.46°, 42.32°, 61.4° and 73.54°) were hardly distinguished in these catalysts because of the broadened peaks of MgO,

[80]

Figure 2. XRD patterns of (a) Cu-TOAB/MgO, (b) Cu-CTAB/MgO, (c) Cu-SDS/MgO, (d) Cu-DDAO/MgO, (e) Cu-TX100/MgO and (f) Cu-None/MgO. The various recognized phases are shown as CuO (open circle, ○), Cu_2O (closed square, ■) and MgO (open triangle, △).

whose diffraction peaks are at close proximities to that of Cu_2O (Figure 3). This complicated the phase recognition and thereby the relative intensity of CuO and MgO as observed in these catalyst were plotted against their catalytic activities (Figure 4). The peak at 38.78° and 78.64° were observed as peak with highest intensity in the XRD patterns of reference CuO and MgO, respectively. The intensity ratio of these peaks were plotted as a function of surfactant and their respective catalytic activities to reveal the structural characteristics of Cu-surfactant/MgO catalysts. However, the trend of catalytic activity and relative intensity ratio of CuO to MgO differed from each other. These results indicate that although CuO is known to chemical upgrade glucose to LA,[31] but CuO is not the active species for this catalytic reaction. Also, the co-presence of both
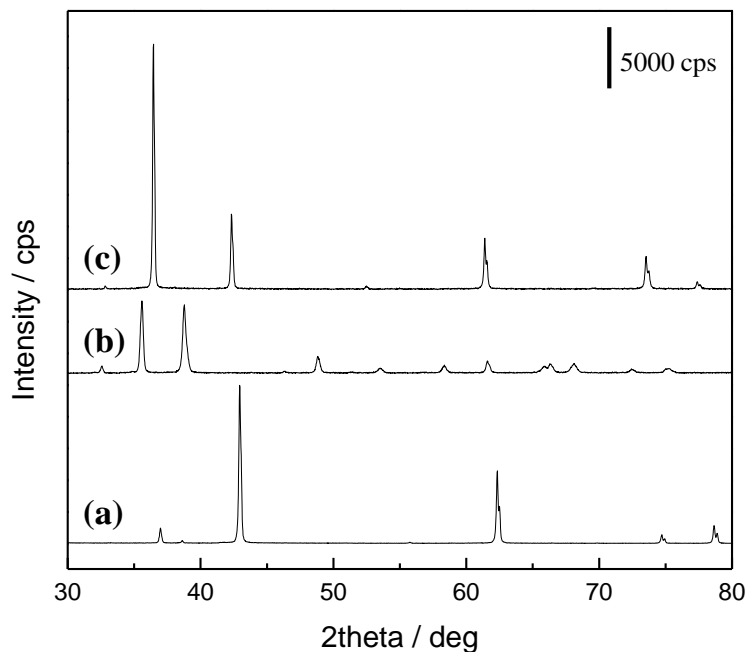
Figure 3. XRD patterns of (a) MgO, (b) CuO and (c) Cu_2O.
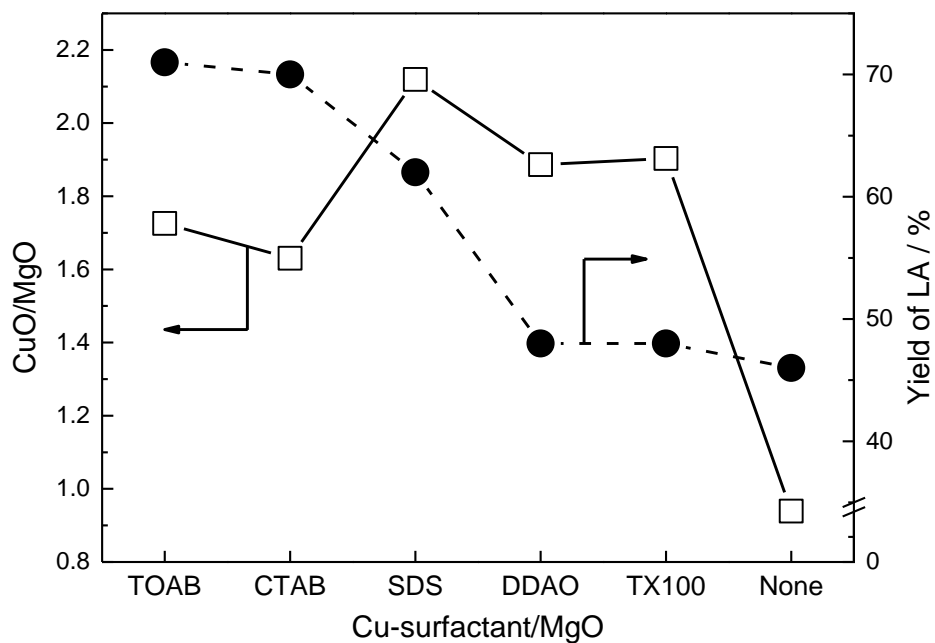
Figure 4. Relative intensities of CuO to MgO in the XRD patterns of Cu-surfactant/MgO and their catalytic activities for the production of LA from glucose.

Cu₂O and CuO were expected in these catalysts as catalytically active sites at this time.

The XRD patterns of the uncalcined catalyst were interesting and unfolded few mysteries about copper oxide species (Figure 5). The hydrothermal treatment of MgO afforded $Mg(OH)_2$ as the main phase, which converted into MgO after calcination at 773 K (Figure 2). The arrows in Figure 5B(d) highlights the absence of tenorite (or CuO) phase on the use of DDAO as surfactant. The use of DDAO as surfactant afforded only cuprite (or Cu_2O) phase on $Mg(OH)_2$ after the hydrothermal treatment and before calcination. These Cu_2O phase can be preferentially converted into CuO on calcining the catalyst at 773 K for 6 h in air (Figure 2). These results also show the incapability of DDAO-surfactant in preserving a particular species on calcination. I found that the DDAO capping decomposed at higher temperatures leaving the copper oxide species naked.

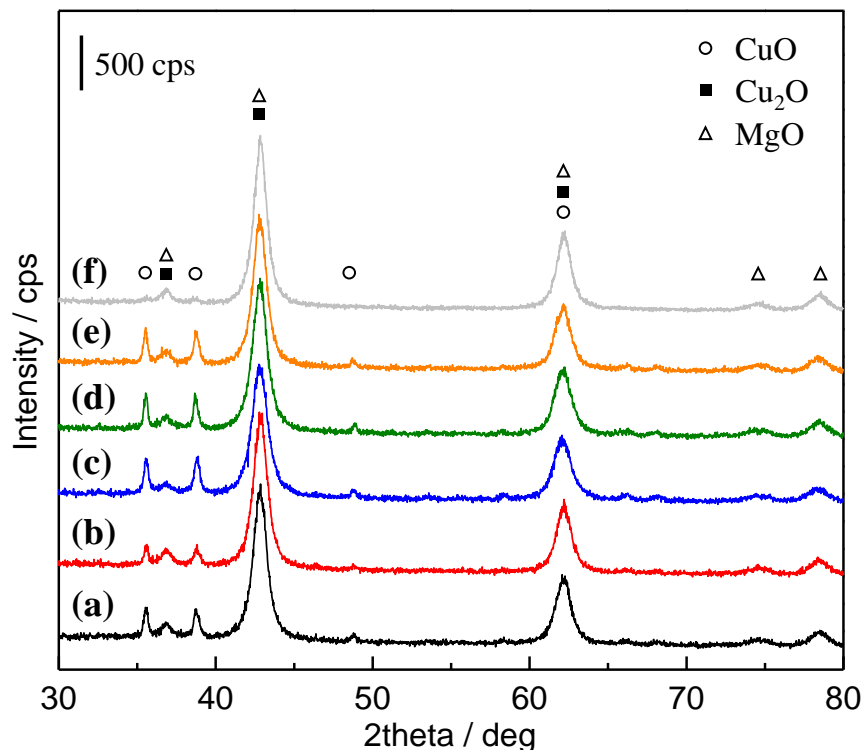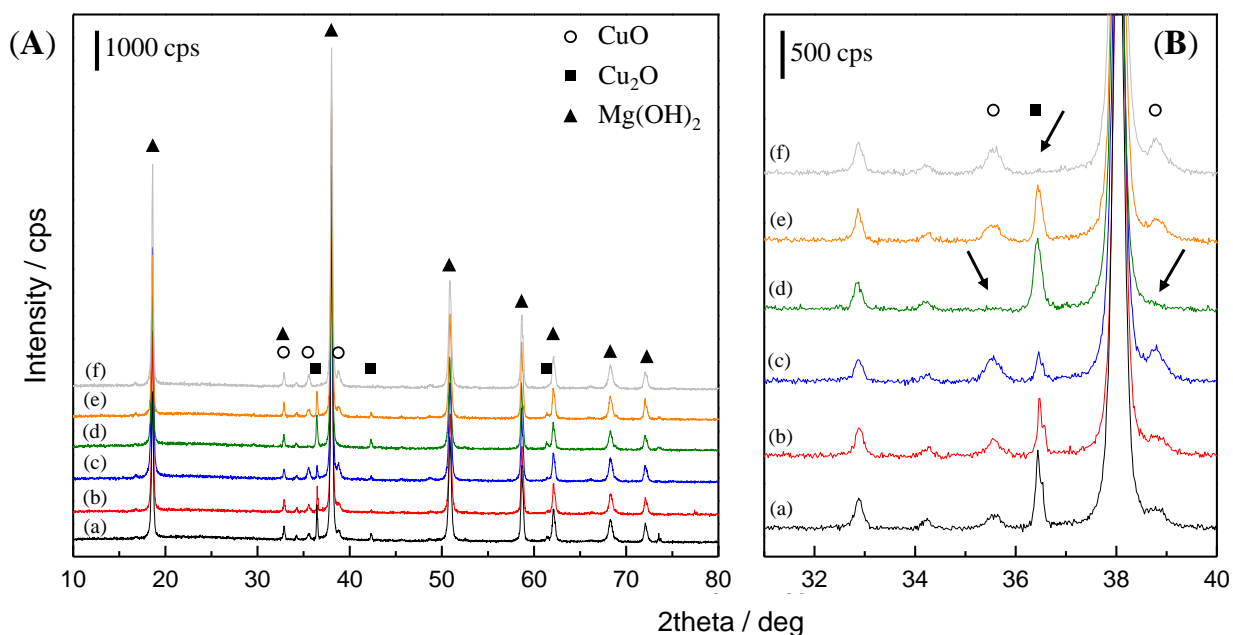**Figure 5.** (A) XRD patterns in 10-80° and (B) emphasized details in 31-40° of uncalcined (a) Cu-TOAB/MgO, (b) Cu-CTAB/MgO, (c) Cu-SDS/MgO, (d) Cu-DDAO/MgO, (e) Cu-TX100/MgO and (f) Cu-None/MgO. The various recognized phases are shown as CuO (open circle, ○), Cu_2O (closed square, ■) and $Mg(OH)_2$ (closed triangle, ▲).

Similarly, the arrow in Figure 5B(f) marks the absence of Cu_2O phase in absence of any surfactant during hydrothermal synthesis of copper catalysts. The only phase obtained in the absence of surfactant was expectedly CuO which could also be observed after calcination of the catalyst at 773 K for 6 h in air (Figure 2). Just after the hydrothermal treatment three kinds of copper species can be afforded on the magnesia surface as a function of surfactant. From the XRD patterns, it was realized that the use of DDAO afforded Cu_2O as the single phase on magnesia. On the other hand, the catalysts prepared without any surfactant had diffraction patterns for only CuO phase. Other surfactants gave both Cu_2O and CuO phases in various ratio on magnesia. Since, a clear picture of the catalyst could not deciphered from the XRD patterns, it becomes necessary to employ other techniques for defining the structure-activity relationship more clearly.

Recently, Debbichi et al. have reported an excellent combination of experimental and theoretical study on the vibrational properties of three different phases of copper oxide.[32] The Raman spectra of the three oxides of copper differed from each other because of the different vibrational modes. The Raman spectra for the Cu-surfactant/MgO catalysts were recorded to reveal the true copper oxide phase in each catalyst (Figure 6). An unexpected copper oxide phase, paramelaconite was observed for Cu-TOAB/MgO, Cu-CTAB/MgO and Cu-SDS/MgO catalysts (Figures 6a-c). Although, the obtained results are not so surprising as per the DFT calculations according to which Cu_4O_3 is much more stable than CuO with 25% oxygen vacancies.[33] In the reduction of CuO to Cu, Cu_4O_3 is expected as an ideal intermediate, however, most of the studies either found it in traces or failed to observe any such phases during the reaction monitoring.[33-35] The reason of failed transformation of CuO to Cu_4O_3 during reduction reactions have been explained using DFT studie.[33] According to the literature, (a) O atoms need to be removed from well-defined positions
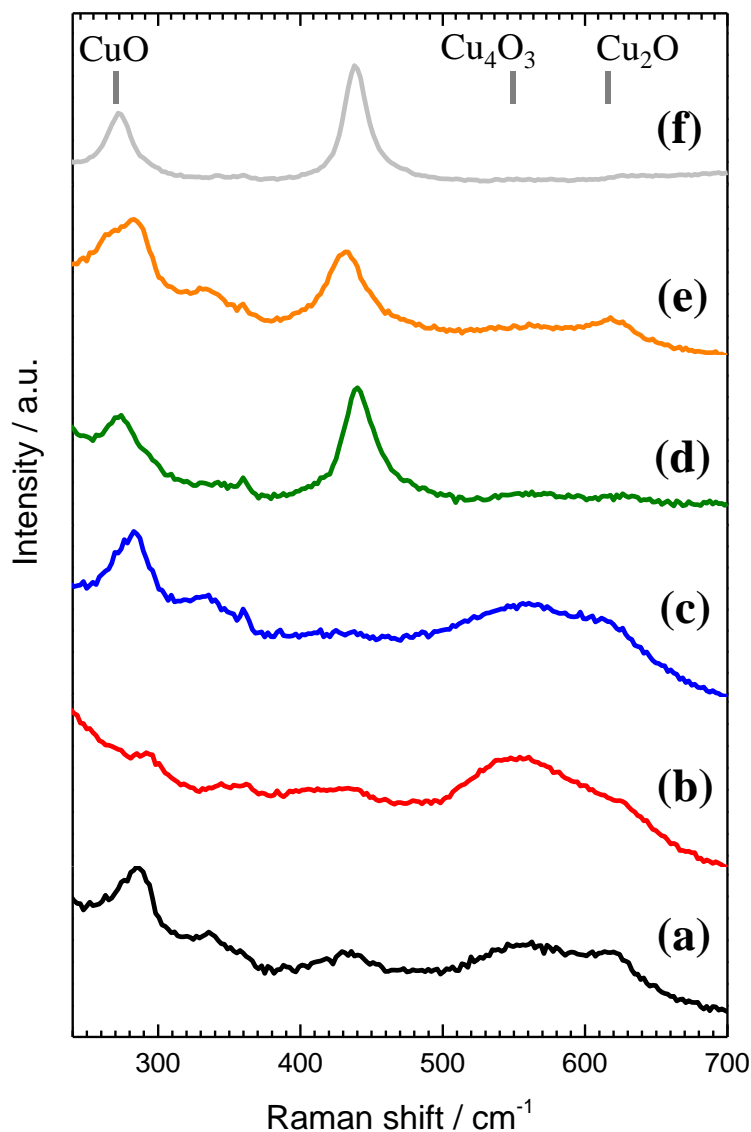
Figure 6. Raman spectra of (a) Cu-TOAB/MgO, (b) Cu-CTAB/MgO, (c) Cu-SDS/MgO, (d) Cu-DDAO/MgO, (e) Cu-TX100/MgO and (f) Cu-None/MgO. The vibrational frequencies for CuO (tenorite), Cu_4O_3 (paramelaconite) and Cu_2O (cuprite) are indicated by vertical bars.

of the Cu-O lattice, and (b) a substantial distortion (activation energy of about 0.06 eV/atom) in the cell parameters of CuO is required to obtain Cu_4O_3. The first unequivocal synthesis of paramelaconite was reported by Morgan et al. by extraction of copper source with concentrated aq. ammonia solution in a Soxhlet apparatus to afford a mineral containing 35% Cu_4O_3.[36] To the

[85]

best of my knowledge, this is the first successful report of grafting paramelaconite on a basic support. In Cu-CTAB/MgO, the only recognizable phase from Raman spectroscopy was of Cu_4O_3. Cu-TOAB/MgO and Cu-SDS/MgO demonstrated signals for CuO in addition to Cu_4O_3, whereas, CuO was found to be the only phase present in the Cu-DDAO/MgO and Cu-None/MgO catalysts. The catalyst prepared using TX-100 as surfactant afforded both CuO and Cu_2O phases on MgO by hydrothermal treatment (Figure 6e). An unknown peak around 440 cm^{-1} were observed for the non-ionic and surfactant-less copper catalysts. The spinel $CuMgO_x$ were held responsible for such unknown peaks, however, I have no experimental evidence for any such phase in the catalyst. These results clearly indicated that the surfactant controlled the formation of copper oxide species under hydrothermal conditions.

Interestingly, the catalytic activity was found to be dependent on the presence of Cu_4O_3. Cu_4O_3 was observed as the main phase for the catalysts synthesized using TOAB, CTAB and SDS. Also, these catalysts afforded high catalytic activity (>60% LA yield; see Table 2). On contrary, the catalysts (such as Cu-DDAO/MgO, Cu-TX100/MgO and Cu-None/MgO) that lacked Cu_4O_3 phase demonstrated lower catalytic activity (<50% LA yield; Table 2). These results clearly indicated Cu_4O_3 as the catalytically active species in the chemical upgradation of glucose to LA.

Temperature programmed reduction (TPR) forms a substantial tool for the investigation of redox behavior of copper catalysts.[37-38] I measured the H_2-TPR profiles for prepared catalysts to further understand the differences in the catalytic behavior based on redox properties, if any. The graphical representation of the reduction profiles is shown in Figure 7. It has been understood well that the signals at lower temperatures in the reduction contour is due to the easily reducible species, while the peaks appearing at higher temperatures correspond to species that are difficult to reduce. Although, Cu-SDS/MgO contains Cu_4O_3 species as in Cu-TOAB/MgO, but the redox nature of
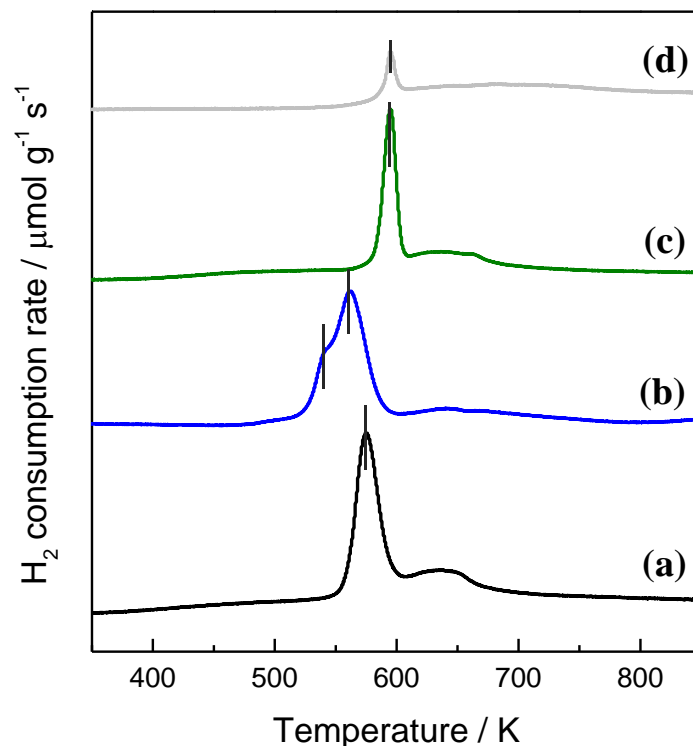
Figure 7. H_2-TPR profiles of (a) Cu-TOAB/MgO, (b) Cu-SDS/MgO, (c) Cu-DDAO/MgO and (d) Cu-None/MgO catalysts.

the two catalysts are much different (Figures 7a-b). The maxima in the TPR spectra was observed at a temperature of 575 K for the Cu-TOAB/MgO catalysts. The main peak in Cu-SDS/MgO was observed at lower temperatures (560 K) with a shoulder at temperatures lower than 550 K. This suggest that the redox behavior of the two copper oxide are somewhat different and thereby a difference in the catalytic activity is also observed among the two catalyst. On the other hand, Cu-DDAO/MgO and Cu-None/MgO catalysts were reduced at higher temperatures implying that the CuO in these catalysts are mainly large sized or bulk-type (Figures 7c-d).

The transmission electron microscopy (TEM) analysis of these catalysts were carried out to observe a variety of morphology (Figure 8). Cu-TOAB/MgO, Cu-CTAB/MgO afforded fine

[87]

dispersion of small sized copper oxide species. Cu-DDAO/MgO also had small particles along with particles of size about 70 nm. In Cu-TX100/MgO, a wide distribution of particle size was observed. Very large sized particle were seen in the Cu-SDS/MgO catalyst along with few small particles. Cu-None/MgO was seen as dark blocks containing very small dispersed particles at few places. The TEM analysis hardly contributed in defining structure-activity relationship. However, as observed in TPR studies, large-sized copper species were formed in Cu-DDAO/MgO and Cu-None/MgO.
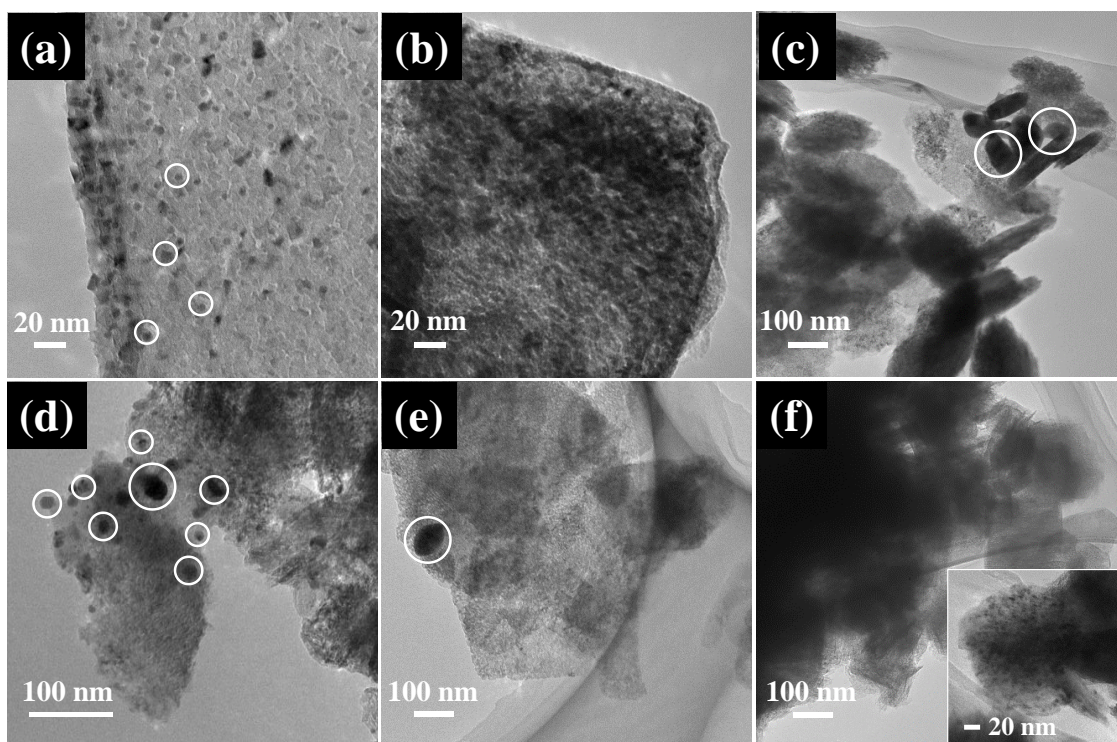
Figure 8. TEM images of (a) Cu-TOAB/MgO, (b) Cu-CTAB/MgO, (c) Cu-SDS/MgO, (d) Cu-TX100/MgO, (e) Cu-DDAO/MgO and (f) Cu-None/MgO.

X-ray absorption spectroscopy (XAS) were also measured for the various Cu-surfactant/MgO catalysts. Figure 9 displays the XAS for selected Cu-surfactant catalysts. All the catalyst showed a great similarity in XANES area at Cu K-edge (Figure 9A) but had a much different EXAFS

region (Figure 9B). The distances between Cu-O and/or Cu-Cu were diverse when the FT of k^3-weighted EXAFS were plotted (Figure 9C). Most catalyst had a dominant peak in the range of 1-2 Å whereas in Cu-None/MgO the dominant peak was observed in the range of 2-3 Å. Neither of the catalyst had high similarity to the bulk type CuO or Cu$_2$O in the XAS profiles (Figures 9A,C).
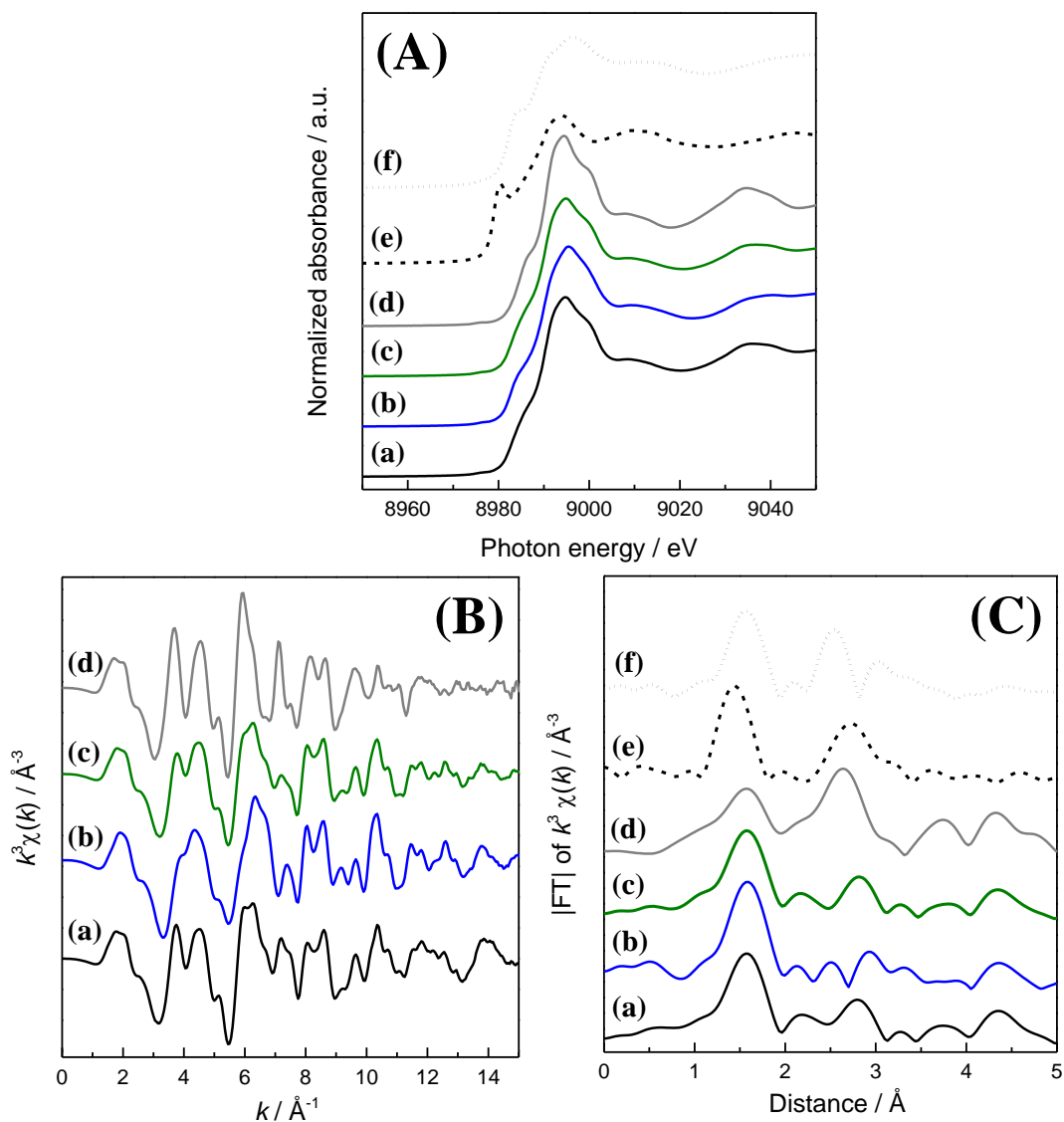
Figure 9. (A) Normalized XANES, (B) EXAFS and (C) FT of k^3-weighted EXAFS spectra at the Cu K-edge of (a) Cu-TOAB/MgO, (b) Cu-SDS/MgO, (c) Cu-DDAO/MgO, (d) Cu-None/MgO, (e) Cu$_2$O and (f) CuO.

The concentrated aq. ammonia solution was used in the earlier reported synthesis of paramelaconite using copper or its oxides.[36] The use of quaternary ammonium salt-based surfactants (TOAB and CTAB) could be the reason for the formation of Cu_4O_3 phase on magnesia starting with copper salt in Cu-TOAB/MgO and Cu-CTAB/MgO. Supposedly, these surfactants under hydrothermal conditions decompose to form ammoniacal solution. Because of the terminal ammonium ion in CTAB (see Table 1 for structure), the formation of Cu_4O_3 is favored and Cu_4O_3 is formed as the main phase, whereas, in TOAB ammonium ion is tertiary that delays the formation rate of Cu_4O_3 and other phases are formed as well (Figure 6). At this stage I am clueless about the formation of Cu_4O_3 species in the presence of SDS. However, the TPR data clearly demonstrates the different redox behavior of Cu-TOAB/MgO and Cu-SDS/MgO (Figure 7). A more detailed and rigorous study is required to define the essential synthetic parameters and/or the formation mechanism of Cu_4O_3 on magnesia using surfactants.

4. CONCLUSIONS

In summary, I have successfully achieved a convenient and simple surfactant-mediated hydrothermal strategy for controlling the supported copper oxide species (Figure 10). In addition, the various prepared catalyst were investigated for their activity in the chemical upgradation reaction of glucose to LA. The analysis of XRD patterns, Raman spectra and H_2-TPR profiles and their correlation with the catalytic activity data drew a clear image of the catalytic active species on magnesia. Also, the careful inspection of these data depicted the facile surfactant-mediated approach to control the supported copper oxide species. From the XRD patterns (of the uncalcined catalyst) it was inferred that Cu_2O (cuprite) phase is formed predominantly in the presence of
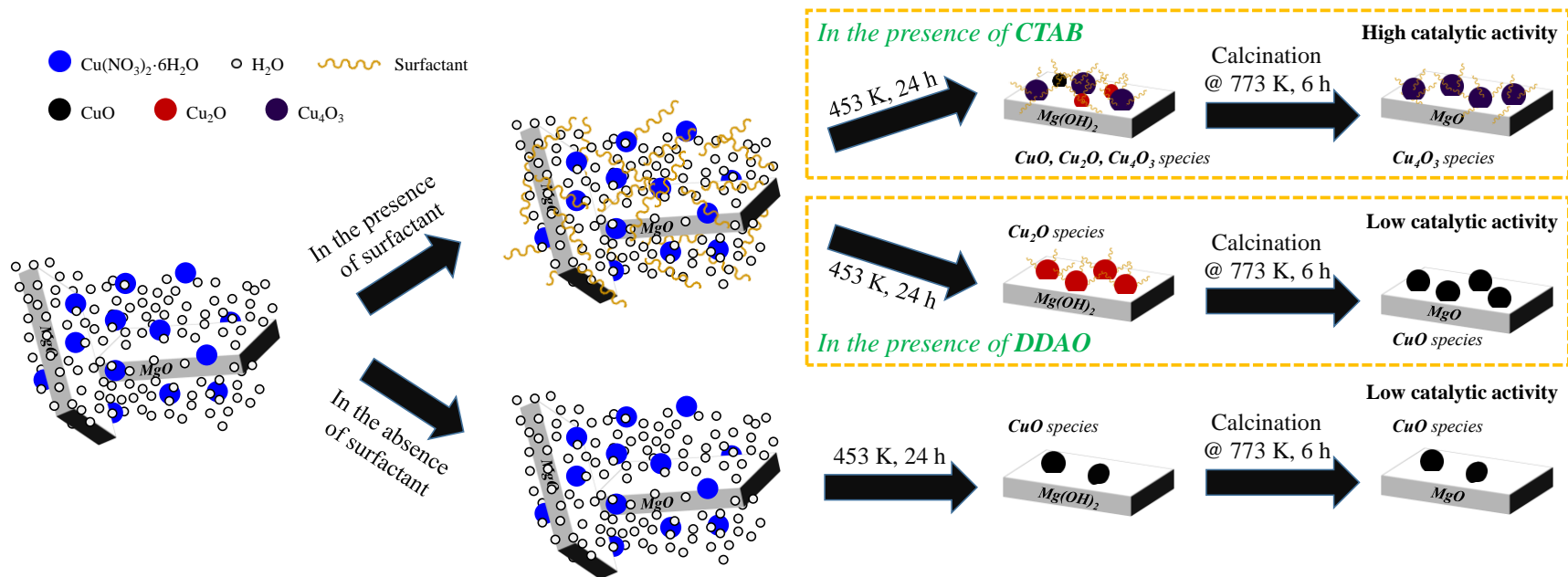
Figure 10. Schematic summary of surfactant-mediated synthesis of supported copper oxide species on MgO.

DDAO after hydrothermal treatment which can be selectively converted into CuO (tenorite) on calcination, where calcination decomposes the capping agent. On the other hand, the catalyst prepared without using surfactant afforded only tenorite phase. The quaternary ammonium salt containing surfactants, selectively formed Cu_4O_3 (paramelaconite) phase and preserved them even after calcination. The correlation with the catalytic activity clearly portrayed paramelaconite or Cu_4O_3 phase as the active species. Such facile control of copper oxide species using a simple and inexpensive hydrothermal strategy makes this process attractive and promising for applications in advanced materials and devices.

REFERENCES

1. D. Lu, T. Takata, N. Saito, Y. Inoue, K. Domen, *Nature* **2006**, *440*, 295.

2. M. Eddaoudi, J. Kim, N. L. Rosi, D. T. Vodak, J. Wachter, M. O'Keeffe, O. M. Yaghi, *Science* **2002**, *295*, 469.

3. J. R. Heath, *Acc. Chem. Res.* **1999**, *32*, 388.

4. C. M. Lieber, *Solid State Commun.* **1998**, *107*, 607.

5. H. Meyssamy, K. Riwotzki, A. Kornowski, S. Naused, M. Haase, *Adv. Mater.* **1999**, *11*, 840.

6. M. −P. Pileni, *Nat. Mater.* **2003**, *2*, 145.

7. L. Manna, E. C. Scher, A. P. Alivisatos, *J. Am. Chem. Soc.* **2000**, *122*, 12700.

8. G. Schmid, *Chem. Rev.* **1992**, *92*, 1709.

9. "*Nanoscale materials in chemistry*", K. J. Klabunde, (ed.), Wiley-Interscience, New York, **2001**.

10. A. Chowdhuri, V. Gupta, V. Sreenivas, *Appl. Phys. Lett.* **2004**, *84*, 1180.

11. R. X. Zhou, T. M. Yu, X. Y. Jiang, F. Chen, X. M. Zheng, *Appl. Surf. Sci.* **1999**, *148*, 263.

12. Y. She, Q. Zheng, L. Li, Y. Zhan, C. Chen, Y. Zheng, X. Lin, *Int. J. Hydrogen Energy* **2009**, *34*, 8929.

13. P. P. C. Udani, P. V. D. S. Gunawardana, H. C. Lee, D. H. Kim, *Int. J. Hydrogen Energy* **2009**, *34*, 7648.

14. J. L. Cao, G. S. Shao, Y. Wang, Y. Liu, Z. Y. Yuan, *Catal. Commun.* **2008**, *9*, 2555.

15. *PDF #41-0254, JCPDS Powder Diffraction File*; Int. Center for Diffraction Data: Swarthmore, PA, **1989**.

16. *PDF #05-0667, JCPDS Powder Diffraction File*; Int. Center for Diffraction Data: Swarthmore, PA, **1989**.

17. *PDF #083-1665, JCPDS Powder Diffraction File*; Int. Center for Diffraction Data: Swarthmore, PA, **2004**.

18. M. O'Keeffe, J. –O. Bovin, *Am. Mineral.* **1978**, *63*, 180.

19. C. Frondel, *Am. Mineral.* **1941**, *26*, 657.

20. N. Datta, J. W. Jeffery, *Acta Cryst.* **1978**, *B34*, 22.

21. M. O'Keeffe, W. J. Moore, *J. Chem. Phys.* **1962**, *36*, 3009.

22. T. J. Huang, D. –H. Tsai, *Catal. Lett.* **2003**, *87*, 173.

23. S. Royer, D. Durpez, *ChemCatChem* **2011**, *3*, 24.

24. For example, Y. Feng, X. Zheng, *Nano Lett.* **2010**, *10*, 4762.

25. M. Leng, M. Liu, Y. Zhang. Z. Wang, C. Yu, X. Yang, H. Zhang, C. Wang, *J. Am. Chem. Soc.* **2010**, *132*, 17084.

26. M. Y. Guo, F. Liu, J. Tsui, A. A. Voskanyan, A. M. C. Ng, A. B. Djurisic, W. K. Chan, K. –Y. Chan, C. Liao, K. Shih, C. Surya, *J. Mater. Chem. A* **2015**, *3*, 3627.

27. H. Choudhary, S. Nishimura, K. Ebitani, *Appl. Catal. B: Environ.* **2015**, *162*, 1

28. X. Yan, F. Jin, K. Tohji, A. Kishita, H. Enomoto, H. *AIChE J.* **2010**, *56*, 2727.

29. D. Esposito, M. Antonietti, *ChemSusChem* **2013**, *6*, 989.

30. A. Onda, T. Ochi, K. Kajiyoshi, K. Yanagisawa, *Catal. Commun.* **2008**, *9*, 1050.

31. Y. Wang, F. Jin, M. Sasaki, Wahyudiono, F. Wang, Z. Jing, M. Goto, *AIChE J.* **2013**, *59*, 2096.

32. L. Debbichi, M. C. Marco, J. F. Pierson, P. Kruger, *J. Phys. Chem. C* **2012**, *116*, 10232.

33. J. –Y. Kim, J. A. Rodriguez, J. C. Hanson. A. I. Frenkel, P. L. Lee, *J. Am. Chem. Soc.* **2003**, *125*, 10684.

34. X. Wang, J. C. Hanson, A. I. Frenkel, J. –Y. Kim, J. A. Rodriguez, *J. Phys. Chem. B* **2004**, *108*, 13667.

35. D. A. Svintsitskiy, T. Y. Kardash, O. A. Stonkus, E. M. Slavinskaya, A. I. Stadnichenko, S. V. Koscheev, A. P. Chupakhin, A. I. Boronin, *J. Phys. Chem. C* **2013**, *117*, 14588.

36. P. E. D. Morgan, D. E. Partin, B. L. Chamberland, M. O'Keeffe, *J. Solid State Chem.* **1996**, *121*, 33.

37. L. Kundakovic, M. –F. Stephanopoulos, *Appl. Catal. A* **1998**, *171*, 13.

38. S. Nishimura, T. Shishido, J. Ohyama, K. Teramura, A. Takagaki, T. Tanaka, K. Ebitani, *Catal. Sci. Technol.* **2012**, *2*, 1685.

Chapter 3

Utilization of inedible-biomass derived formic acid as a potential hydrogen source using hydrothermally prepared supported CoPd bimetallic catalyst

ABSTRACT

Bimetallic CoPd nanoparticles (NPs) on boehmite (AlOOH) were synthesized under hydrothermal conditions using three different capping agents. Their catalyses were evaluated for the facile utilization of formic acid (HCO$_2$H; FA) as a hydrogen source in the hydrogenation reaction of maleic anhydride (MAn). Among compared capped bimetallic CoPd catalysts, *N,N*-dimethyldodecylamine *N*-oxide (DDAO) capped bimetallic CoPd NPs supported on AlOOH (CoPd-DDAO/AlOOH) exhibited superior catalysis with enhanced rate of the reaction and excellent reusability without metal(s) leaching. To further understand the prominent activity of CoPd-DDAO/AlOOH catalyst, several spectroscopic techniques were applied. Transmission electron microscopy studies indicated the formation of mono-dispersed NPs containing both cobalt and palladium atoms in each NP on AlOOH. X-ray diffraction and X-ray absorption spectroscopy (XAS) supported the alloy structure of CoPd NP in CoPd-DDAO/AlOOH which was composed with Co oxides and CoPd alloy. The partial electron transfer in DDAO-capped CoPd NPs was observed by X-ray photoelectron spectroscopy and XAS analysis. In summary, it is suggested that CoPd-DDAO/AlOOH catalyst possessed remarkable catalytic activity for MAn hydrogenation using FA because of both enhanced stability (metal leaching inhibition) and favorable electronic/geometric changes for adsorption of substrates caused by alloying in the presence of DDAO capping agent.

1. INTRODUCTION

The recent research to overcome the economical hurdles in fuel cell technology has introduced various systems for catalytic dehydrogenation of formic acid (HCO_2H; FA) into hydrogen.[1-6] In addition to the realization of FA being sustainable and convenient hydrogen storage material,[7-9] it is also an important aspect that FA can be obtained from biomass in high yields.[10-13] In spite of spectacular research accomplishments for dehydrogenation of FA, a limited effort has been made to replace the dangerous and hazardous H_2 by FA for catalytic hydrogenation reactions. On the other hand, the scopes for synthesizing efficacious heterogeneous catalysts have been kept wide open, among which supported metal NPs are of prime interest. The resulting interactions of dispersed nanoparticles (NPs) on support and their impact on composition, structure and catalytic performances of NPs have been understood very well in the past decades.[14-18] It has been reported that not only the metal-support interactions but also the type of capping agent influences the electronic properties of NPs in a noticeable way.[14-18] The Pd-based catalysts were found to be more efficient for FA decomposition than the commonly used overpriced Pt catalysts, because of the facilitated 2-electron oxidation step of FA promoting dehydrogenation pathway (toward H_2 and CO_2) rather than dehydration pathway (toward H_2O and CO).[19-20] Unfortunately, the limiting step is the adsorption/dissociation of FA on the Pd catalyst surface, which demands increased quantity of catalysts (and in turn increases cost) to achieve high catalytic activity. Of late, it has been also found that the incorporation of earlier transition metal can dramatically enhance the 2-electron oxidation process owing to their oxophilic properties.[6] Similar effects of alloying Pd with transition metals have been observed for oxygen reduction reaction.[21-23]

A significant accomplishment has been made in the synthesis of colloidal alloy NPs using various methods,[24-29] and some studies exist for the simplistic synthesis of stable supported MPd (M = Fe, Ni, Co, Au) alloy NPs for catalytic research.[15-16,30-31] Homogeneous polymer protected metal NPs endure obvious advantages of higher degree of dispersion with serious issues of separation and sustainability for wider applications. Thus, it becomes necessary to develop stable and highly active heterogeneous NPs (or supported NPs) catalysts.

Hydrothermal methods have gained popularity in the synthesis of advanced materials including nanomaterials mainly due to the reasonable product quality (narrow size distribution and good crystallinity) and high reproducibility.[32-34] In the Chapter 1, CuO_x NPs supported on MgO catalyst using cetyltrimethylammonium bromide (CTAB) as a capping agent (denoted as CuCTAB/MgO) by a simple hydrothermal methodology to obtain a stable and active catalyst for the synthesis of FA and lactic acid from biomass resources were synthesized.[13] These results motivated me to extend the preparation method for bimetallic catalyst such as CoPd, and to examine the catalytic activity for the industrially important maleic anhydride (MAn) hydrogenation reaction towards succinic acid (SA), a C-4 building block chemical[35]. Also, very recently, our group synthesized supported metal catalysts for efficient utilization of FA in hydrogenation reactions of 5-hydroxymethylfuraldehyde, levulinic acid and nitroarenes.[36-38] The continuous research efforts in the effective and facile utilization of FA under moderate conditions with decreased metal content for industrially important catalytic reactions paved the path for this research.

As one of the pioneers in this research field, Toshima et al., have extensively reported the role of poly(*N*-vinyl-2-pyrrolidone) (PVP) on the geometric, physical and chemical properties of NPs.[39-42] Our research group has also demonstrated PVP[16], acrylate[43], starch[17-18] and CTAB[13] as an efficient capping agent that influences formation mechanism of NPs and/or properties of

constructed active centers on supported NPs catalyst. For the hydrothermal synthesis of CoPd catalyst in this study, I chose *N,N*-dimethyldodecylamine *N*-oxide (DDAO) (see Figure 1 for structure), a non-ionic surfactant, as the capping agent. Because the DDAO possessed strong hydrophilicity and similar functionality as PVP, it is expected to affect both physical and chemical properties of NPs.
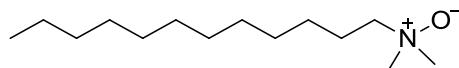
Figure 1. Chemical structure of *N,N*-dimethyldodecylamine *N*-oxide (DDAO).

To the best of my knowledge, this is the first report to introduce DDAO as a novel capping agent for the synthesis of metallic NPs under hydrothermal condition. Herein, I demonstrate the novel preparation and superior catalysis of supported and capped robust bimetallic CoPd catalyst for the hydrogenation of MAn to SA using FA as an inexpensive and sustainable hydrogen source. In this paper, the characterization of the DDAO-stabilized bimetallic CoPd NPs by means of TEM, XRD, XPS and XAS; and one-pot synthesis of SA using FA formed from glucose are also described.

2. EXPERIMENTAL SECTION

Chemicals. Cobalt acetate (Co(OAc)$_2$·4H$_2$O), palladium acetate (Pd(OAc)$_2$), boehmite (AlOOH)[44], 5 wt% Pd/Al$_2$O$_3$, D(+)-glucose, cetyltrimethylammonium bromide (CTAB), formic acid (FA), copper nitrate hexahydrate (Cu(NO$_3$)$_2$·6H$_2$O), 30% hydrogen peroxide (H$_2$O$_2$) and standard solutions (1000 ppm) of palladium and cobalt were purchased from Wako Pure Chemical Industries, Ltd.. Acetic acid, succinic acid (SA), magnesium oxide (MgO), and sulfuric acid

(H_2SO_4) were procured from Kanto Chemical Co., Inc.. Tokyo Chemical Industry Co., Ltd. supplied maleic anhydride (MAn) and fumaric acid, whereas *N,N*-dimethyldodecylamine *N*-oxide (DDAO) was obtained from Sigma-Aldrich, Co. LLC.. Acros Organics provided poly(*N*-vinyl-2-pyrrolidone) (PVP K12, average molecular weight 3,500).

Catalyst preparation. Surfactant/polymer capped mono- or bi-metallic NPs supported on AlOOH have been synthesized by a hydrothermal method as demonstrated previously by me with some modifications.[13] In a typical synthetic procedure, of Co(OAc)$_2$·4H$_2$O (0.42 mmol) and/or Pd(OAc)$_2$ (0.24 mmol) were dispersed in acetic acid (150 μL) and capping agent (0.5 mmol), followed by the addition of water (3 mL) into the paste. AlOOH (1.0 g) was dispersed in deionized water (25 mL), and then the above mentioned metal-capping solution was added dropwise under stirring, and vigorously stirred for additional 3 h at room temperature. The obtained mixture was sealed in a 100 mL Teflon lined autoclave, and heated to 453 K at a heating rate of 6 K min^{-1} in an oven, and maintained at the same temperature for 24 h. The oven was allowed to cool slowly to room temperature. The obtained solid was washed with deionized water till the pH of filtrate became neutral, followed by washing with ethanol before drying *in vacuo* overnight at room temperature.

Catalytic testing. All experiments to test the catalytic activity were performed in a 50 mL Teflon lined autoclave, unless stated. The catalytic activity was evaluated for MAn hydrogenation into SA in an aqueous media. In a typical reaction procedure, MAn (0.5 mmol) was dissolved in 5 mL deionized water. Catalyst (25 mg) was added to the solution, followed by the addition of FA (1.9 mmol). The autoclave was sealed and mounted on a preheated oil bath at 353 K. The mixture was allowed to react for various time intervals with continuous magnetic stirring. After the reaction, a part of the resultant solution was diluted 20 times with deionized water, and the catalyst was

filtered off using a Milex®-LG 0.20 μm filter. The obtained filtrate was analyzed by high performance liquid chromatography (HPLC, WATERS 600) using an Aminex HPX-87H column (Bio-Rad Laboratories, Inc.) attached to a refractive index detector. An aqueous 10 mM H_2SO_4 (as a mobile phase) was run through the column (maintained at 323 K) at a flow rate of 0.5 mL min^{-1}. The conversion and yield(s) were determined with a calibration curve method.

Recycling tests were performed to check stability of the synthesized CoPd-DDAO/AlOOH catalyst during the reaction. The catalyst was separated from the reaction mixture by centrifugation. The supernatant liquid was stored, and then analysis of products and leaching test of catalysts were performed. The residual catalyst was washed by centrifugation with deionized water. Finally, the catalyst was dried *in vacuo* overnight. Fresh substrates and reagents were added to the catalyst, and then the reaction was performed again.

Characterization. Crystal structure was analyzed by powder X-ray diffraction (PXRD) with a SmartLab (Rigaku Co.) using a Cu Kα radiation (λ= 0.154 nm) at 40 kV and 30 mA in the range of $2\theta = 8-80°$. The diffraction patterns were analyzed with the database in the joint committee of powder diffraction standards (JCPDS). For inductively coupled plasma atomic emission spectroscopy (ICP-AES) analysis, an ICPS-7000 ver. 2 (Shimadzu Co.) was employed to quantify the real amounts of Co and Pd on AlOOH and to evaluate the metal leaching, if any, during the reaction. Contents of metal (Co and/or Pd) in the catalyst and/or the reaction medium were estimated by a calibration curve method using the standard solutions. A H-7650 (Hitachi, Ltd.) operating at 100 kV was utilized to acquire the morphology of catalyst by a transmission electron microscopy (TEM) image. High-angle annular dark-field and scanning TEM (HAADF-STEM) images and elemental mapping analyses were recorded on JEM-ARM200F (JEOL USA, Inc.) operating at 200 kV. The samples for TEM measurements were dispersed in water, and the

supernatant liquid was dropped onto a copper/carbon grid before drying *in vacuo* overnight. The electronic state of Co/Pd on AlOOH was analyzed by X-ray photoelectron spectroscopy (XPS). The experiments were conducted on an AXIS-ULTRA DLD spectrometer system (Shimadzu Co. and Kratos Analytical Ltd.) using an Al target at 15 kV and 10 mA in an energy range of 0-1200 eV. The binding energies were calibrated with the C 1s level (284.5 eV) as an internal standard reference. X-ray absorption spectroscopy (XAS) was performed at a BL-9C (Co K-edge) and a BL-9A (Pd L_3-edge) in KEK-PF under the approval of the Photon Factory Program Advisory Committee (Proposal No. 2013G586) and a BL01B1 (Pd K-edge) in SPring-8 under the approval of Japan Synchrotron Radiation Research Institute (JASRI) (Proposal Nos. 2013B1478 and 2014B1472). Fourier transforms (FT) of k^3-weighted extended X-ray absorption fine structure (EXAFS) were performed in the range of 3-12 $Å^{-1}$ for Co-K and 3-13 $Å^{-1}$ for Pd K-edge XAS. All samples were grained and pressed to pellets with a diameter of 10 mm. The obtained XAS spectra were analyzed with Rigaku REX2000 software (ver. 2.5.92). The IR measurements of samples were carried out on a PerkinElmer Spectrum 100 FT-IR spectrometer.

3. RESULTS AND DISCUSSION

Hydrogenation of MAn to SA using FA. The hydrogenation of MAn, an industrially important pathway to produce SA,[35] was chosen as the test reaction to evaluate the catalytic activity of supported mono- and bimetallic catalysts. The hydrogenation was carried out using FA as a hydrogen source. The catalytic activity was carefully investigated as a function of temperature (Table 1), time (Figure 2), and amount of FA (Table 2) in the reaction medium. At lower

temperature values (333 K), MAn could not be converted efficiently (Table 1, entry 1). The increase in temperature increased the catalytic activity; however, the use of open reactor (schlenk

Table 1. Temperature variation for MAn hydrogenation using CoPd-DDAO/AlOOH.[a]

Entry	Temperature /K	Conv.[b] /%	SA Yield[b] /%
1	333	30	22
2	353	>99	>99
3	373	>99	>99
4[c]	353	50	38

[a]Reaction conditions: Maleic Anhydride (MAn, 0.5 mmol), CoPd-DDAO/AlOOH (25 mg), FA (2 mmol), 5 h, H_2O (5 mL), Teflon lined autoclave. [b]Calculated by HPLC analysis using a calibration curve method. [c]Schlenk tube, 16 h.
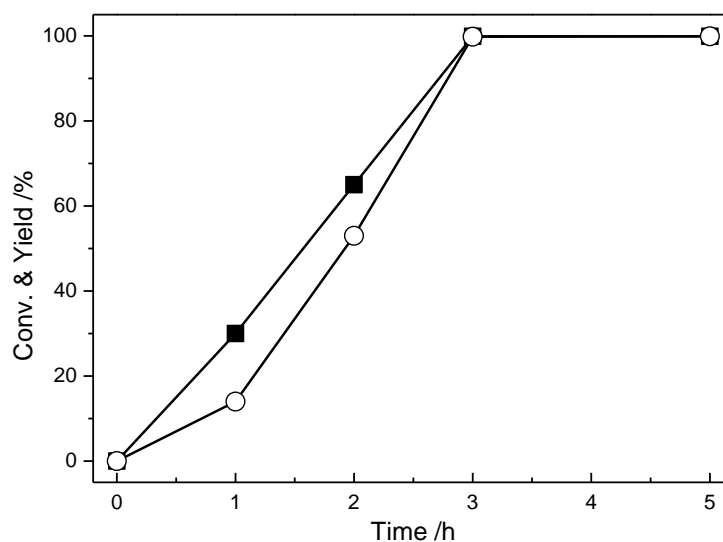
Figure 2. Time course of CoPd-DDAO/AlOOH catalyst for the hydrogenation of MAn to SA. The conversion of MAn (closed square) and yield of SA (open circle) are shown in black. *Reaction conditions*: Maleic anhydride (MAn, 0.5 mmol), Formic acid (FA, 1.9 mmol), CoPd-DDAO/AlOOH (25 mg), 353 K, H_2O (5 mL), Teflon lined autoclave.

tube) decrease the catalytic activity even at the elevated temperature (Table 1, entry 4). The reaction progressed smoothly with the progress of time and a maximum conversion were attained

[103]

after 3 h (Figure 2). In order to evaluate the dependency of the reaction rate on FA amounts, the effect of FA amounts was examined (Table 2). The reaction was found to be of second order with the reaction rate depending on both the amount of MAn and FA. On optimization, 3 h and 353 K with 1.9 mmol of FA were found to be the best reaction condition for MAn hydrogenation over the CoPd-DDAO/AlOOH catalyst.

Table 2. Effect of formic acid (FA) amount on MAn hydrogenation.[a]

Entry	FA /mmol	MAn Conv.[b] /%	SA Yield[b] /%
1	0	0	0
2	1	34.7	20
3	1.5	68.1	56.8
4	1.9	>99	>99
5	2	>99	>99

[a]Reaction conditions: Maleic Anhydride (MAn, 0.5 mmol), CoPd-DDAO/AlOOH (25 mg), H_2O (5 mL), 353 K, 3 h, Teflon lined autoclave. [b]Calculated by HPLC analysis using a calibration curve method.

As the results summarized in Table 3, DDAO capped bimetallic CoPd NPs supported on AlOOH (CoPd-DDAO/AlOOH) exhibited excellent catalytic activity for the selective hydrogenation of MAn to SA (>99% yield) (Table 3, entry 1).[45] The superiority of bimetallic CoPd catalyst was established by the experiments performed with the corresponding monometallic Pd or Co catalysts prepared by same procedure (Table 3, entries 2-3). Pd-DDAO/AlOOH possessed some catalytic activity (29% yields) for the hydrogenation reaction, whereas Co-DDAO/AlOOH catalyst failed to show any activity even after 5 h of reaction time.

To elucidate the novelty of DDAO capping agent, CoPd catalysts with/without other commonly known capping agents were also prepared with the same procedure. From our previous studies on

[104]

use of capping agents, I selected cationic CTAB surfactant[13] and PVP polymer[16] to compare the

activity with DDAO capped CoPd catalyst. As shown in entries 5-6 in Table 3, however, both

CoPd catalysts capped with CTAB or PVP hardly facilitated the hydrogenation reaction with FA

(ca. 35% yields). Fumaric acid was observed as the only by-product in some of the catalytic

hydrogenations of MAn under my reaction conditions.

Table 3. Hydrogenation of Maleic anhydride using formic acid.[a]

maleic anhydride (MAn)   succinic acid (SA)
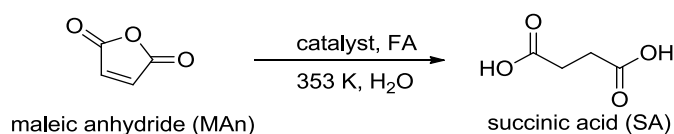
Entry	Catalyst	t /h	Co[b] /wt%	Pd[b] /wt%	Conv.[c] /%	Yield[c] /%
1	CoPd-DDAO/AlOOH	3	0.75, 0.71[d]	2.53, 2.52[d]	>99, >99[d]	>99, >99[d]
2	Pd-DDAO/AlOOH	5	0	2.64	40	29
3	Co-DDAO/AlOOH	5	1.02	0	0	0
4	CoPd/AlOOH	3	0.94, 0.39[e]	2.44, 2.41[e]	72	56
5	CoPd-CTAB/AlOOH	3	0.63	2.49	52	36
6	CoPd-PVP/AlOOH	3	0.55	2.51	49	35
7	Pd/Al$_2$O$_3$ (comm)	3	0	5[f]	98	74
8	AlOOH	3	0	0	0	0
9	blank	3	0	0	0	0
10[g]	CoPd-DDAO/AlOOH	3	0.75	2.53	0	0
11[h]	CoPd-DDAO/AlOOH	3	0.75	2.53	>99	98

[a]Reaction conditions: Maleic anhydride (MAn, 0.5 mmol), Formic acid (FA, 1.9 mmol), Catalyst (25 mg), 353 K, H$_2$O (5 mL), Teflon lined autoclave. [b]Determined by ICP-AES analysis. [c]Calculated by HPLC analysis using a calibration curve method. [d]5th catalytic run. [e]After 1st catalytic run. [f]Quoted from manufacturer's product specifications. [g]Without FA. [h]0.15 mmol of 2,6-di-*tert*-butyl-*p*-cresol was used as a radical scavenger.

The real amounts of Co loading were in the range of 0.55-1.02 wt% which were much lower

than the theoretical value (2.5 wt%) in all catalysts including Co element (Table 3, entries 1 and

3-6). The molar compositions of the capped CoPd catalyst by ICP-AES analysis were found to be $Co_{0.23}Pd_{0.77}$-DDAO/AlOOH (*i.e.* 0.75 wt% Co and 2.53 wt% Pd loading), $Co_{0.20}Pd_{0.80}$-CTAB/AlOOH, and $Co_{0.18}Pd_{0.82}$-PVP/AlOOH, respectively. The loading amount of Co seems to be inefficient to explain the differences in catalysis.
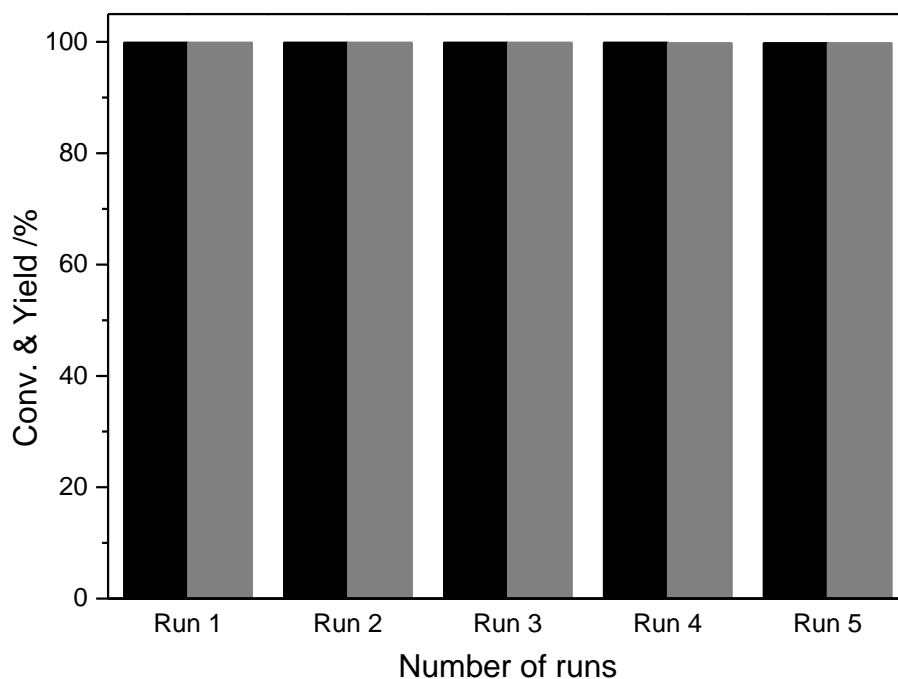
Figure 3. Reusability graph of CoPd-DDAO/AlOOH catalyst for the hydrogenation of MAn to SA. The conversion of MAn and yield of SA are shown in black and gray column, respectively. *Reaction conditions*: Maleic anhydride (MAn, 0.5 mmol), Formic acid (FA, 1.9 mmol), CoPd-DDAO/AlOOH (25 mg), 353 K, 4 h, H_2O (5 mL), Teflon lined autoclave.

On the other hand, the non-capped CoPd catalyst, $Co_{0.28}Pd_{0.72}$/AlOOH estimated by ICP-AES, had considerable activity (56% yield) for the 1st run with high Co loading (Table 3, entry 4). However, a significant cobalt leaching was observed after the 1st catalytic cycle; *i.e.* initial loaded amount of Co (0.94 wt%) was drastically decreased to 0.39 wt% (Table 3, entry 4e). Thus, Co species were hardly preserved on catalyst surface during reaction without any capping agent. In

other words, this result established the efficient capability of DDAO to retain metal species on AlOOH during catalytic runs.

The 5 wt% Pd/Al_2O_3 (commercial catalyst) afforded high conversion (98%) owing to the high Pd amount with moderate SA yields (74%) (Table 3, entry 7). The reaction could not progress in the absence of Pd at all (Table 3, entries 3, 8, 9), indicating that the Pd species acted as the active center for the catalysis. Without FA (hydrogen source), the reaction did not proceed (Table 3, entry 10). Notably, the CoPd-DDAO/AlOOH catalyst retained high catalytic activity even after the 5th run of hydrogenation (entry 1 in Table 3, and Figure 3). It was ascertained that the CoPd-DDAO/AlOOH preserved similar composition as $Co_{0.22}Pd_{0.78}$-DDAO/AlOOH (*ie.* 0.71 wt% Co and 2.52 wt% Pd loading) even after 5th runs (entry 1d).
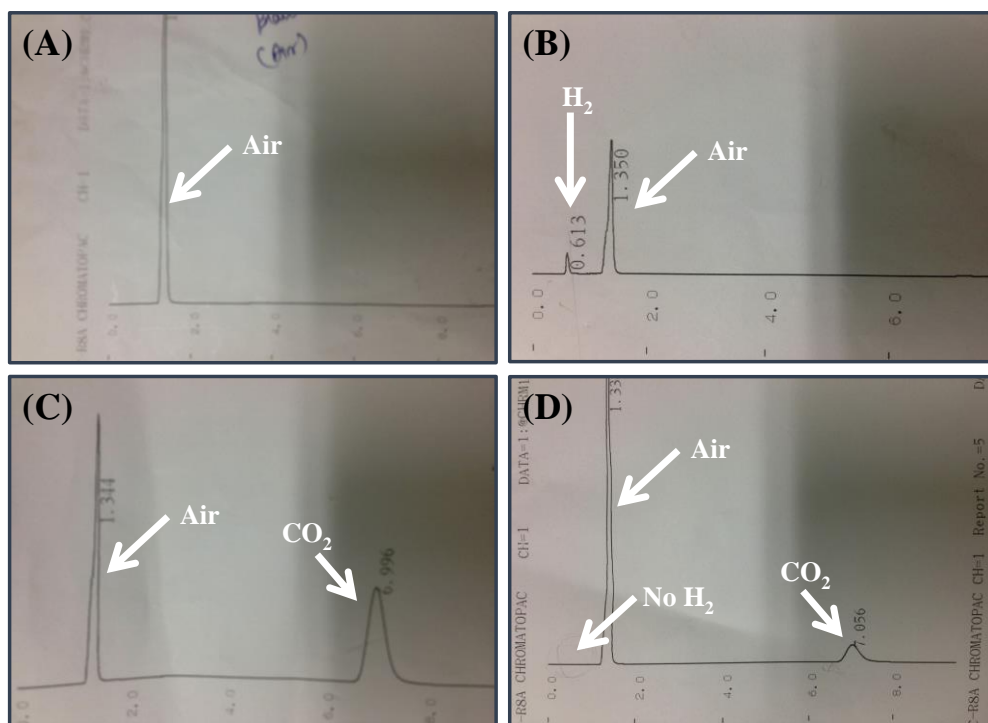

Figure 4. Gas chromatograph of (A) Blank/Air, (B) Pure hydrogen, (C) Pure carbon dioxide, and (D) After 1 h of stirring of aqueous solution of FA with CoPd-DDAO/AlOOH at 353 K.

To understand the nature of FA dissociation and clarify the reaction pathway over CoPd-DDAO/AlOOH, a radical scavenger was added into the reaction mixture. The result in Table 3 (entry 11) declined the influences of radical scavenger (2,6-di-*tert*-butyl-*p*-cresol, 0.15 mmol) on the hydrogenation of MAn using FA over the CoPd-DDAO/AlOOH catalyst. These results ruled out the possibility of any radical intermediate (hydrogen radical or carbon-centered free radical) within the reaction medium. Additionally, the gaseous product after treatment of only FA (without MAn) with the CoPd-DDAO/AlOOH were collected and analyzed by gas chromatography (GC-TCD, an active carbon column). Although a peak corresponding to CO_2 was detected, no signals for H_2 appeared in the GC chart (Figure 4). The dissociation of FA to CO_2 by dehydrogenation pathway[20] and the presence of adsorbed hydrogen as ionic species in the reaction medium were proposed by these observations.

TEM analyses of CoPd-capping/AlOOH. TEM was measured to characterize the bimetallic CoPd NPs. Figure 5 shows a typical TEM images and particle size distribution of capped or non-capped bimetallic CoPd NPs on AlOOH. Well-dispersed and well-shaped NPs were obtained for all catalysts. Interestingly, the DDAO capped bimetallic CoPd NPs exhibited a wider particle size distribution with an average diameter of 6.4 nm than those of other bimetallic CoPd NPs. CTAB capped CoPd NPs afforded the biggest size of 7.5 nm whereas non-capped CoPd NPs had the lowest size of 5.5 nm in average diameter of the particles. PVP capped CoPd NPs exhibited the middle average particle size of 6.2 nm among them. These results suggest that the formation process and/or the growth rate of bimetallic CoPd NPs is varied with the co-existence of capping agents under the hydrothermal conditions. The TEM images and size distribution of CoPd-DDAO/AlOOH after 5th catalytic run were similar to that of the fresh catalyst, demonstrating the stability of the catalyst capped with DDAO.
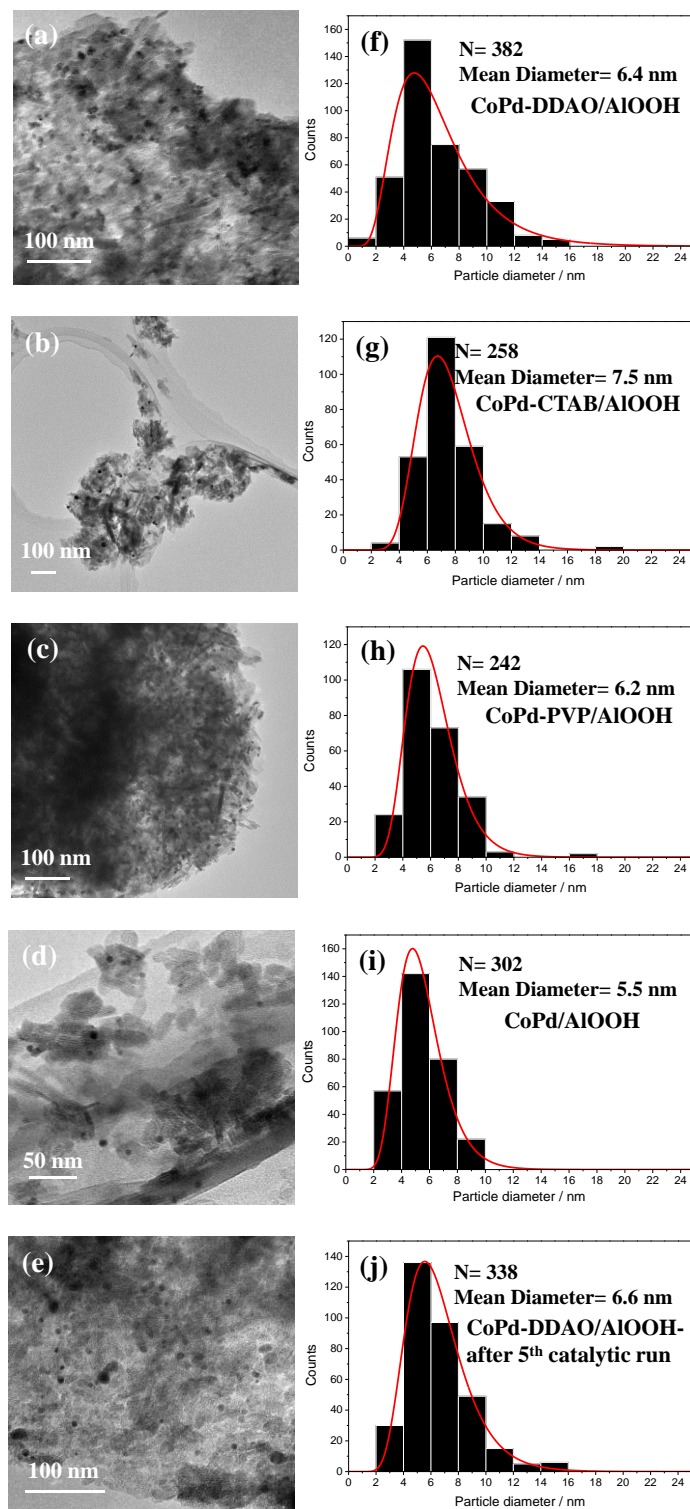
Figure 5. TEM images (a-e) and particle size distributions (f-j) of CoPd-DDAO/AlOOH (a,f), CoPd-CTAB/AlOOH (b,g), CoPd-PVP/AlOOH (c,h), CoPd/AlOOH (d,i), and CoPd-DDAO/AlOOH-after 5th catalytic run (e,j).
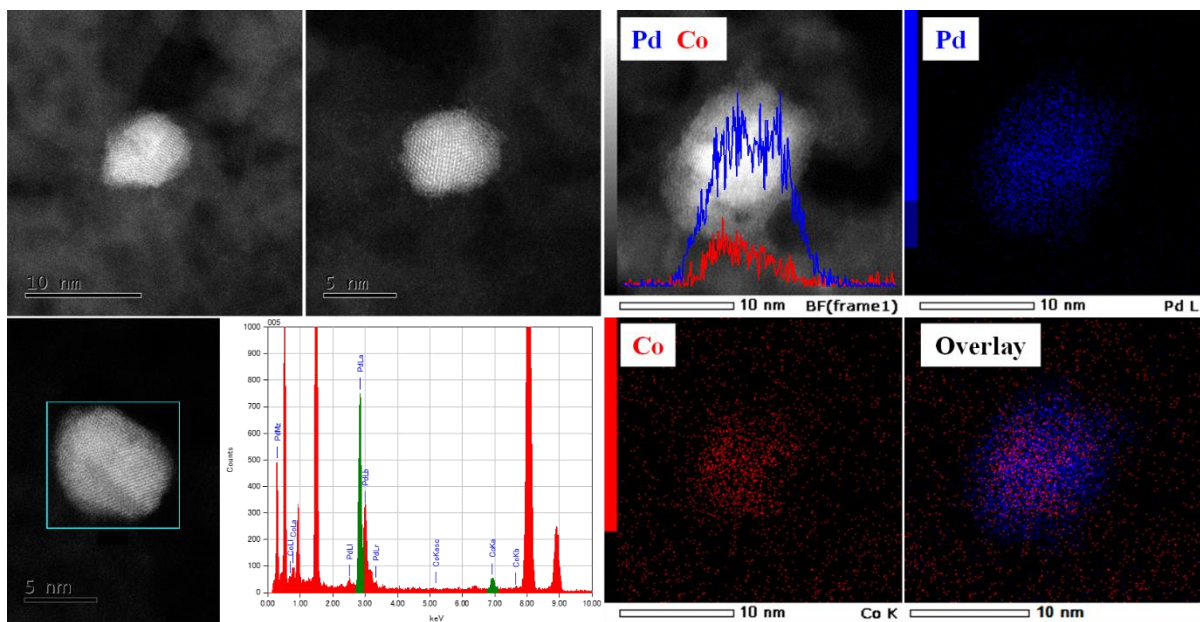
Figure 6. HAADF-STEM images of CoPd-DDAO/AlOOH with an EDS elemental mapping.

The HAADF-STEM images shown in Figure 6 revealed the crystalline nature of CoPd-DDAO/AlOOH catalyst. The compositional mapping was done by STEM-EDS mapping and HAADF-STEM techniques. The inspection of the elemental mapping image shows the uniform distribution of Co and Pd elements within bimetallic CoPd NP with higher concentration of Pd in it. HAADF-STEM line analysis shown in Figure 6 suggests the composition is $Co_{0.1}Pd_{0.9}$. Similar results in elemental mapping images were observed at various places designating the homogeneity of the bimetallic CoPd NPs (consistent compositional distribution within each NP) throughout the catalyst structure. The existence of bimetallic CoPd NPs over the AlOOH surface as alloy is substantiated by the electron microscopy. At some places darker and brighter regions were observed in NP, however, the line analyses declined the formation of core-shell structure. While, the composition of NP estimated by STEM-EDS line analyses ($Co_{0.1}Pd_{0.9}$) differed from that of the ICP-AES analysis of catalyst ($Co_{0.23}Pd_{0.77}$) results. It implied that the $Co_{0.23}Pd_{0.77}$-DDAO/AlOOH catalyst was composed by not only the CoPd-alloy NPs with high concentration

[110]

of Pd but also the isolated Co species, though the latter hardly exhibited any activity for the reaction (see Table 3, entry 3). Neither large sized isolated CoO_x particles nor particles with high Co composition were observed by microscopic analyses. To account for such differences, more detailed investigations of the CoPd-DDAO/AlOOH were carried out by other spectroscopic methods.
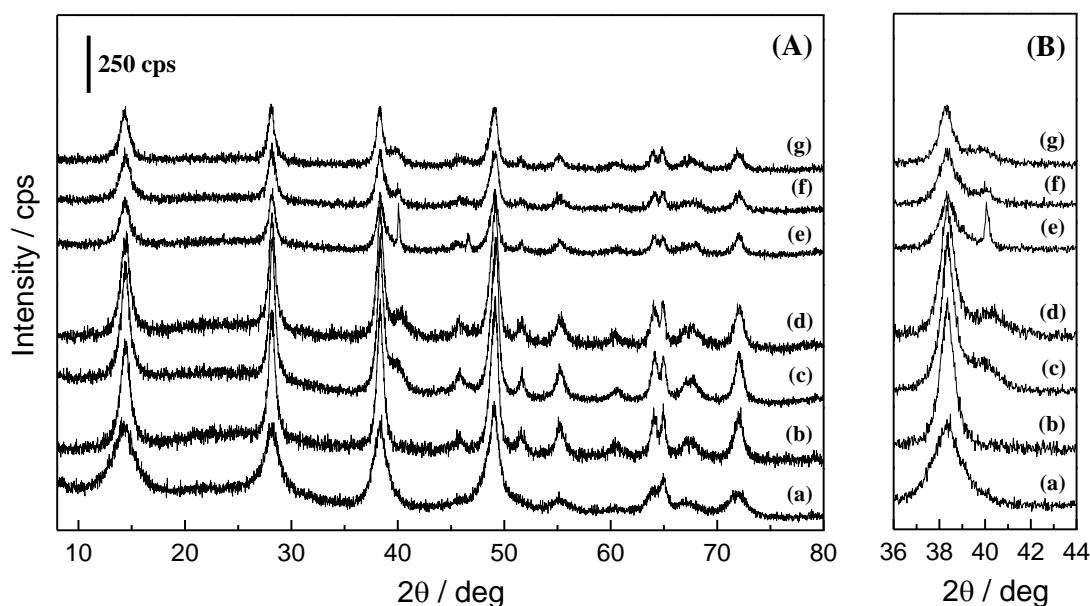
Figure 7. XRD patterns (A) in the range of 8-80° and (B) with emphasized detail in the range of 36-44° of (a) AlOOH, (b) Co-DDAO/AlOOH, (c) Pd-DDAO/AlOOH, (d) CoPd-DDAO/AlOOH, (e) CoPd-CTAB/AlOOH, (f) CoPd-PVP/AlOOH, and (g) CoPd/AlOOH.

XRD patterns of CoPd-capping/AlOOH. To get more insights of the bimetallic CoPd alloy, the X-ray diffraction patterns (XRD) were obtained for CoPd-capping/AlOOH catalysts and patterns for various AlOOH supported monometallic and bimetallic catalysts are shown in Figure 7A. Diffraction patterns of AlOOH structure appeared at $2\theta = 14.04°, 28.36°, 38.42°, 49.06°, 55.14°,$ 64.94°, and 71.84° for all catalysts. No diffraction signals corresponding to CoO or Co_3O_4 were found in all samples. It indicates that either these species were absent or the crystalline sizes of

[111]

isolated Co species were too small to be detected by the XRD. At 2θ value around 40°, the bimetallic CoPd NPs catalyst showed a diffraction peak at higher 2θ values in comparison to Pd-DDAO/AlOOH (Figures 7c-g). The area $2\theta = 36\text{-}44°$ is shown as Figure 7B to highlight the differences in monometallic and bimetallic catalysts. The similar shift for the (111) lattice spacing of the CoPd (also observed as striped pattern for the closed packing plane of the fcc structure in TEM) had been reported earlier.[31,46] The shift in diffraction peak for the bimetallic nanostructure could be explained in terms of d-d bonding and the s-d charge transfer effects as reported for other bimetallic systems such as Ni/Pt, Pd/Au and Pd/Ag.[47-48]

An intense line corresponding to CoPd in XRD pattern of CoPd-CTAB/AlOOH (Figure 7e) imply the presence of large crystals of the bimetallic CoPd particles (crystalline size in (111) phase is estimated to be 49.4 nm), though these were hardly observed in TEM analysis. It is also shown that the CoPd-DDAO/AlOOH has stable structure under the reaction condition; similar electron micrographs (Figure 5e and j) and XRD patterns (Figure 8) are obtained even after 5th catalytic run of the MAn hydrogenation.
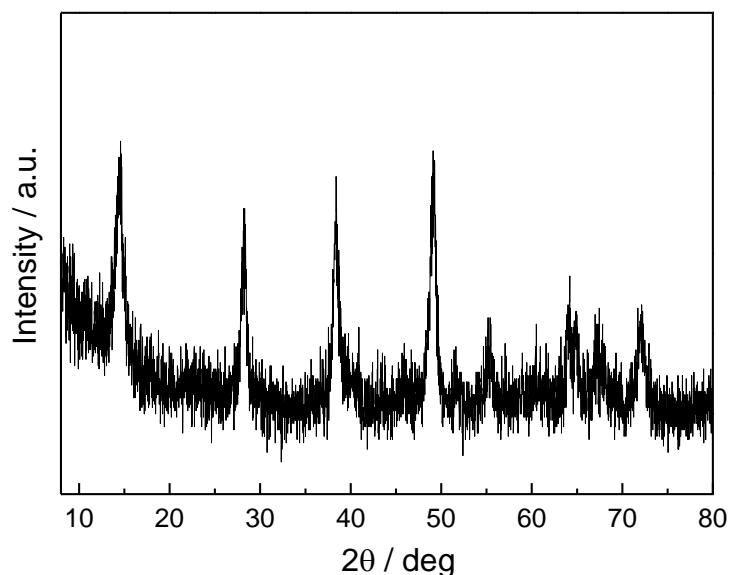
Figure 8. XRD patterns of CoPd-DDAO/AlOOH after 5th catalytic run.

[112]

XPS of supported CoPd catalysts. XPS measurements were employed to investigate the oxidation states of Co and Pd species and the effect of alloying on each. In Figure 9A, Pd 3d states of various catalysts are shown, where the Pd $3d_{5/2}$ spectral lines were observed at around 334 eV. A significant negative shift in the binding energy values for all catalysts was noticed in comparison to pure palladium (bulk Pd $3d_{5/2}$ 335.1 eV).[49-53] The binding energies of Pd 3d in these catalysts are attributed to the electron-rich metallic state of palladium as they were much lower than the palladium oxide (bulk PdO $3d_{5/2}$ 337.0 eV).[49-53] In the cases of bimetallic CoPd catalysts, the negative shifts in binding energy supposedly indicate the electron transfer phenomenon from Co to Pd in CoPd NP which is in agreement with the Pauling's electronegativities of Pd (2.2) and Co (1.88).
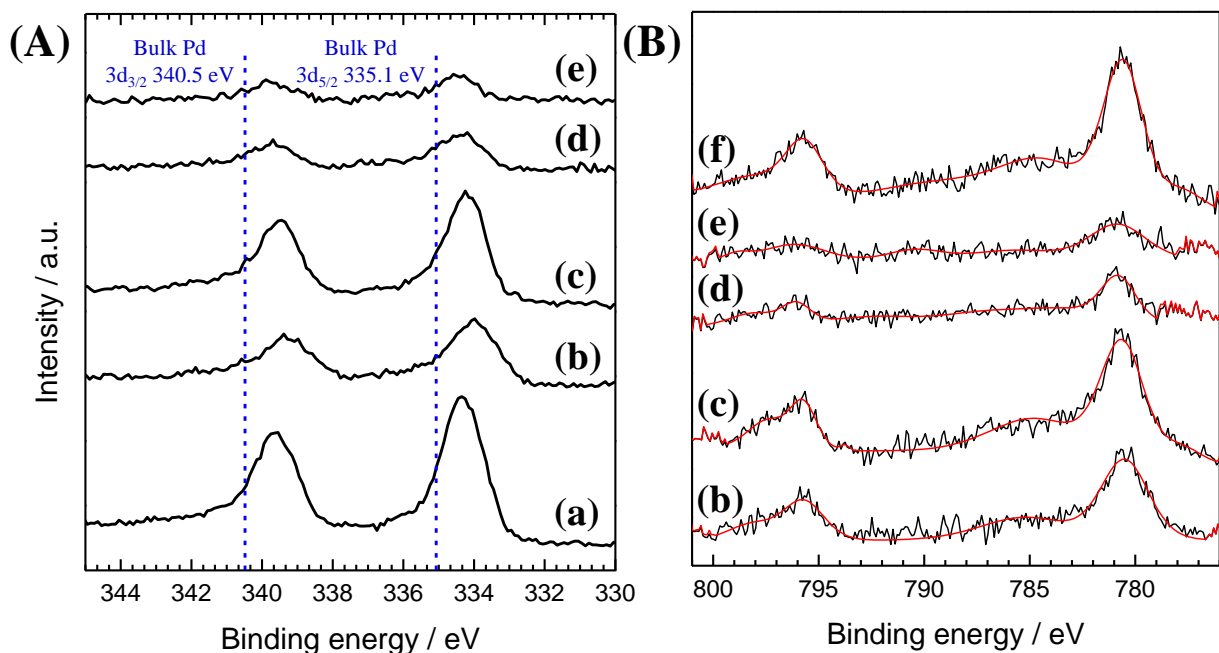
Figure 9. (A) Pd 3d states and (B) Co 2p XPS of (a) Pd-DDAO/AlOOH, (b) CoPd/AlOOH, (c) CoPd-DDAO/AlOOH, (d) CoPd-PVP/AlOOH, (e) CoPd-CTAB/AlOOH and (f) Co-DDAO/AlOOH catalysts. Due to the poor signal to noise ratio, the peaks were hardly realized, and thus the peak was shaped by a synthetic peak using Gaussian-Lorentzian product formula (GL30) shown in red line.

[113]

Additionally, from comparison in capped and non-capped bimetallic CoPd catalyst, the lowest binding energy value (334.0 eV) of non-capped bimetallic CoPd catalyst (CoPd/AlOOH) could be distinguished from other capped bimetallic CoPd catalysts, where the energy in $3d_{5/2}$ position increased in order from CoPd-DDAO/AlOOH (334.2 eV), CoPd-PVP/AlOOH (334.4 eV) and CoPd-CTAB/AlOOH (334.5 eV). The higher binding energies of the capped CoPd catalysts than the non-capped CoPd/AlOOH would be accounted by the synergistic effect owing to capping coordination. When the capping coordinates to metal NP, the electron donation from capping to coordinated metal is expected. Because it may enhance the negative flow onto Pd atoms in bimetallic CoPd NP, back donation from d states in Pd towards neighbor Co and/or capping agent (CTAB, PVP and DDAO) occurs. These synergistic phenomena supposedly determine the back shifts in capped CoPd catalysts to higher energy side in binding energy rather than non-capped CoPd catalyst. Among the three capped CoPd catalysts, DDAO capping agent favored an electron rich Pd in CoPd NP. However, as observed in Figure 9A, the peak in $3d_{5/2}$ for the DDAO capped monometallic Pd catalyst (Pd-DDAO/AlOOH, 29% yield) appeared at 334.3 eV which is little higher than bimetallic CoPd-DDAO/AlOOH (334.2 eV) possessing higher catalytic activity (>99% yield). Thus, further effect of co-existence of Co in bimetallic CoPd catalysts needs to be discussed (*vide infra*).

It was expected by XPS of Co 2p that the cobalt in catalysts existed as oxide (namely CoO and Co_3O_4) instead of metallic cobalt. In a typical case of the CoPd-DDAO/AlOOH, Co $2p_{3/2}$ was observed in the region of 780.2-780.9 eV (Figure 9B) which are consistent with the binding energies for cobalt oxides (bulk CoO $2p_{3/2}$ 780.6 eV and bulk Co_3O_4 780.7 eV).[54-56] The absence

of widely-used reducing agent such as H_2 during the synthetic process of CoPd catalysts is supposed to be as one of the reason for the presence of cobalt oxide.

In addition, much peak broadenings for the CoPd-CTAB/AlOOH and CoPd-PVP/AlOOH were observed in both Pd 3d and Co 2p XPS results, it could be due to the following two reasons: (a) various oxidation states of Pd and/or Co species, and/or (b) change in electronic density on the Pd and/or Co states. Thus, it is suggested that CTAB and PVP capped CoPd catalysts possessed various states in Co and Pd rather than DDAO capped CoPd catalyst.

On the basis of the above observations, I tentatively summarize that the CoPd-DDAO/AlOOH included these novel points: 1) the active CoPd alloy NPs were formed more uniformly (*i.e.*, with fewer variation of species than other capped CoPd), 2) the more electron rich Pd atoms were kept on the AlOOH (rather than other capped CoPd), 3) the more stable Co species in CoPd alloy was produced (rather than non-capped CoPd), leading to the highest activity for the hydrogenation of MAn using FA.

XAS analyses of CoPd catalysts. XAS has been recognized as a powerful technique for detailed inspection of electronic states and structure of nanomaterials.[43,57-60] XAS experiments were, therefore, conducted for bimetallic CoPd catalysts to further clarify the nanostructure and electronic interactions induced by capping agent. Figure 10 represent X-ray absorption near edge structure (XANES) of the catalysts and references (metal foils, oxides and salts) at Pd K-edge and Co K-edge. The Pd K-edge XANES features of all catalysts (Figure 10A) were similar to that of Pd foil, indicating the presence of zero valent Pd as the dominant state in the catalysts. In accordance with XPS of Co 2p, the Co K-edge XANES (Figure 10B) had close resemblance to the cobalt oxides and was much different from the Co foil.
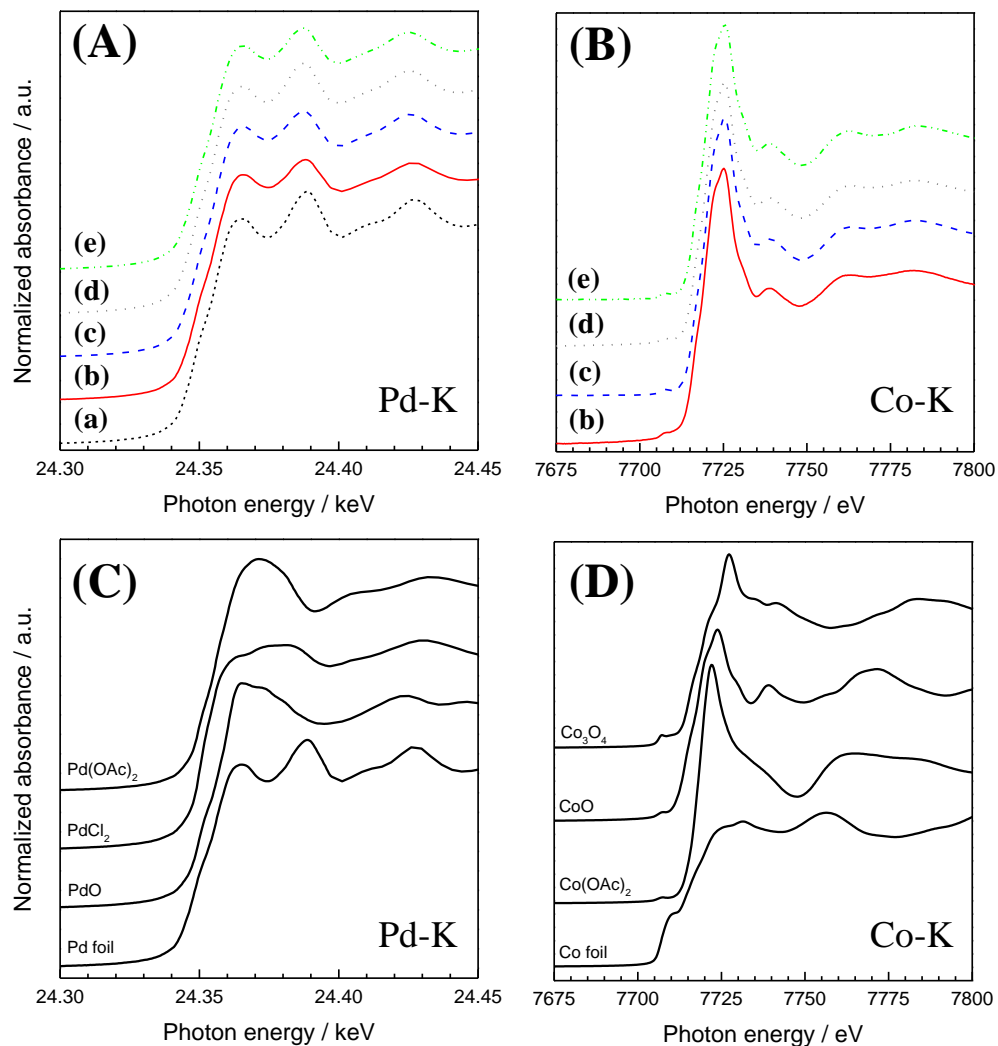
Figure 10. (A) Pd K-edge and (B) Co K-edge XANES spectra of (a) Pd foil, (b) CoPd-DDAO/AlOOH, (c) CoPd/AlOOH, (d) CoPd-CTAB/AlOOH, and (e) CoPd-PVP/AlOOH catalysts. (C) Pd K-edge and (B) Co K-edge XANES of references.

The L-edge XANES, being electric-dipole allowed transition (p→d), affords more intense and high-resolution observations.[57,61-62] The most prominent feature in the Pd L-edge XANES is the white-line (WL) at around 3175 eV, observed due to the excitation of electrons from the degenerate 2p states to the 4d band.[57,61-62] The intensity of the WL is proportional to the number of holes in the nd valence band of the transition metal species. It has also been understood that as the

hybridization of the d state becomes weaker, the peak at L_3 threshold is enhanced.[61-62] The Pd L_3-edge XANES of bi-metallic catalysts are included as Figure 11. In all samples, their heights were higher than Pd black (Pd metal), and thus the partial oxidation on NP by air or capping coordination and/or the stronger hybridization phenomenon in Pd states in each sample were expected. The CoPd-CTAB/AlOOH displayed the lowest WL intensity among all bimetallic catalysts. The WL intensity profile for CoPd-PVP/AlOOH, CoPd-DDAO/AlOOH and CoPd/AlOOH were close to
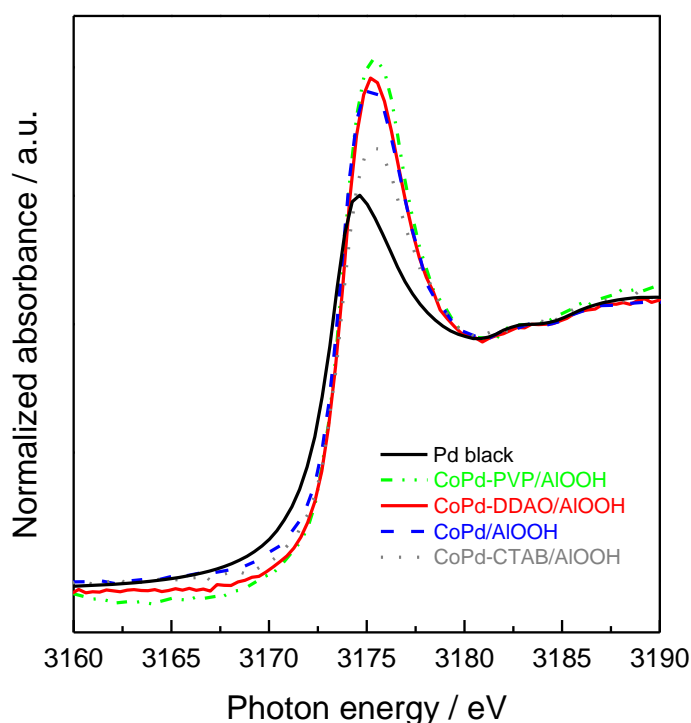
Figure 11. Pd L_3-edge of Pd black and various bimetallic CoPd catalysts.

each other lying above CoPd-CTAB/AlOOH catalyst. These suggested that the order of electron density in Pd 4d state is CoPd-CTAB/AlOOH > CoPd/AlOOH > CoPd-DDAO/AlOOH > CoPd-PVP/AlOOH. The tendency among non-capped and DDAO or PVP capped CoPd/AlOOH nicely supported the XPS results in Pd 3d states. Thus, the proposed synergistic phenomena among Co, Pd and capping agent described in XPS section were also supported here. The CTAB capped

CoPd/AlOOH catalyst demonstrated the highest electron density on Pd 4d. Because of the large CoPd crystallites observed in XRD patterns, the surface CTAB cappings in CoPd-CTAB/AlOOH seems to have a little influence on CoPd alloy. So, the electron density profile of CoPd-CTAB/AlOOH in Pd L_3-edge XANES (which includes average information in the sample) differed significantly from that in Pd 3d XPS (selectively showing surface information).

To understand the detailed structure, I further discuss the EXAFS of these catalysts in both Pd-K and Co-K edge. The EXAFS at Pd K-edge and the FT of k^3-weighted Pd K-edge EXAFS could be hardly distinguished for all catalyst, and were similar to Pd metal in all cases (Figure 12). This is because of high concentration of Pd in CoPd alloy NP leading to small information of Pd-Co interaction in Pd XAS measurements. On the other hand, the Co K-edge EXAFS would be much informative about the Co-Pd interactions owing to the low concentration of Co in bimetallic CoPd NPs. As shown in Figure 13, the Co K-edge EXAFS of bimetallic CoPd catalysts showed
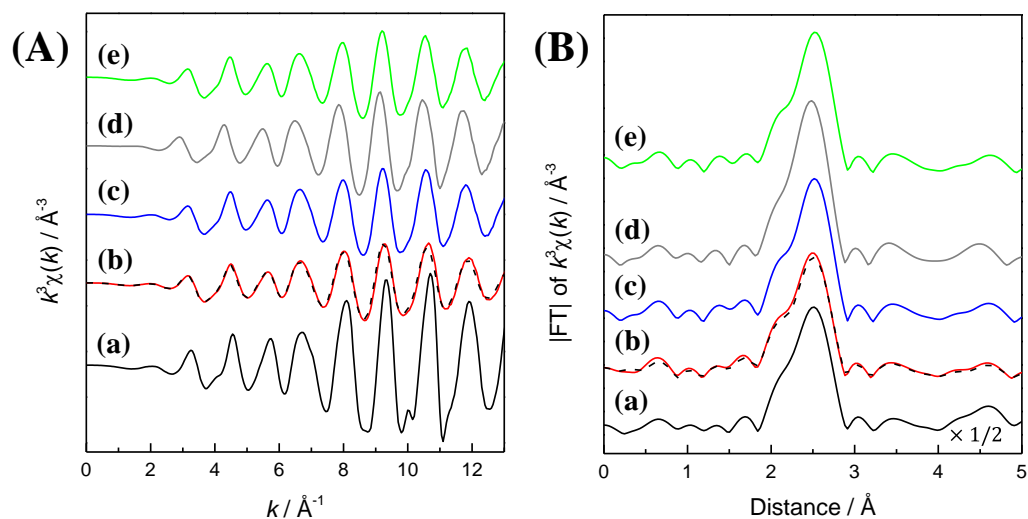
Figure 12. Pd K-edge (A) EXAFS and (B) FT of k^3-weighted EXAFS of (a) Pd foil, (b) CoPd-DDAO/AlOOH (fresh in red, and after 5th run of hydrogenation in black dashed line), (c) CoPd/AlOOH, (d) CoPd-CTAB/AlOOH, and (e) CoPd-PVP/AlOOH.
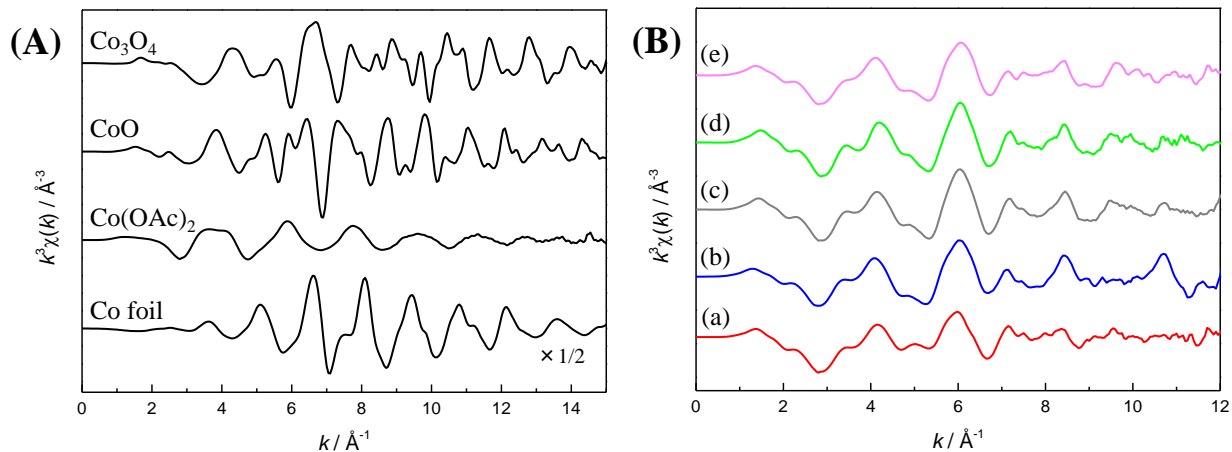
Figure 13. k^3-weighted EXAFS at Co K-edge of (A) references and (B) Various CoPd catalysts; (a) CoPd-DDAO/AlOOH, (b) CoPd/AlOOH, (c) CoPd-CTAB/AlOOH, and (d) CoPd-PVP/AlOOH.

significantly different oscillations from CoO and Co_3O_4, though they had large similarity with CoO in XANES area (Figure 10). Such marked differences in the EXAFS oscillations from that of the oxide species is a strong proof that there was not only the isolated CoO_x species but also the alloying of Co species with Pd and/or further variety in bimetallic CoPd catalysts.

The FT of k^3-weighted Co K-edge EXAFS of three capped bimetallic CoPd catalysts displayed two broadening peaks (Figure 14). In the previous literature,[31] CoPd-alloy showed a peak at 2.1 Å with a shoulder at 1.6 Å in FT of Co-K edge. Though the PVP and DDAO capped CoPd catalysts had peaks around at 2.35 Å, it seemed hard to discuss their origin from the FTs at this stage. The FTs of CoPd-DDAO/AlOOH and CoPd-PVP/AlOOH were much different from that of CoPd-CTAB/AlOOH catalyst which had peaks at lower distances. Additionally, the non-capped bimetallic CoPd catalyst, on which the XRD patterns suggested the presence of CoPd-alloy, showed three distinct peaks at 1.44 Å, 1.98 Å and 2.72 Å. These results implied that each bimetallic CoPd catalysts (capped and non-capped) differed in phases and/or coordination around Co, however, further distinction in FT had large problem owing to poor information of possible

variation and low concentration of Co species in the catalysts. The detailed study of the structural analysis of the NPs will be published elsewhere in near future.
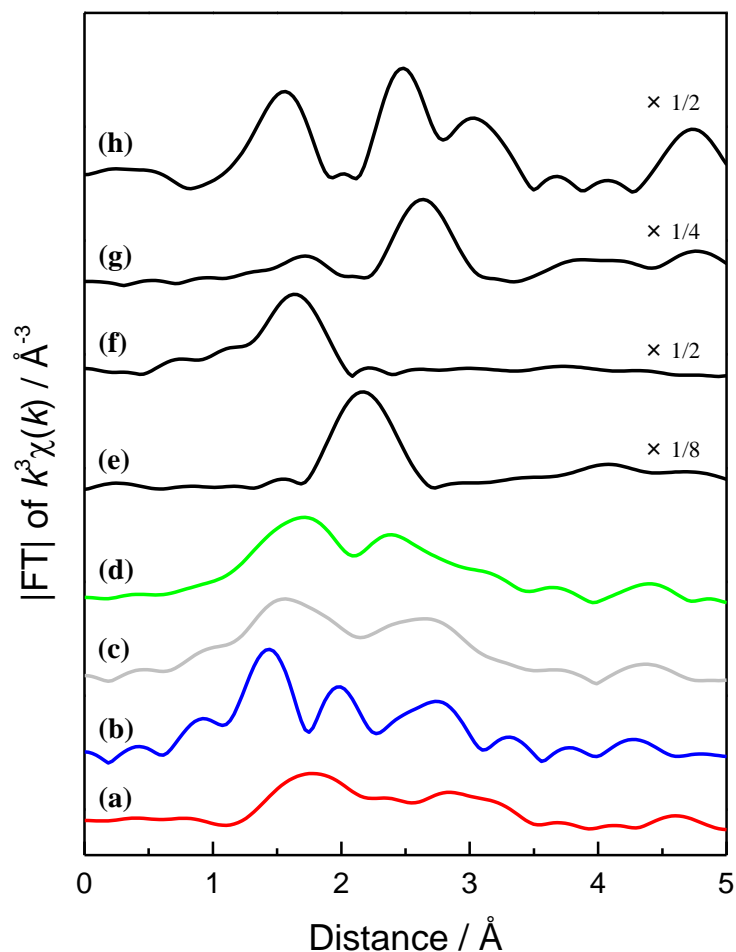
Figure 14. FT of k^3-weighted EXAFS at Co K-edge XAS of (a) CoPd-DDAO/AlOOH, (b) CoPd/AlOOH, (c) CoPd-CTAB/AlOOH, (d) CoPd-PVP/AlOOH, (e) Co foil, (f) Co(OAc)$_2$, (g) CoO, and (h) Co$_3$O$_4$.

Mechanistic considerations. According to the work by Yoo et al.,[20] I propose that the CoPd-DDAO/AlOOH decomposed FA through dehydrogenation pathway via adsorbing FA on oxophilic Co (*vide supra*) and enhancing the rate of FA dissociation. Another theoretical approach by Pallassana et al. for the hydrogenation of MAn, proposed the adsorption of MAn in a more favorable di-σ conformation onto the catalyst surface.[63-64] This is supported by IR measurements

[120]

carried out before and during the reaction to observe the adsorption and thereby the ring opening of MAn into a di-acid on the catalyst surface (Figure 15). Because of the differences in the electronic charges on the surface of bimetallic CoPd-DDAO/AlOOH catalyst and the modification in the Pd-Pd bond distance owing to the insertion of Co into the catalyst structure, a better alignment of the surface Pd atoms for improved overlap between the metal d-orbitals and the π-orbitals of the carbonyl group is expected.[63] Such geometric effect decreased the adsorption energy and hence the CoPd-DDAO/AlOOH shows enhanced rate of the hydrogenation. These results also suggested that the reaction proceeded over catalyst surface as proposed in Figure 16.

In the reaction progress, FA adsorbs on the surface of the CoPd-DDAO/AlOOH catalyst and CO_2 is released. Because of the differential charge on the CoPd-DDAO/AlOOH (*vide supra*) the
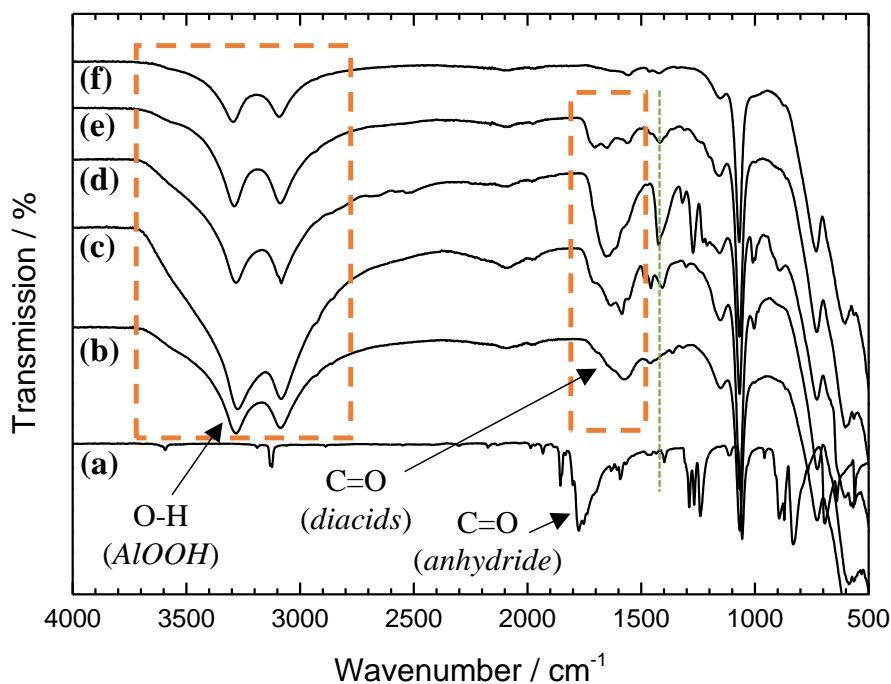
Figure 15. Infrared spectroscopy of (a) MAn, (b) Maleic acid adsorbed on CoPd-DDAO/AlOOH, (c) Succinic acid adsorbed on CoPd-DDAO/AlOOH, (d) Fumaric acid adsorbed on CoPd-DDAO/AlOOH, (e) CoPd-DDAO/AlOOH-after 1 h of MAn hydrogenation, and (f) CoPd-DDAO/AlOOH.

[121]

hydride dwells on electron deficient Co species and Pd, being electron rich, adsorbs the proton (see Figure 16). Simultaneously, MAn attaches to the CoPd surface through di-σ conformation.[63] The ring opens up in water into a di-acid form and the proton from the Pd atom is transferred to the C=C. The dashed green line (in Figure 15) highlights the similarity between the IR spectra of succinic acid and fumaric acid (proposed intermediate during the hydrogenation of MAn) with the IR spectra of CoPd-DDAO/AlOOH-after 1 h of MAn hydrogenation. Again, another hydrogen is transferred to the other carbon to finally produce SA and regenerate active catalyst. The rate of MAn hydrogenation was found to vary as a function of concentration of both MAn and FA, indicating the competitive adsorption between them. In accordance with the previous study,[6] I propose the adsorption/dissociation of MAn and/or FA on the catalyst surface as the rate-
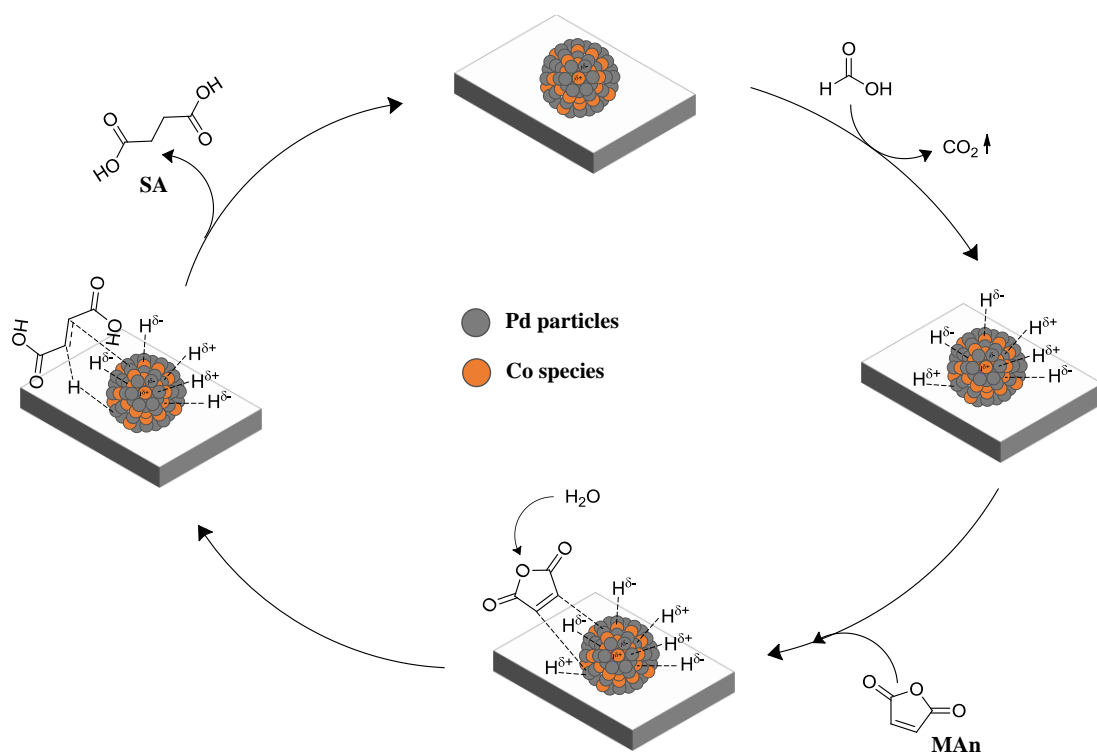
Figure 16. Proposed pathway for the hydrogenation of MAn over CoPd-DDAO/AlOOH using FA as a hydrogen source.

determining step in this catalysis. These results are in agreement with the activity profiles of CoPd catalysts and also explains the high catalytic activity of the CoPd-DDAO/AlOOH. The presence of electron-rich Pd (and oxophilic Co) in the CoPd-DDAO/AlOOH accelerated the adsorption and thereby dissociation of FA under the reaction conditions, and thus an efficient catalysis was observed.

Direct utilization of glucose as a hydrogen source over CoPd-DDAO/AlOOH. My previous efforts have succeeded in the effective production of FA from glucose using the CuCTAB/MgO catalyst.[13] The fruitful outcome of hydrogenation using the CoPd-DDAO/AlOOH catalyst motivated me to combine the two reactions as a one-pot two-step strategy (Table 4). The strategy focused on the synthesis and utilization of FA in the same reaction flask. I elucidated that the filtration of the Cu catalyst after step 1 and maintaining the temperature at 393 K for hydrogenation could utilize glucose as a hydrogen source yielding 8% SA after 3 h of the reaction (Table 4).

Table 4. One-pot utilization of biomass derived FA for MAn hydrogenation reaction.[a]

OH
HO
HO
OH OH
D-glucose

CuOx-CTAB/MgO
30% H_2O_2 (aq.)
(*Step 1*)

O
H OH
formic acid (FA)

O O O
maleic anhydride (MAn)

CoPd-DDAO/AlOOH
(*Step 2*)

O
HO OH
O
succinic acid (SA)
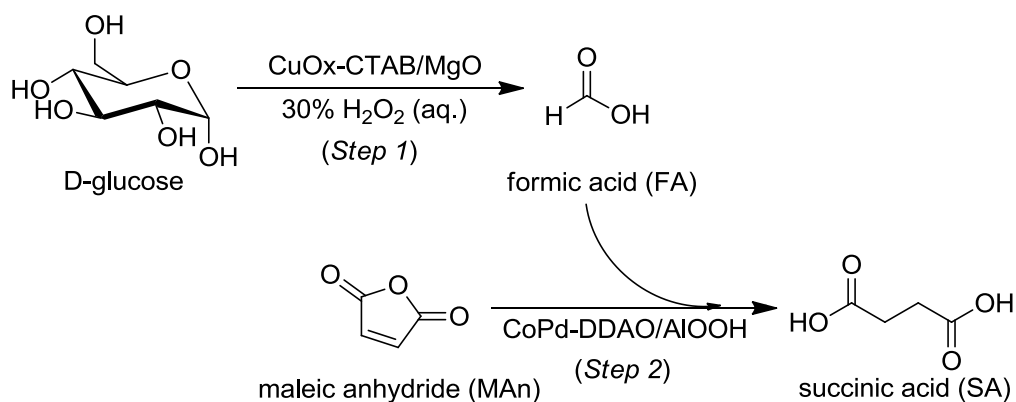
Entry	Catalyst		FA	MAn	SA
	Step 1	Step 2	Yield /%[b]	Conv. /%[b]	Yield /%[b]
1	Cu-CTAB/MgO	None	54.6	0	0
2	None	CoPd-DDAO/AlOOH	4.5	0	0
3	Cu-CTAB/MgO + CoPd-DDAO/AlOOH	None	6.2	0	0
4	Cu-CTAB/MgO	CoPd-DDAO/AlOOH	49.9	0	0
5[c]	Cu-CTAB/MgO	CoPd-DDAO/AlOOH	42.7	2.4	0
6[d]	Cu-CTAB/MgO	CoPd-DDAO/AlOOH	40.0	3.1	1.6
7[c,d]	Cu-CTAB/MgO	CoPd-DDAO/AlOOH	38.9	8.9	7.8

[a]Reaction conditions: **Step 1**: Glucose (0.5 mmol), Catalyst (60 mg), 30% H_2O_2 (4 mmol), H_2O (5 mL), Ar (0.4 MPa), 393 K, 6 h. **Step 2**: MAn (0.5 mmol), Catalyst (25 mg), 353 K, 3 h. [b]Conversion and yields were estimated by HPLC after Step 2. [c]393 K for Step 2. [d]The Cu catalyst was removed by centrifugation and filtration.

4. CONCLUSIONS

The CoPd-DDAO/AlOOH catalyst was prepared under a hydrothermal condition in the presence of *N,N*-dimethyldodecylamine *N*-oxide (DDAO) without any widely-used reducing agent. The DDAO capped bimetallic CoPd catalyst not only exhibited higher activity than the corresponding

monometallic or bimetallic CoPd catalysts with other capping agents (like PVP or CTAB) for the hydrogenation of MAn using FA as a sustainable hydrogen source, but could also be reused effectively. The electron microscopy observations show that such catalyst had a mean particle size of 6.4 nm with uniform distribution of Co and Pd within each bimetallic CoPd NP. Also, the XRD, XPS and XAS analyses suggested the presence of Co-Pd interactions in the bimetallic CoPd catalyst. Furthermore, based on the theoretical studies (in literature) and my experimental observations, the alloying of Co with Pd in the presence of DDAO, afforded electron rich Pd and modified the Pd-Pd bond distance. The electron rich Pd enhanced the adsorption/dissociation of substrates and the change in inter-atomic distances facilitated the better alignment of metal d-orbital with the carbonyl π-orbitals onto the catalyst surface, and in turn enhanced the rate of MAn hydrogenation into SA. Additionally, the catalyst in combination with CuCTAB/MgO catalyst provides a possibility for the direct utilization of abundant biomass-based glucose as hydrogen source for various hydrogenation reactions.

REFERENCES

1. V. Mazumder, S. Sun, *J. Am. Chem. Soc.* **2009**, *131*, 4588.

2. V. Mazumder, Y. Lee, S. Sun, *Adv. Funct. Mater.* **2010**, *20*, 1224.

3. A. Majewski, D. J. Morris, K. Kendall, M. Wills, *ChemSusChem* **2010**, *3*, 431.

4. A. Boddien, D. Mellmann, F. Gartner, R. Jackstell, H. Junge, P. J. Dyson, G. Laurenczy, R. Ludwig, M. Beller, *Science* **2011**, *333*, 1733.

5. K. Tedsree, T. Li, S. Jones, C. W. A. Chan, K. M. K. Yu, P. A. J. Bagot, E. A. Marquis, G. D. W. Smith, S. C. E. Tsang, *Nat. Nanotech.* **2011**, *6*, 302.

6. V. Mazumder, M. Chi, M. N. Mankin, Y. Liu, O. Metin, D. Sun, K. L. More, S. Sun, *Nano Lett.* **2012**, *12*, 1102.

7. F. Joo, *ChemSusChem* **2008**, *1*, 805.

8. T. C. Johnson, D. J. Morris, M. Wills, *Chem. Soc. Rev.* **2010**, *39*, 81.

9. M. Grasemann, G. Laurenczy, *Energy Environ. Sci.* **2012**, *5*, 8171.

10. J. J. Bozell, *Science* **2010**, *329*, 522.

11. R. Xing, W. Qi, G. W. Huber, *Energy Environ. Sci.* **2011**, *4*, 2193.

12. Z. Tang, W. Deng, Y. Wang, E. Zhu, X. Wan, Q. Zhang, Y. Wang, *ChemSusChem* **2014**, *7*, 1557.

13. H. Choudhary, S. Nishmura, K. Ebitani, *App. Catal. B: Environ.* **2015**, *162*, 1.

14. J. H. A. Martens, R. Prins, D. C. Konningsberger, *J. Phys. Chem.* **1989**, *93*, 3179.

15. R. W. Wunder, J. Phillips, *J. Phys. Chem.* **1996**, *100*, 14430.

16. S. Nishimura, Y. Yakita, M. Katayama, K. Higashimine, K. Ebitani, *Catal. Sci. Technol.* **2013**, *3*, 351.

17. D. Tongsakul, S. Nishimura, K. Ebitani, *ACS Catal.* **2013**, *3*, 2199.

18. D. Tongsakul, S. Nishimura, K. Ebitani, *J. Phys. Chem. C* **2014**, *118*, 11723.

19. J. Wang, G. Yin, Y. Chen, R. Li, X. Sun, *Int. J. Hydrogen Energy* **2009**, *34*, 8270.

20. J. S. Yoo, F. Ablid-Pedersen, J. K. Nørskov, F. Studt, *ACS Catal.* **2014**, *4*, 1226.

21. J. L. Fernandez, D. A. Walsh, A. J. Bard, *J. Am. Chem. Soc.* **2005**, *127*, 357.

22. V. Raghuveer, A. Manthiram, A. J. Bard, *J. Phys. Chem. B* **2005**, *109*, 22909.

23. M. H. Shao, K. Sasaki, R. R. Adzic, *J. Am. Chem. Soc.* **2006**, *128*, 3526.

24. N. Toshima, T. Yonezawa, *New J. Chem.* **1998**, 1179.

25. B. L. Cushing, V. L. Kolesnichenko, C. J. O'Connor, *Chem. Rev.* **2004**, *104*, 3893.

26. R. Ferrando, J. Jellinek, R. L. Johnston, *Chem. Rev.* **2008**, *108*, 845.

27. T. K. Sau, A. L. Rogach, *Adv. Mater.* **2010**, *22*, 1781.

28. M. Sankar, N. Dimitratos, P. J. Miedziak, P. P. Wells, C. J. Kiely, G. J. Hutchings, *Chem. Soc. Rev.* **2012**, *41*, 8099.

29. B. H. Kim, M. J. Hackett, J. Park, T. Hyeon, *Chem. Mater.* **2014**, *26*, 59.

30. P. Lu, T. Teranishi, K. Asakura, M. Miyake, N. Toshima, *J. Phys. Chem. B* **1999**, *103*, 9673.

31. S. Takenaka, T. Tsukamoto, H. Matsune, M. Kishida, *Catal. Sci. Technol.* **2013**, *3*, 2723.

32. G. Demazeau, *J. Mater. Chem.* **1999**, *9*, 15.

33. J. Li, Z. Chen, R. –J. Wang, D. M. Proserpio, *Coord. Chem. Rev.* **1999**, *190-192*, 707.

34. K. Byrappa, T. Adschiri, *Prog. Cryst. Growth Charact. Mater.* **2007**, *53*, 117.

35. C. Delhomme, D. Weuster-Botz, F. E. Kühn, *Green Chem.* **2009**, *11*, 13 and references cited therein.

36. J. Tuteja, H. Choudhary, S. Nishimura, K. Ebitani, *ChemSusChem* **2014**, *7*, 96.

37. P. A. Son, S. Nishimura, K. Ebitani, *RSC Adv.* **2014**, *4*, 10525.

38. J. Tuteja, S. Nishimura, K. Ebitani, *RSC Adv.* **2014**, *4*, 38241.

39. N. Toshima, M. Harada, T. Yonezawa, K. Kushihashi, K. Asakura, *J. Phys. Chem.* **1991**, *95*, 7448.

40. M. Harada, K. Asakura, Y. Ueki, N. Toshima, *J. Phys. Chem.* **1993**, *97*, 10742.

41. Y. Wang, N. Toshima, *J. Phys. Chem. B* **1997**, *101*, 5301.

42. H. Zhang, T. Watanbe, M. Okumura, M. Haruta, N. Toshima, *Nat. Mater.* **2012**, *11*, 49.

43. S. Nishimura, D. Mott, A. Takagaki, S. Maenosono, K. Ebitani, *Phys. Chem. Chem. Phys.* **2011**, *13*, 9335.

44. The BET surface area and pore volume of the boehmite employed in this study are 465 m^2 g^{-1} and 0.79 mL g^{-1}, respectively.

45. The turnover number for hydrogenation of MAn (0.5 mmol) with the CoPd-DDAO/AlOOH is 84 based on total palladium amount in the catalyst.

46. D. Sun, V. Mazumder, Ö. Metin, S. Sun, *ACS Nano* **2011**, *5*, 6458.

47. E. G. Allison, G. C. Bond, *Catal. Rev.* **1972**, *7*, 233.

48. J. M. Dominguez, A. Vazquez, A. J. Renouprez, M. J. Jose Yacaman, *J. Catal.* **1982**, *75*, 101.

49. B. Schleich, D. Schmeisser, W. Gopel, *Surf. Sci.* **1987**, *191*, 367.

50. J. M. Tura, P. Regull, L. Victori, M. Dolors de Castellar, *Surf. Interface Anal.* **1988**, *11*, 447.

51. I. Z. Shyu, K. Otto, W. L. H. Watkins, G. W. Graham, R. K. Belitz, H. S. Gandhi, *J. Catal.* **1988**, *114*, 23.

52. T. J. Sarapatka, *J. Phys. Chem.* **1993**, *97*, 11274.

53. C. J. Jenks, S. –L. Chang, J. W. Anderegg, P A. Thiel, D. W. Lynch, *Phys. Rev. B* **1996**, *54*, 6301.

54. T. J. Chuang, C. R. Brundle, D. W. Rice, *Surf. Sci.* **1976**, *59*, 413.

55. M. Oku, K. Hirokawa, *J. Electron Spectrosc. Relat. Phenom.* **1976**, *8*, 475.

56. B. J. Tan, K. J. Klabunde, P. M. A. Sherwood, *J. Am. Chem. Soc.* **1991**, *113*, 855.

57. X-ray Absorption: Techniques of EXAFS, SEXAFS and XANES; Eds. D. C. Koningsberger, R. Prins, J. Wiley & Sons: New York, 1988.

58. M. Harada, K. Asakura, N. Toshima, *J. Phys. Chem.* **1994**, *98*, 2653.

59. U. Kolb, S. A. Quaiser, M. Winter, M. T. Reetz, *Chem. Mater.* **1996**, *8*, 1889.

60. S. Nishimura, A. T. N. Dao, D. Mott, S. Maenosono, K. Ebitani, *J. Phys. Chem. C* **2012**, *116*, 4511.

61. T. K. Sham, *Phys. Rev. B* **1985**, *31*, 1888.

62. T. K. Sham, *Phys. Rev. B* **1985**, *31*, 1903.

63. V. Pallassana, M. Neurock, G. W. Coulston, *J. Phys. Chem. B*. **1999**, *103*, 8973.

64. V. Pallassana, M. Neurock, *J. Phys. Chem. B*. **2000**, *104*, 9449.

Part II

Design of efficacious heterogeneous Pd catalyst for industrially important organic transformations

Chapter 1

Design of highly active palladium grafted on amino-functionalized organozinc coordination polymer for Suzuki-Miyaura coupling reaction

ABSTRACT

The design of highly active and stable heterogeneous palladium catalyst is gaining a lot of attention because of its increasing importance in organic syntheses of commodity chemicals. Herein, I report the tailored synthesis of palladium species grafted on highly stable amino functionalized organozinc coordination polymer (denoted as Pd/AZC) and its extraordinary catalytic performances on Suzuki-Miyaura coupling (SMC) reaction. It achieved the highest turnover number of 2,106,720 (>99% yield) in air among the most reported palladium catalysts for the SMC reaction of bromobenzene. As-prepared Pd/AZC composite is also successfully applied for the catalysis of the Mizoroki-Heck coupling, hydrogenation of nitro, and C=C functional groups. Since the developed AZC support has the thermal stability at least up to 573 K, it posesses high potentials for grafting various metal species as catalytically active centers for wide range of metal-catalyzed reactions.

1. INTRODUCTION

In recent decades, porous coordination polymers (PCPs) have been an area of interest in many fields, namely energy, catalysis and separation. PCPs are inorganic-organic hybrid advanced materials with metal ions as the inorganic center and organic ligands as the linker with well-defined channels/pores. The prime reason of increasing attentions on the PCPs materials lies in the ease of tuning their structural features and relative properties for the wide-range potential applications.[1-3] For instance in terms of catalytic performances, because of this tunability, its structure can be precisely controlled to similarly incorporate active catalytic centers (in channels/pores) as enzymes which are extremely active and selective catalysts owing to the architectural active pockets in well-defined cavities.

Organic transformations such as C-Z (Z= C, O, N, etc.) coupling, hydrogenations, and oxidations have found potential industrial applications using transition metals (such as Au, Pd, Pt, etc.) catalysts. Among these, the Suzuki-Miyaura coupling (SMC) reaction using Pd catalyst[4-7] has become more like a ritual for the regioselective formation of C-C bonds in modern organic chemistry.[8-13] Because of the tolerance of the SMC reaction for wide range of substrates under milder conditions in the presence of readily available organoboronic acids, the SMC reaction has been extensively employed as a handy methodology in the syntheses of natural products, pharmaceuticals and supra-molecular assemblies throughout the globe.[8-13] The homogeneous Pd catalytic processes have higher activity and selectivity than their heterogeneous counterparts, however, have serious issues of recovery and reusability. The reasons for the limited activity of heterogeneous catalyst might be the poor accessibility of reactants to the active sites and/or fast deactivation by agglomeration of unstable Pd species into inactive Pd particles. Thus, designing a

highly active and stable, heterogeneous Pd catalyst constitutes one of the important objectives for the transition metal-catalyzed SMC reaction and other catalytic reaction.[14-15]

I have successfully fabricated such coordination polymer to graft drastically low palladium using a ligand design methdology. Herein, the synthesis, catalysis and structural characterization of a monomeric palladium species grafted on amino functionalized organozinc coordination polymer (denoted as Pd/AZC) as a highly active and easily reusable heterogeneous catalyst for the SMC reaction with high turnover number (TON) is demonstrated. Recently, Deraedt and Astruc compiled a report on Pd nanoparticles (both homogeneous and heterogeneous) for cross coupling reaction with concluding remarks on forthcoming challenges of both stabilization and improvement of catalytic efficiency.[16] Various researchers have reported TON in the range of 100-3,500,000 for haloarenes (average TON being 85,000 for bromobenzene) by homogeneous and heterogeneous catalyses.[17-30] Different supports such as activated carbon or carbon nanotubes,[31-34] metal organic frameworks,[21,29,35-36] zeolites,[23,37-39] and mesoporous silica[25,40-42] have been utilized for the SMC reaction.[43-45] The activities were observed as a function of easy access of the substrates and reagents to active species. Okumura et al. demonstrated that Pd/USY catalyst can give a TON of 13,000,000 using bromobenzene as substrate only under H_2 atmosphere without commenting on catalyst reusability.[23]

In this contribution, an organozinc coordination polymer with amino functionality was designed for efficient grafting of Pd species leading to highly dispsersed and easily accessible active centers. Because such PCPs have a regular microporous structure and a significant high surface area,[1-3] the synthesized organometallic coordination polymer are believed to possess highly porous structure that facilitates the access of substrates to the firmly held active Pd species with amino moieties. The catalytic system described here is supposed to be a promising synthetic protocol for the

development of advanced metal-supported catalysts because of the following advantages: (i) high catalytic activity and selectivity under air atmosphere, (ii) easy recovery and high reusability, and (iii) restricted homo-coupling of phenyl boronic acid in the Pd-catalyzed SMC reaction.

2. EXPERIMENTAL SECTION

Chemicals. Phenylboronic acid, palladium chloride, zinc nitrate hexahydrate ($Zn(NO_3)_2 \cdot 6H_2O$), toluene, methyl isobutyl ketone, benzyl alcohol, benzaldehyde, nitrobenzene, aniline, cinnamaldehyde, 3-phenylpropionaldehyde and standard solutions (1000 ppm) of palladium and zinc were purchased from Wako Pure Chemical Industries, Ltd. Potassium chloride, potassium carbonate (K_2CO_3), lithium carbonate, cesium carbonate, calcium carbonate, styrene, dimethylsulfoxide, acetone, N,N-dimethylformamide (DMF), methanol, acetonitrile, ethanol, N,N-dimethylacetamide, zinc oxide, succinic acid and sodium hydroxide were procured from Kanto Chemical Co., Inc. Tokyo Chemical Industry Co., Ltd. supplied bromobenzene, maleic anhydride and naphthalene whereas chlorobenzene was bought from Junsei Chemical Co., Ltd. QuadraPure® TU, 1-methyl-2-pyrrolidinone, 2-aminoterephthalic acid (ATA), tetrabutylammonium bromide (TBAB), stilbene, 1,1-diphenylethylene and zinc acetate ($Zn(OAc)_2$) were obtained from Sigma-Aldrich, Co. LLC.

Strategy for catalyst design. In general, the inclusion of facile access to the active species and firm binding of the supported active species have proved as an extra advantage to heterogeneous catalyst. I really desired to fabricate such heterogeneous material for SMC reaction with features to hold easily-accesible active Pd firmly. The PCPs could be synthesized by controlled stitching of organic molecules with inorganic molecules especially the transition metal fascinated us. In

principle, the Pd-N bonds are relatively strong, and thus I craved to choose an organic moiety with a nitrogen containing functional group such as amine, and thereby I selected 2-aminoterephthalic acid (ATA) as the organic linker for PCP. While, zinc as the metal center was selected owing to its relative abundance, low cost and significant catalytic characteristics. The obtained amino functionalized organozinc coordination polymer (AZC) may facilitate to hold active Pd species with high dispersibility derived from amino functionality and porous framework of PCP compounds.

Catalyst preparation. *(a) Synthesis of amino-functionalized organo-zinc coordination polymer (AZC):* ATA (5 mmol) and $Zn(NO_3)_2 \cdot 6H_2O$ (5 mmol) in DMF (35 mL) were sealed in a 100 mL teflon lined autoclave, and heated to 413 K (heating rate; 4 K/min) in a programmable oven and maintained at same temperature for 24 h. The synthesis method involved the use of DMF as solvent which slowly dissociate at higher temperature to deprotonate ATA, which in turn reacts with $Zn(NO_3)_2 \cdot 6H_2O$ to form organozinc coordination polymer. The oven was allowed to cool to room temperature slowly. The solid residue obtained was filtered and washed with small amount of DMF. A brownish blocks were obtained and dried in vacuo before grinding them to afford light brown powder in pestle mortar. These dried brown powders were further treated with ethanol at 353 K for 24 h in order to remove DMF and filtered and dried in vacuo to obtain "AZC". Elemental analysis (%) for prepared AZC was found as C, 37.2; H, 2.0; N, 6.2; Zn, 27.3. To account for the result, a molecular formulae was suggested as $Zn_4(ATA)_3(NO_3)_2$ (or $C_{24}H_{15}N_5O_{18}Zn_4$): C, 31.2; H, 1.6; N, 7.6; Zn, 28.4. *(b) Synthesis of palladium grafted amino-functionalized organo-zinc coordination polymer (Pd/AZC):* About 0.5 g of palladium chloride with 0.5 g potassium chloride were weighed and suspended in 50 mL water. The solution was sonicated with occasional stirring for 30 minutes to obtain a homogeneous palladium stock solution with a concentration of about 10

mg of PdCl₂ per mL of the stock solution. In a typical synthesis of 0.5wt%Pd/AZC, calculated amount of solution (208 μL, if the concentration of stock solution is 10 mg PdCl₂ per mL) was taken in a round bottomed flask and 15 mL of water was added. To this solution, 250 mg AZC was added and stirred at room temperature for 6 h, and then at 353 K for 14 h. The obtained brown colored solution was filtered, washed with about 1 L of water and dried in vacuo at room temperature. The dried powder was grinded to obtain Pd/AZC (238 mg). Various palladium grafted AZC catalysts were denoted as xPd/AZC; where the x is Pd content on support as (wt/wt) in theory.

Catalytic testing. All experiments to evaluate the catalytic activity were performed under air in a round bottomed flask, unless mentioned. In a general reaction procedure, catalyst was weighed in to the flask followed by the addition of base, phenylboronic acid and substrate (bromobenzene or chlorobenzene) in a molar ratio of 4:3:2. The solvent (5 mL) was added to disperse the reactants well and the flask was mounted on a preheated oil bath at T K and the reaction was continued for t h. After the passage of desired time, the flask was allowed to cool to room temperature and naphthalene was added as an internal standard. The reaction mixture was stirred at room temperature, diluted and the catalyst was filtered off using a Milex®-LG 0.20 μm. The obtained filtrate was analyzed by a gas chromatogram (GC-17A, Shimadzu Co.) using an Agilent DB-1 column (30 m×0.25 mm×0.25 μm) attached to a FID detector. The conversion and selectivity were determined with a calibration curve method using naphthalene as an internal standard.

Recycling tests were performed to check stability of the Pd/AZC catalysts during the reaction. The catalyst was separated from the reaction mixture by centrifugation. The supernatant liquid was stored, and then analysis of products and leaching test of catalysts were performed. The residual catalyst and base were washed by centrifugation with ethanol and dried in vacuo overnight. Fresh

substrates and reagents were added to the catalyst, and then the reusability of the catalyst was verified under similar reaction conditions.

In a typical case of isolation of 4-phenylbenzoic acid (Table 2, entry 4), naphthalene was not added in the reaction mixture. The reaction mixture was centrifuged and the resulting supernatant liquid was filtered to remove any suspended solid particles. The ethanol solution was concentrated followed by the addition of water to precipitate the organics. The reaction mixture containing water, ethanol and white solid were centrifuged again and supernantant liquid was collected separately to remove traces of bromobenzene (liquid). The solid was dissolved in very small amount of ethanol and sufficient water was added to achieve precipitation and was then centrifuged. The mixture was left overnight to obtain colourless crystals to record ^{1}H NMR spectra.

Heterogeneity test and solid-phase poisioning test. *(a) Hot-filtration test:* 0.5wt%Pd/AZC (1 mg) was weighed into the flask followed by K_2CO_3 (4 mmol), phenylboronic acid (3 mmol) and bromobenzene (2 mmol). Finally ethanol (5 mL) was added to disperse the reactants and the reaction mixture was heated at 353 K. After 20 minutes of reaction progress, naphthalene (as an internal standard) was added and the catalyst was separated at the reaction temperature by centrifugation followed by filtration using a Milex®-LG 0.20 μm. Additional amount of K_2CO_3 (3 mmol) was introduced to the filtrate and the reaction was continued at 353 K for additional 40 minutes. Furthermore, as a separate experiment 0.5wt%Pd/AZC (1 mg) was weighed in to the flask followed by the addition of base, phenylboronic acid and bromobenzene in a molar ratio of 4:3:2 and ethanol (5 mL). The resulting solution was stirred at 353 K for 1 h. After 1 h of reaction progress, naphthalene was added and the subjected to GC analysis. The catalyst was removed by centrifugation followed by filtration using a Milex®-LG 0.20 μm and fresh reagents (base, phenylboronic acid and bromobenzene in a molar ratio of 4:3:2) were added and the reaction was

[138]

continued for another 1 h at 353 K. The product concentration was determined by GC analysis. ***(b)***

Solid-phase poisoning test: The catalyst poison candidate was added to the reaction flask before

the addition of the reagents for SMC reaction of bromobenzene. The amount of QuadraPure® TU

was used four times of that required to bind total Pd as indicated by manufacturer (scavenging

limit; 0.19 mmol Pd per gram QuadraPure TU). As a control experiment aq. $PdCl_2$ (47 nmol Pd)

was used as catalyst with two equivalents of QuadraPure TU (twice the amount required to bind

all the palladium in the reaction mixture).

Characterization. Structure was analyzed by powder X-ray diffraction (PXRD) patterens with a

SmartLab (Rigaku Co.) using a Cu Kα radiation (λ = 0.154 nm) at 40 kV and 30 mA in the range

of 2θ = 4-60°. The diffraction patterns were analyzed with the database in the joint committee of

powder diffraction standards (JCPDS). For inductively coupled plasma atomic emission

spectroscopy (ICP-AES) analysis, an ICPS-7000 ver. 2 (Shimadzu Co.) was employed to quantify

the actual Pd amount and to evaluate the Pd leaching, if any, during the reaction. Contents of Pd

in the catalyst and/or the reaction medium were estimated by a calibration curve method. A H-

7100 (Hitachi, Ltd.) operating at 100 kV was utilized to acquire the morphology of catalyst by a

transmission electron microscopy (TEM) image. The samples for TEM measurements were

dispersed in water or ethanol, and the supernatant liquid was dropped onto a copper grid before

drying in vacuo overnight. Scanning electron microscopy (SEM) micrographs were observed using

S-4100 (Hitachi, Ltd.). The electronic state of Pd and Zn was analyzed by X-ray photoelectron

spectroscopy (XPS). The XPS experiments were conducted on an AXIS-ULTRA DLD

spectrometer system (Shimadzu Co. and Kratos Analytical Ltd.) using an Al target at 15 kV and

10 mA in an energy range of 0-1200 eV. The binding energies were calibrated with the O 1s level

(531.0 eV) as an internal standard reference. X-ray absorption spectroscopy (XAS) was performed

[139]

with a transmission and/or fluorescence mode at a BL-9C in KEK-PF under the approval of the Photon Factory Program Advisory Committee (Proposal No. 2013G586) and BL01B1 in SPring-8 under the approval of Japan Synchrotron Radiation Research Institute (JASRI) (Proposal No. 2012B1610 and 2013B1478). The obtained XAS spectra were analyzed with Rigaku REX2000 software (ver. 2.5.92). The IR measurements of samples were carried out on a PerkinElmer Spectrum 100 FT-IR spectrometer. Nuclear Magnetic Resonance (NMR) spectra were recorded on 400 MHz Bruker (AVANCE III 400) using DMSO-d_6 as the solvent with TMS as internal standard. Gas Chromatogram (GC-17A, Shimadzu Co.) coupled Mass Spectrometer (QP5000, Shimadzu Co.) (GC-MS) were employed to obtain the mass fragmentation spectra of synthesized compounds.

3. RESULTS AND DISCUSSION

Morphology and crystallinity of AZC and Pd/AZC. Solvothermal treatment of $Zn(NO_3)_2 \cdot 6H_2O$ with ATA in DMF at 413 K, followed by ethanol treatment afforded brownish material (denoted as AZC). The SEM (Figure 1a) and TEM (Figure 1b) analyses of the sample captured porous blocks with irregular size and shape having thread/tube like features at the edges. The AZC and Pd/AZC consisted of a phase with PXRD patterns observed at 2θ = 11.2, 14.4, 18.1, 20.3, 23.6, 25.8 and 27.2° corresponding to (111), (210), (220), (310), (320), (400) and (411) planes, respectively (Figure 2), which were much different from the PXRD patterns of IRMOF-3 and MIL-53 reported, previously.[2,46] The co-existence of agglomerates and large crystals of impurities such as ZnO, $PdCl_2$ and PdO in these materials were excluded on the basis of TEM images and XRD patterns. Requisite amounts of $PdCl_2$ were loaded on AZC by an adsorption method to afford

xPd/AZC, where the x is Pd content (wt%) in theory. The Pd grafting process on AZC preserved its original structure as evidenced by XRD (Figure 2).
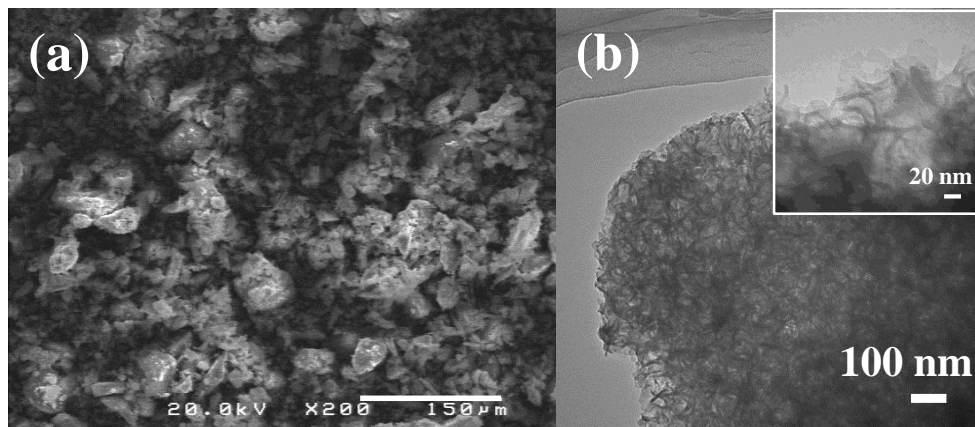

Figure 1. (a) SEM micrograph of AZC showing irregular blocks. (b) TEM images of AZC at different magnifications.
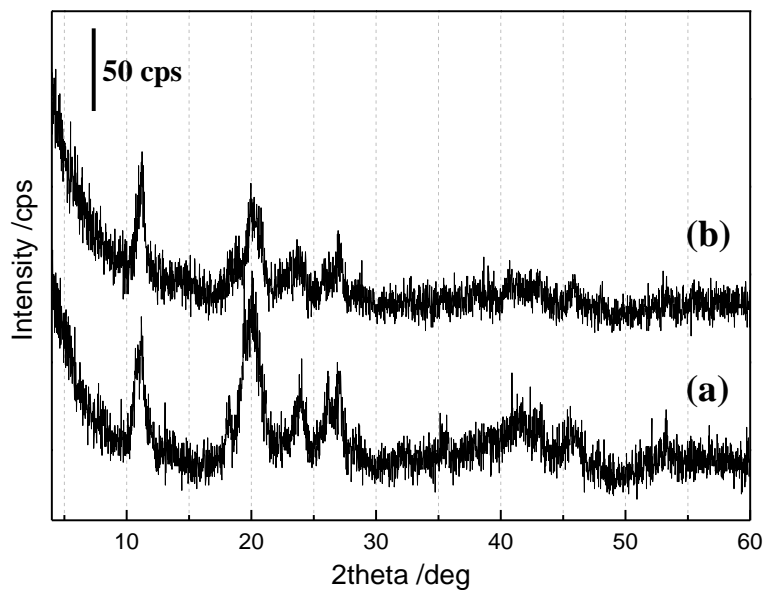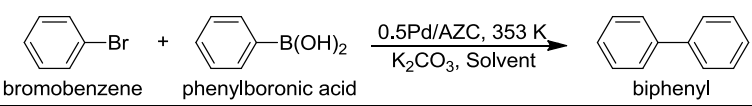

Figure 2. XRD patterns of (a) AZC and (b) Pd/AZC.

Catalytic activity of Pd/AZC for SMC reaction. The catalytic activity of Pd/AZC was investigated for the SMC reaction and was found to be highly active for bromobenzene (Table 1).

[141]

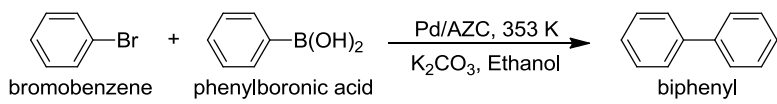**Table 1.** Effect of solvent on SMC reaction of bromobenzene using 0.5Pd/AZC catalyst[a]

Entry	Solvent	t /h	Conv. /%[b]	Yield /%[b]
1	Ethanol	0.5	>99	>99
2[c]			92.3, 91.4[d]	92.7, 93.2[d]
3[e]			-	0.5
4[f]		1	10.5	0
5[g]			0	0
6	DMF	2	42.9	44.1
7	Toluene		18.2	23.8
8	Water		10.6	4.2
9	DMF:Water (4:1)		44.0	48.0
10	Ethanol:Water (4:1)	0.5	>99	>99

[a]Reaction conditions: Bromobenzene (2 mmol), Phenylboronic acid (3 mmol), K_2CO_3 (4 mmol), Solvent (5 mL), 0.5Pd/AZC (30 mg), 353 K. [b]Determined by GC using naphthalene as internal standard on the basis of bromobenzene. [c]0.5Pd/AZC (5 mg). [d]1st reuse. [e]Without bromobenzene. [f]Without Pd loading (AZC, 5 mg). [g]Without catalyst.

All experiments were performed under air atmosphere. High activities for bromobenzene were realized at shorter reaction time (Table 1, entry 1). Even with decreased amount of Pd. The catalyst retained high catalytic activity with excellent reusability (Table 1, entry 2). The control experiment without bromobenzene (Table 1, entry 3) pronounced the catalytic activity to be restricted to cross-coupling under the present reaction conditions. The reaction did not progressed in the absence of both catalysts and palladium (Table 1, entries 4-5). Solvents have a drastic effect on the progress of a catalytic reaction, and thereby various solvents were used to optimize the catalytic activity for SMC reaction (Table 1, entries 6-10). Although some of the current reports have demonstrated highly efficient SMC reaction in aqueous media, I found my catalytic system to be fruitful in ethanol solvent. While optimizing the activity of Pd/AZC in ethanol, a remarkable TON value of 2,106,720 was reached with 4.7 nmol of Pd for 10 mmol of bromobenzene (Table 2).

Table 2. Highly efficient SMC reaction by Pd/AZC catalyst[a]

bromobenzene —Br + phenylboronic acid —B(OH)$_2$ $\xrightarrow[\text{K}_2\text{CO}_3,\ \text{Ethanol}]{\text{Pd/AZC, 353 K}}$ biphenyl

Entry	PhBr /mmol	Pd /nmol[b]	t /h	Conv. /%[c]	Yield /%[c]	TON[d]
1[e]	2	235	1	83.7	88.8	7,576
2	4	47	6	81.6	84.2	71,501
3	15	47	14.5	86.6	85.2	271,320
4	30	47	24.5	80.7	81.3	517,104
5	75	47	40	74.7	64.5	1,029,420
6[f]	10	4.7	48	94.4	>99	2,106,720

[a]Reaction conditions: Bromobenzene:Phenylboronic acid:K$_2$CO$_3$ (1:1.5:2) (molar ratio), Ethanol (5 mL), 0.5Pd/AZC (1 mg), 353 K. [b]Estimated by the results of ICP-AES analysis of the xPd/AZC. [c]Determined by GC using naphthalene as an internal standard on the basis of bromobenzene. [d]TON was calculated based on the amount of biphenyl formed. [e]0.5Pd/AZC (5 mg). [f]0.05Pd/AZC (1 mg).

The highly active Pd/AZC could keep its potential at least up to recycling 7 runs without any significant loss of activity (Figure 3). The activities of Pd/AZC showed gradual decrease from 3rd to 5th run, however, the activity could be re-achieved by increasing the reaction time as seen in 6th and 7th run. Thus, the Pd/AZC could possess its original potential even after 7th run. The observation, increase in activity with the increase in reaction time, indicated that the rate of reaction was affected during recycling runs. I supposed that the accessibility of substrates towards catalyst was compromised by increase in the base (K$_2$CO$_3$) amount against the small quantity of Pd/AZC in five catalytic runs.
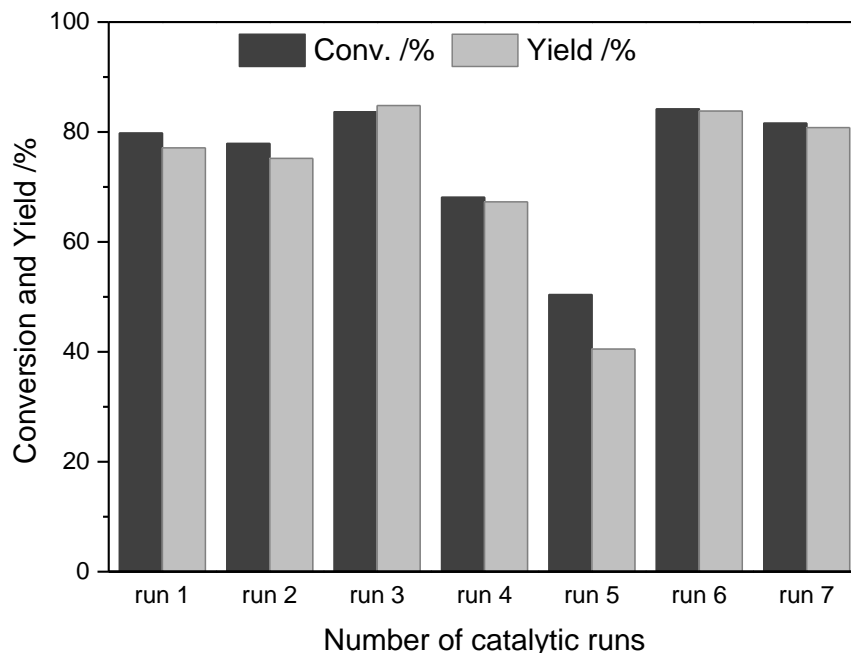
Figure 3. Reusability of 0.5Pd/AZC catalyst for the SMC reaction of bromobenzene. *Reaction conditions*: Bromobenzene (2 mmol), phenylboronic acid (3 mmol), K_2CO_3 (4 mmol), 0.5Pd/AZC (1 mg), Ethanol (5 mL), 353 K, 1 h. The reaction time was increased to 3 h for runs 6 and 7.
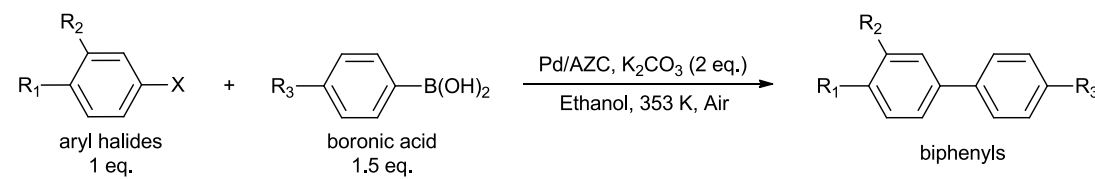
After achieving excellent results with bromobenzenes, chlorobenzenes were employed as substrate. Chlorobenzenes are less reactive in comparison to the bromobenzenes. The catalytic activities were optimized for chlorobenzenes under various conditions to maximise the biphenyl yields from chlorobenzenes (Table 3). The activity was not limited to bromobenzene; the reaction of activated chlorobenzene (p-nitrochlorobenzene) also afforded 4-nitrobiphenyl with >99% yield (>99% conv.) in the absence of additives (Table 3, entry 26). However, it was realized that chlorobenzene could not be coupled effectively with arylboronic acid under which bromobenzene underwent SMC reaction. whereas a higher conversion of chlorobenzenes (58.4%) was observed at 353 K in the presence of TBAB with 18% yield of biphenyl (Table 3, entry 11). In fact,

[144]

Table 3. Optimization of reaction parameters for maximizing biphenyl yield from chlorobenzene (CB)[a]

Entry	Temp. /K	Time /h	Pd /μmol[b]	Solvent	TBAB/CB ratio[c]	Conv. /%[d]	Yield /%[d]
1	353	2	2.4	Ethanol	0	0.6	8.5*
2				Methanol	0	3.8	7.4*
3				MIBK	0	0	0
4				DMSO	0	0	0
5				CH$_3$CN	0	0	0
6				Acetone	0	0	0
7				1,4-Dioxane	0	0	0
8				DMA	0	0	0
9				DMA:Ethanol	0	0	0
10			14.1	Ethanol:water(4:1)	0	8.0	22.3*
11	353	4	5.6	Ethanol	1	58.4	18.4
12			0.7	Ethanol	0.5	49.9	7.4
13	373	6	0.2	Ethanol	1	39.3	3.2
14[e]					1	72.0	24.8
15				DMF	1	46.8	2.0
16					0	0	0
17				H$_2$O	1	72.0	3.0
18				Ethanol:DMF (3:2)	1	49.6	7.6
19[f]			2.8	Ethanol:DMF (1:1)	1	74.5	31.2
20[e]					1	58.2	34.0
21[e]					0.5	46.1	30.0
22[f]				Ethanol:DMF (2:3)	1	76.1	27.8
23[f]				Ethanol:DMF (1:4)	1	72.5	14.1
24[f]				Ethanol:DMF (4:1)	1	72.6	16.1
25[f]				Ethanol:DMF (3:2)	1	73.7	23.7
26[g]	353	3	1.4	Ethanol	0	>99	>99

[a]Reaction conditions: Chlorobenzene (CB, 0.5 mmol), Phenylboronic acid (0.75 mmol), K$_2$CO$_3$ (1 mmol), Pd/AZC, Solvent (5 mL), Round bottomed flask. Abbreviation: TBAB; tetrabutylammonium bromide, MIBK; methyl isobutyl ketone, DMSO; dimethylsulfoxide, DMA; *N,N*-dimethylacetamide. DMF, *N,N*-dimethylformamide. [b]Determined by ICP-AES analysis. [c]TBAB:CB in mmol:mmol. [d]Determined by GC using naphthalene as internal standard on the basis of bromobenzene or chlorobenzene. [e]50 mL Teflon lined Autoclave. [f]Sealed glass tube. [g]*p*-Nitrochlorobenzene (0.5 mmol) was used instead of chlorobenzene. *Note; The higher biphenyl yields than conversions in entries 1, 2 and 10 are due to the homocoupling of phenylboronic acid.

[145]

Table 4. The SMC reaction of aryl halides and boronic acids with Pd/AZC catalyst[a]

Entry	X	R_1	R_2	R_3	Time /h	Conv.[b] /%	Yield[b] /%
1	Br	H	H	H	1.0	80	77
2				OCH_3		83	69
3				F		91	92
4[c]				COOH	3.0	84	73[f,g]
5[d]	Cl	NO_2	H	H		>99	>99
6[d]				OCH_3		26	19[g]
7[d]				F		47	32[g,h]
8	I	H	H	H	0.3	99	96
9				OCH_3	1.0	>99	68
10				F		90	89
11[e]		COOH	OH	H	3.0	82	76[g]

[a] Reaction conditions: Aryl halide (2 mmol), Boronic acid (3 mmol), K_2CO_3 (4 mmol), 0.5Pd/AZC (1 mg), Ethanol (5 mL), Round bottomed flask, 353 K, Air. [b]Determined by GC using naphthalene as internal standard on the basis of aryl halides. [c]Aryl halide (1 mmol), Boronic acid (1.5 mmol), K_2CO_3 (2 mmol), 0.5Pd/AZC (5 mg). [d]Aryl halide (0.5 mmol), Boronic acid (0.75 mmol), K_2CO_3 (1 mmol), 3Pd/AZC (5 mg). [e]0.5Pd/AZC (5 mg). [f]Isolated yield. [g]Product was confirmed by NMR and GC-MS (see ESI). [h]4,4'-Difluorobiphenyl was observed.

chloroarenes required larger Pd amounts in comparison to bromoarenes. Employment of ethanol and DMF as solvent with TBAB additive agent[47-48] could improve the yield of biphenyl moderately in an autoclave reactor (Table 3, entry 20); the implementation of such reaction parameters in an autoclave could afford high conversion of chlorobenzene with decent yields (30-34%) of biphenyl.

For futural and advanced interests, not only the various aryl halides but also the reactivity of them with diverse boronic acids was subjected to the SMC reaction using Pd/AZC catalyst. These reactions were also attempted and tabulated as Table 4. The reactivities of aryl halides in general

were found to decrease with the use of phenylboronic acids (Table 4, entries 1,5,8; R_3 = H) to flurophenylboronic acids (entries 3,7,10; R_3 = F) to methoxyphenylboronic acids (Table 4, entries 2,6,9 R_3 = OCH_3). Because of the high reactivity of fluorophenylboronic acid, large excess of palladium catalyst and low reactivity of aryl chloride produced 4,4'-difluorobiphenyl as the homocoupling product of fluorophenylboronic acid in traces (Table 4, entry 7). The cross-coupling of 4-carboxyphenylboronic acid with bromobenzene required longer reaction times and higher amounts of palladium to accomplish decent yields (Table 4, entry 4). The 2 mmol iodobenzene quickly cross-coupled with phenylboronic acid to produce >90% biphenyl yields within 20 minutes catalyzed by 47 nmol of palladium, whereas in contrast, aryl iodides with hydroxyl and carboxyl functional groups necessitated longer reaction times to reach high conversions (Table 4, entries 8,11).

Investigation of localized Pd/AZC structure around Zn. To account for the high activity and propose a suitable mechanistic pathway for the SMC reaction over Pd/AZC, the structural features were further characterized by spectroscopic methods. The local structure around zinc in AZC and palladium in Pd/AZC were investigated by XAS measurements. The Zn K-edge X-ray absorption near-edge structure (XANES) spectrum of AZC was similar to Zn(II) salts of $Zn(OAc)_2$ and $Zn(NO_3)_2 \cdot 6H_2O$ (Figure 4a); 58% of $Zn(OAc)_2$ with 42% of $Zn(NO_3)_2 \cdot 6H_2O$ were estimated by deconvolution of XANES feature, indicating Zn(II) species as the integral part of electronic states and/or local structure in AZC.

The k^3-weighted extended X-ray absorption fine structure (EXAFS) of AZC at Zn K-edge suggested a high similarity in EXAFS oscillation to $Zn(OAc)_2$ (Figure 4b); merging estimation indicated that the AZC has structural features of $Zn(OAc)_2$ (above 80%) mixed with $Zn(NO_3)_2 \cdot 6H_2O$ (Figures 4b-c). A broad peak in the Fourier transforms (FT) of EXAFS of AZC

[147]

appeared at 1.3-1.7 Å (solid line, Figure 4d) and which was at lower distance of Zn-O coordination compared to Zn(OAc)$_2$ (dashed line, Figure 4d). This shift towards lower bond distance in AZC was supposedly accounted due to differences in side-chain of RCOO- (R= CH$_3$ in Zn(OAc)$_2$ and C$_6$H$_3$(NH$_2$)(COOH) in AZC) and structural complexity relating to higher bond strength of Zn-O.
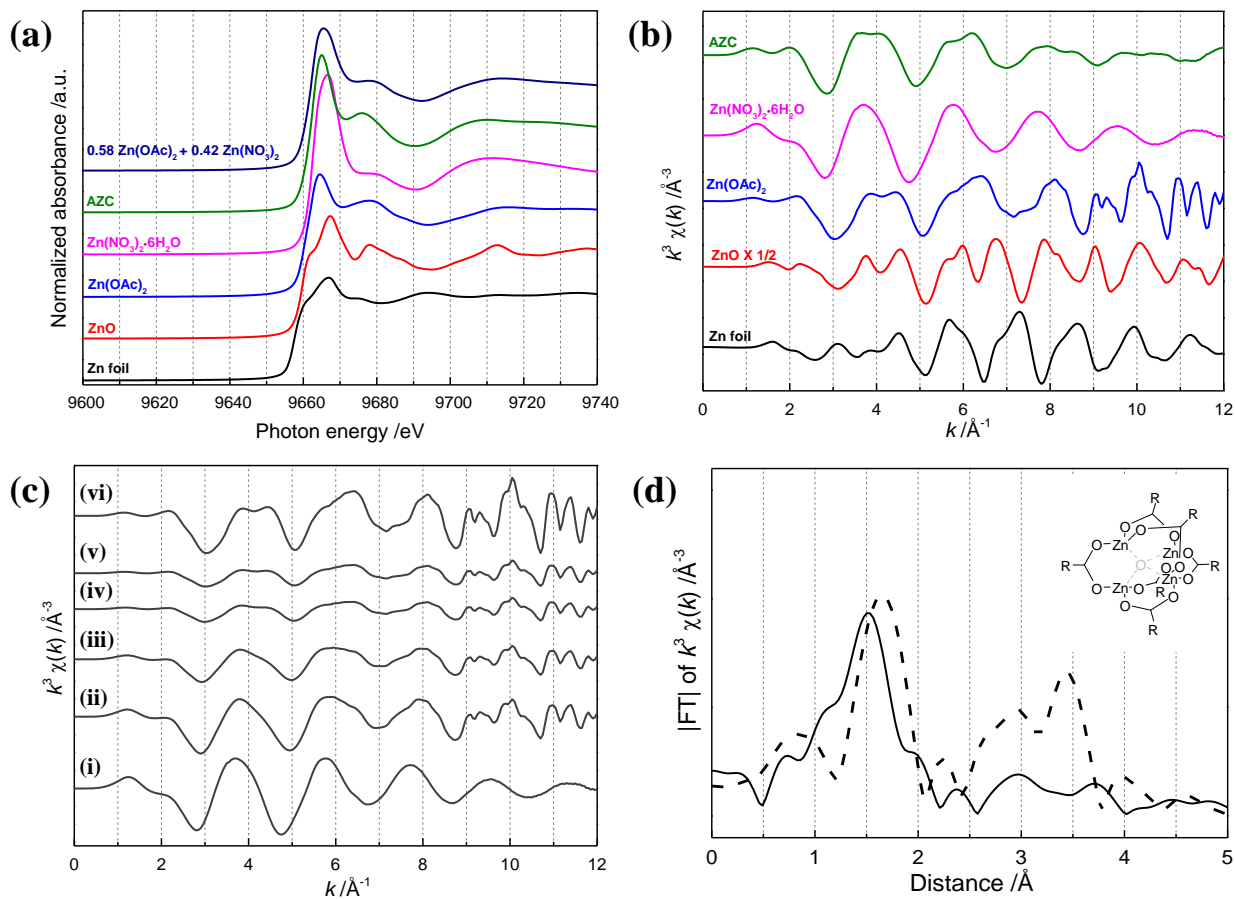

Figure 4. (a) Normalized XANES and (b) EXAFS spectra at Zn K-edge of references and AZC. (c) Calculated Zn K-edge EXAFS spectrum of Zn(NO$_3$)$_2$·6H$_2$O and Zn(OAc)$_2$ in different ratio. The ratio of Zn(NO$_3$)$_2$·6H$_2$O to Zn(OAc)$_2$ are (i) 100:0, (ii) 50:50, (iii) 25:75, (iv) 20:80, (v) 10:90, (vi) 0:100. The merged spectra with higher content of Zn(OAc)$_2$ (above 80%) demonstrated good correlation to the obtained features of AZC (the humped peak). (d) FT of k^3-weighted EXAFS spectrum of AZC (solid line) and Zn(OAc)$_2$ (dashed line) at Zn K-edge. The inset shows the proposed local structure around Zn in AZC.

Investigation of localized Pd/AZC structure around Pd atom. The IR analysis of AZC and Pd/AZC demonstrated that ATA was stable under synthetic conditions forming a palladium- amine complex assembly (N-H and Pd-N stretchings were observed) (Figure 5). The appearance of two peaks (at 477 and 496 cm^{-1}) for Pd-N in IR spectra supports the loading of Pd on AZC through palladium–amine complex with cis geometry.[49] In the Pd 3d XPS shown in Figure 6, the peaks at
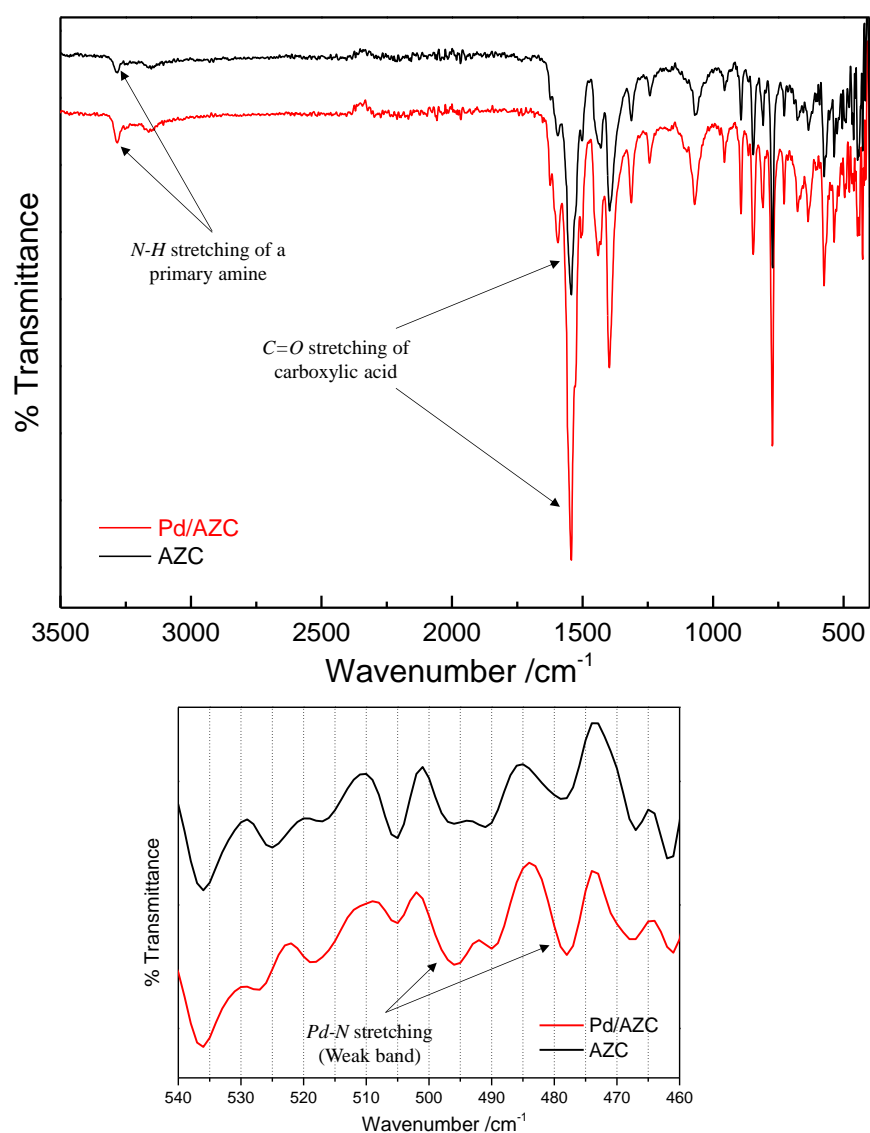

Figure 5. Infrared (IR) spectra of AZC and Pd/AZC. The weak band of Pd-N is also shown.

higher binding energy (than that of Pd foil) distinguished the oxidized/ionic species of palladium in Pd/AZC. Deconvolution analysis of the XPS of Pd/AZC in Pd 3d region: Pd $3d_{3/2}$ (342.2 eV) and $3d_{5/2}$ (336.9 eV), splited each individual peak into two peaks at 341.4 eV and 342.3 eV for Pd $3d_{3/2}$ whereas 335.6 eV and 337.1 eV for Pd $3d_{5/2}$; corresponding to Pd(II) in square planar organopalladium complex and oxygen-coordinated Pd(II) states (Figure 6).[50-51]
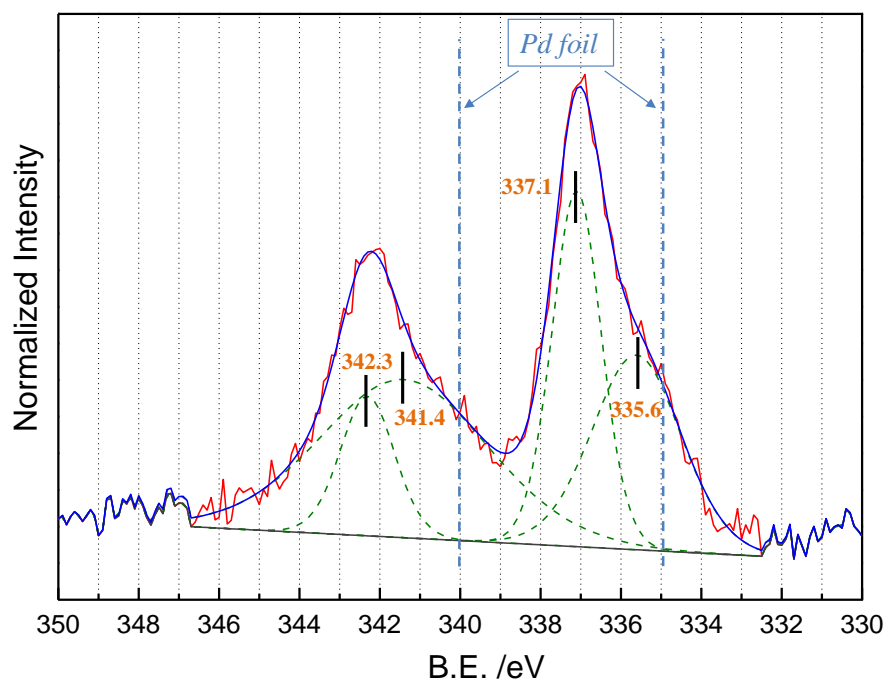

Figure 6. XPS of Pd 3d in Pd/AZC.

The Pd K-edge XAS studies of the Pd/AZC were also performed, and its oxidation states as well as co-ordination of Pd species were estimated. Pd K-edge XANES characteristics (Figure 7a), EXAFS (Figure 7b), and FT of EXAFS (Figure 7c) of Pd/AZC were very different from the Pd foil but had resemblance to the Pd(II) state of Pd(OAc)$_2$ (Figure 8a). The literature survey
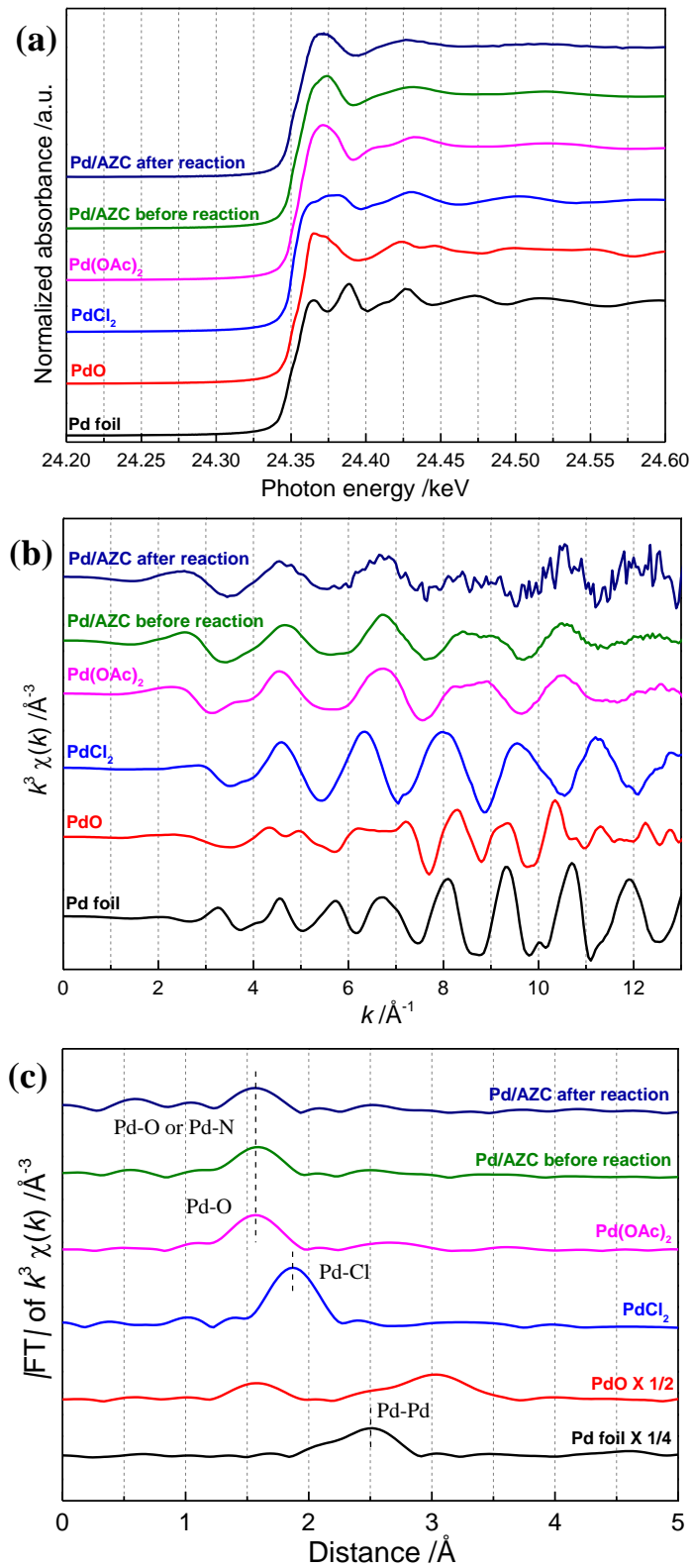
[150]

Figure 7. (a) Normalized XANES, (b) k^3-weighted EXAFS and (c) FT of k^3-weighted EXAFS of references and Pd/AZC at Pd K-edge XAS.
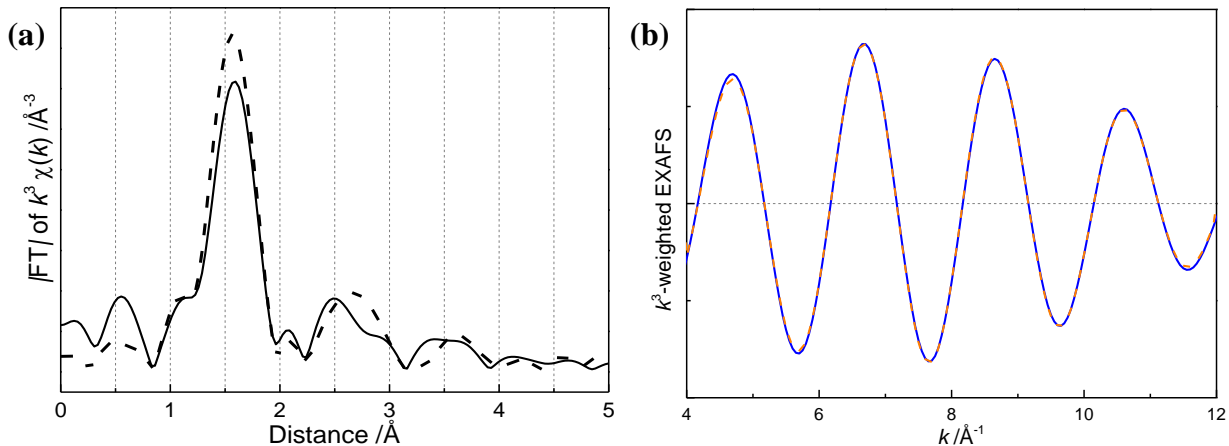
Figure 8. (a) FT of k^3-weighted EXAFS spectrum of Pd/AZC (solid line) and Pd(OAc)$_2$ (dashed line) at Pd K-edge. (b) The inverse FT of Pd/AZC performed in the range of 4-12 Å^{-1}. The dashed orange line shows the results of a curve-fitting analysis.

suggested the species to possess a square planar geometry close to that of Pd(OAc)$_2$ or [Pd(NH$_3$)$_4$]Cl$_2$.[52] The FT of EXAFS exhibited a single peak in the region of 1.4-1.8 Å (Figure 8a), resultant of the backscattering of the adjacent nitrogen and/or oxygen atoms (Figures 7a-c). The inverse FT of the peak was well-fitted using Pd-N (CN= 1.8) and Pd-O (CN= 2.2) shells in the range of k = 4-12 Å^{-1} (Figure 8b and Table 5). Mori et al.[53] reported the loading of Pd on hydroxyapatite (HAP) with Pd coordinated to four oxygens in a Ca-deficient site of HAP. A sound similarity in the FT of Pd/AZC and PdHAP[53] at Pd K-edge were observed.

Table 5. Curve-fitting results for Pd K-edge EXAFS[a]

Shell	CN[b]	R[c] /Å	DW[d] /Å^2
Pd-N	1.8	2.050	0.0004
Pd-O	2.2	2.026	0.0104

[a]The curve fitting was performed using McKale method. FT of the k^3-weighted EXAFS spectrum (k^3c(k)) of Pd/AZC was performed in the range of k = 3–13 Å^{-1} with a window function for 20, and the inverse FT was examined in the ranges of k = 4–12 Å^{-1} and R = 1.258–1.872 Å with a window function for 10. The obtained results were under the R factor of 0.041%; which was defined by the formula of $\frac{\Sigma(k^3\chi_{obs} - k^3\chi_{cal})^2}{\Sigma(k^3\chi_{obs})^2}$. [b]Coordination number. [c]Interatomic distance. [d]Debye–Waller factor.

Proposed structure of Pd/AZC. The local structure around Pd atom was proposed as shown in Figure 9. Neither any characteristics peak for Pd-Pd bond, nor any significant signals at higher distances were observed in FT, supporting the monomeric atomically dispersed Pd ions with AZC. A thoughtful conclusion of these characteristics data inspired us to propose the structures of AZC and Pd/AZC as described in Figure 9. A detailed and minute study with higher accuracy for the structural determination is subject to further investigation and ongoing work.
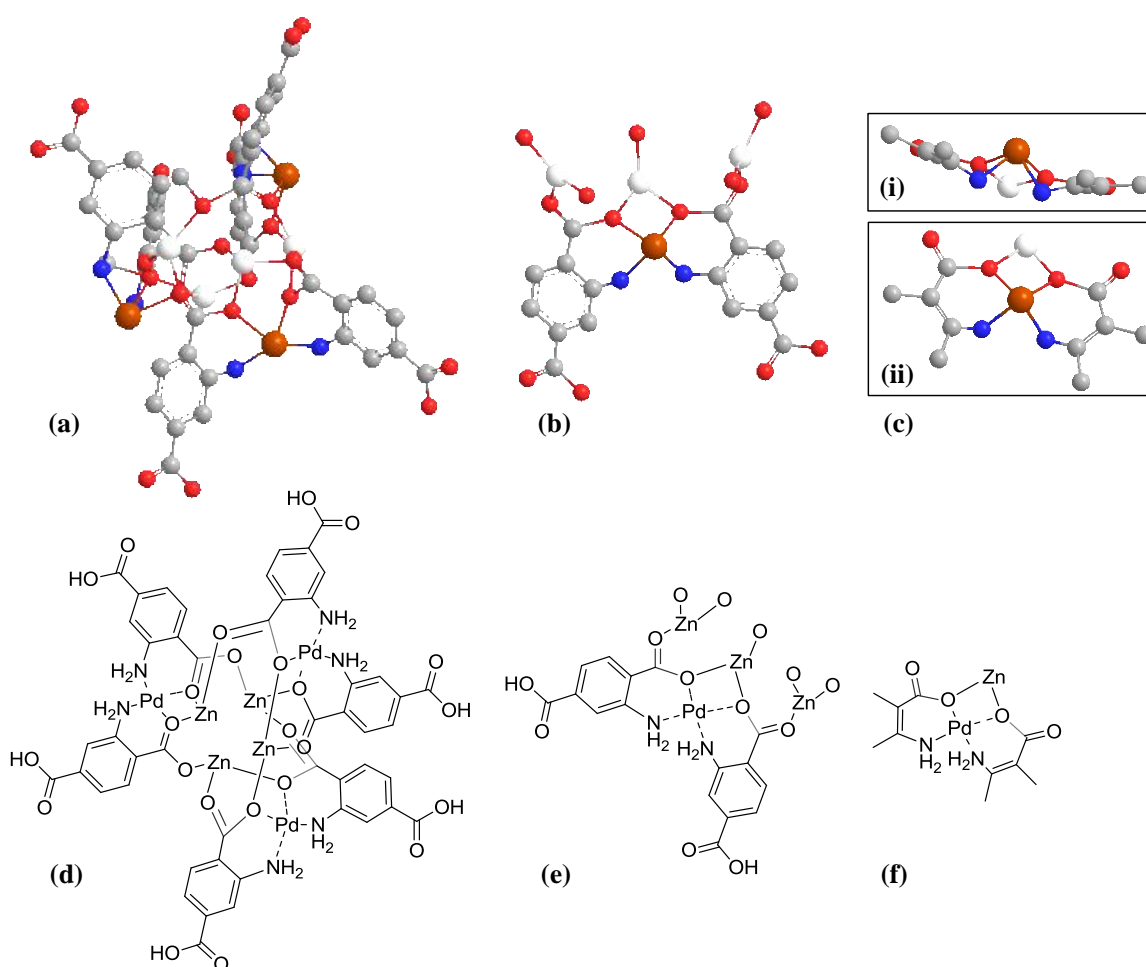
Figure 9. Proposed structure of AZC on the basis of spectroscopic characterizations. Ball and stick model structure of (a) Pd/AZC; (b) Local structure around palladium and zinc in Pd/AZC; (c) (i) Side and (ii) top view of local structure of palladium in Pd/AZC. (d-f) Simplified structure of (a-c). Carbon (gray), Oxygen (red), Nitrogen (blue), Palladium (brown), and Zinc (white). Hydrogen atoms are not shown for simplicity in the ball and stick model.

Heterogeneity of Pd/AZC catalyst during the SMC reaction. The Pd K-edge XANES and EXAFS analysis of the catalyst after the SMC reaction (of bromo- and chlorobenzene) suggested that the catalyst conserved its original structural features (Figures 7a-c). EXAFS oscillation of the spent catalyst was indistinguishable from the fresh catalyst. Besides, the FT of k^3-weighted EXAFS at Pd K-edge denied the presence of any Pd-Pd shell in the spent catalyst, rather bespoke the ionic Pd species with signals for Pd-N/Pd-O shells. The ICP-AES analysis confirmed that neither the supported Pd nor the assembled Zn leached during the SMC reaction under the reaction conditions on ppm order.

The hot-filtration test is a useful method for establishing the heterogeneity of the catalytic reaction. After 20 minutes of SMC reaction progress, the catalyst was quickly filtered off and the filtrate along with additional base was stirred for another 40 minutes at 353 K. The GC analysis showed a high initial rate of reaction with 60% biphenyl yield (62% conv.) within 20 minutes of reaction with just 1 mg of 0.5wt%Pd/AZC. The SMC reaction did not proceed after the separation of solid catalyst after 20 minutes. Additionally, in a separate experiment when fresh reactants (bromobenzene, phenylboronic acid and base with the molar ratio of 2:3:4) were added to the filtrate obtained by centrifugation and filtration with the filter (0.2 μm) after 1 h of SMC reaction, the further reaction did not proceed at all. These results indicate that the catalysis by Pd/AZC is heteorgeneous.

As described by various researchers,[54-58] the solid-phase poisoning tests were performed to ascertain the hetereogeniety of Pd/AZC in SMC reaction. Richardson and Jones reported that two equivalents of QuadraPure TU required for binding all the palladium could completely shutdown the reactivity of solid catalysts that operate through leaching mechanism.[55] In the present case, however, it was found that the use of even four equivalents of QuadraPure TU could not effect the

catalytic activity of Pd/AZC. The control experiment with aq. PdCl$_2$ and two equivalents of QuadraPure TU afforded no product with 4% bromobenzene conversion. It confirms that no homogeneous Pd species catalyze SMC reaction under the conditions. These experiments authenticated the significant heterogeneous nature of Pd/AZC catalyst.

Even after two decades of the SMC reaction, it is still a matter of discussion that whether the genuine catalysis by heterogeneous catalyst is heterogeneous or homogeneous. Some researchers have held the atom-leaching mechanism as the main cause of high activity for such cross-coupling reactions.[54,59-60] The non-leaching of the palladium species into the reaction medium is supposed to be the reason for low activity (34% biphenyl yield) for chlorobenzene in the present case. As discussed above, no black-colored Pd or reduced Pd was observed after the SMC reaction over Pd/AZC, and these reflects the stability of heterogeneous Pd/AZC. The results also indicate that Pd/AZC, and these reflects the stability of heterogeneous Pd/AZC. The results also indicate that the Pd precipitation during the reaction and its effect on catalytic activity of Pd species could be negligible with enduring AZC as support. Strong affinity of Pd to N and interaction of ionic Pd with oxygen could prevent the active Pd species from leaching or undergo agglomeration under the reaction conditions.
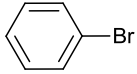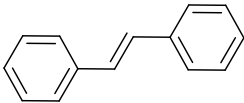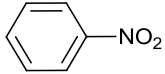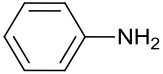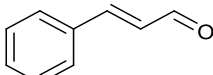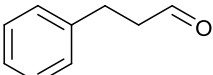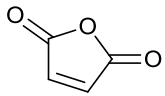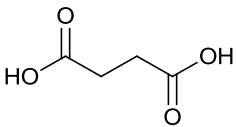
Proposed reaction pathway. A general reaction mechanism by divalent Pd has been considered and sketched accordingly (Scheme 1). An oxidative addition of bromobenzene on the exposed Pd(II) center of Pd(O)$_2$(NH$_3$)$_2$ followed by the ligand exchange with base and arylboronic acid are considered as the sequential steps. Reductive elimination of biphenyl regenerates the active naked Pd and thereby the hetero-coupling of bromoarenes and arylboronic acid takes place consecutively. Since the active Pd species is generated, no further regeneration step is required and could be effectively recycled and thus afforded product with high TON.
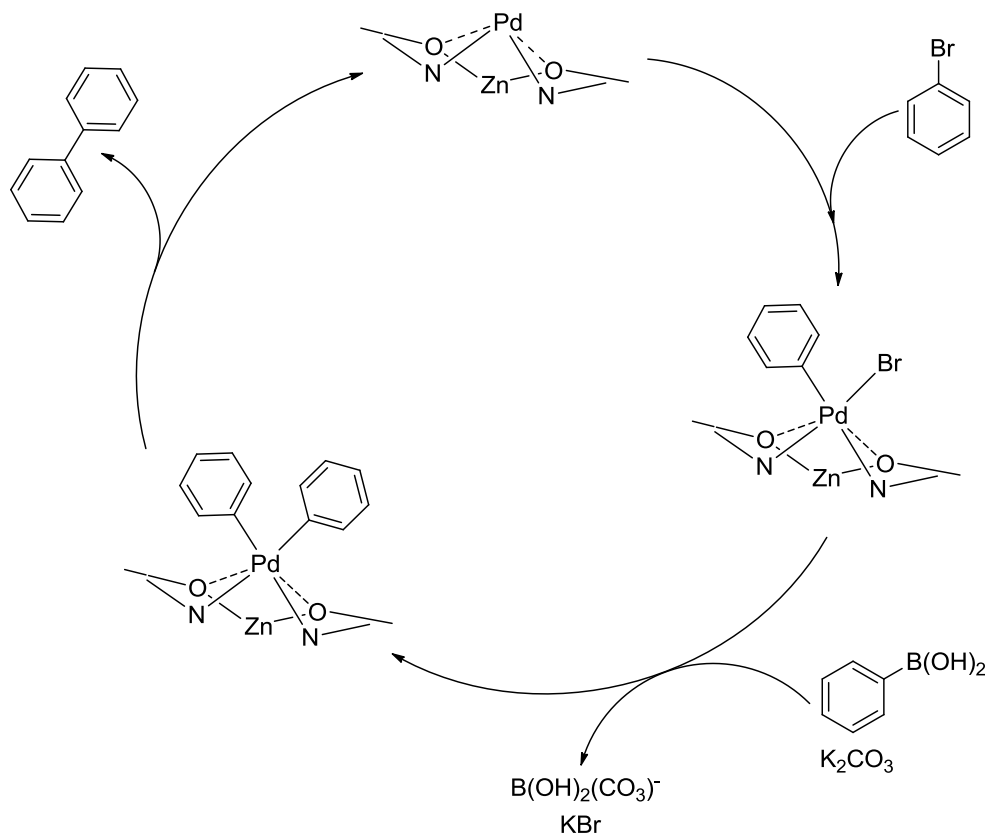
Scheme 1. An illustrative sketch of proposed mechanism of the SMC reaction of bromobenzene in the presence of Pd/AZC catalyst. Hydrogen atoms on nitrogen atoms are not shown for simplicity.

Catalytic scope of Pd/AZC for other organic reactions. The Pd/AZC catalyst was also attempted to use for various Pd-catalyzed reactions as shown in Table 6. I found that the present Pd/AZC catalyst efficiently catalyzed the Mizoroki-Heck reaction of bromobenzene and styrene (Table 6, entry 1). The catalyst also efficaciously promoted hydrogenation reactions of $-NO_2$ group (in nitrobenzene), and $-C=C-$ group (in cinnamaldehyde and maleic anhydride) under mild conditions using hydrogen at an atmospheric pressure (Table 6, entries 2-4). Since the structure of AZC is stable against heat treatment (at least upto 573 K) (Figure 10), the synthesized support

Table 6. Scope of catalysis by Pd/AZC

Entry	Substrate	Product	t /h	Conv.[a] /%	Yield[b] /%
1[b]	bromobenzene	*trans*-stilbene	24	97	84
2[c]	nitrobenzene	aniline	2.5	>99	>99
3[c]	cinnamaldehyde	3-phenylpropanol	6	>99	>99
4[c,d,e]	maleic anhydride	succinic acid	6	>99	98

[a]Determined by GC using naphthalene as internal standard. [b]Reaction conditions: Bromobenzene (3.75 mmol), Styrene (4.5 mmol), K_2CO_3 (4.5 mmol), 0.5Pd/AZC (25 mg), 1-methyl-2-pyrrolidinone (5 mL), 403 K, N_2 flow. [c]Reaction conditions: Substrate (1 mmol), 3Pd/AZC (25 mg), Ethanol (5 mL), H_2 balloon (1 atm), 353 K. [d]Water was used instead of ethanol.
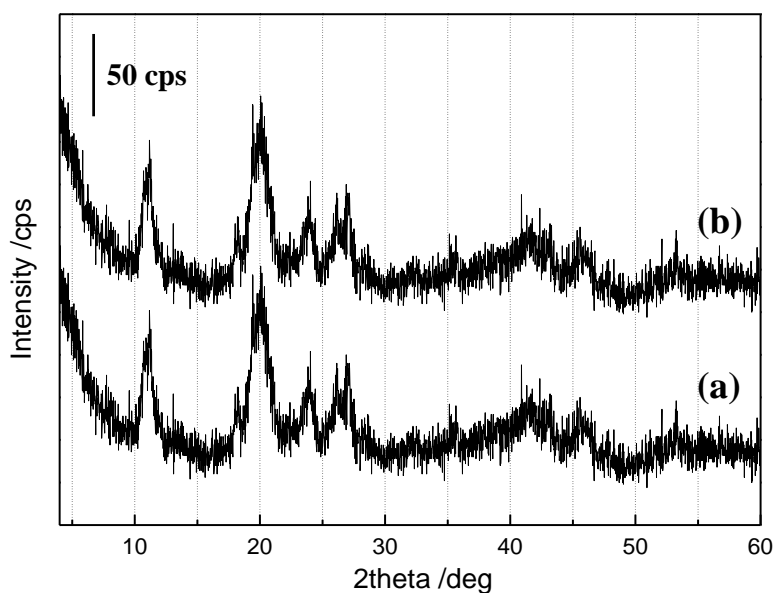
Figure 10. XRD patterns of (a) AZC and (b) AZC treated at 573 K.

(AZC) is believed to be capable of grafting various metal species as catalytically active centers for wide range of industrially-important metal-catalyzed reactions.

4. CONCLUSIONS

In conclusion, I found that ionic palladium species grafted on amino-functionalized organozinc coordination polymer (Pd/AZC) as a robust catalyst for the SMC reaction for bromobenzene. The reusable Pd/AZC demonstrated impressive high turnover numbers (TON= 2,106,720) without any additives under atmospheric conditions. The SMC reaction of other aryl halides and aryl boronic acids could also be efficaciously catalyzed by Pd/AZC under similar conditions. The characterization evidences the stability and durability of Pd/AZC catalyst, highlighting it as a candidate for potential industrial catalyst.

The Pd/AZC also successfully catalyzed the Mizoroki-Heck coupling, hydrogenation of nitro, and C=C functional groups. The high thermal stability, reflect its high potentials for grafting various metal species as catalytically active centers for wide range of metal-catalyzed reactions.

REFERENCES

1. O. M. Yaghi, H. Li and T. L. Groy, *J. Am. Chem. Soc.* **1996**, *118*, 9096.

2. M. Eddaoudi, J. Kim N. Rosi, D. Vodak, J. Watcher, M. O'Keeffe and O. M. Yaghi, *Science* **2002**, *295*, 469.

3. S. Kitagawa, R. Kitamura and S. Noro, *Angew. Chem. Int. Ed.* **2004**, *43*, 2334.

4. N. Miyaura, K. Yamada and A. Suzuki, *Tetrahedron Lett.* **1979**, *20*, 3437.

5. N. Miyaura, T. Yanagi and A. Suzuki, *Synth. Commun.* **1981**, *11*, 513.

6. N. Miyaura and A. Suzuki, *Chem. Rev.* **1995**, *95*, 2457.

7. A. Suzuki, *J. Organomet. Chem.* **2002**, *653*, 83.

8. A. F. Littke and G. C. Fu, *Angew. Chem. Int. Ed.* **2002**, *41*, 4176.

9. A. Molnar, *Chem. Rev.* **2011**, *111*, 2251.

10. C. -J. Li, *Chem. Rev.* **2005**, *105*, 3095.

11. S. Grunder, C. Valente, A. C. Whalley, A. Sampath, J. Portmann, Y. Y. Botros and J. F. Stoddart, *Chem. Eur. J.* **2012**, *18*, 15632.

12. K. -Y. Park, B. T. Kim and J. -N. Heo, *Eur. J. Org. Chem.* **2014**, 164.

13. K. D. Hesp, D. P. Fernando, W. Jiao and A. T. Londregan, *Org. Lett.* **201**4, *16*, 413.

14. V. Polshettiwar and R. S. Varma, *Che*m. Soc. Re*v.* **2008**, *37*, 1546.

15. V. Polshettiwar and R. S. Varma, *Acc. Chem. Res.* **2008**, *41*, 629.

16. C. Deraedt and D. Astruc, *Acc. Chem. Res.* **2014**, *47*, 494.

17. M. Pittelkow, K. Moth-Poulsen, U. Boas and J. B. Christensen, *Langmuir* **2003**, *19*, 7682.

18. J.-H. Li and W.-J. Liu, *Org. Lett.* **2004**, *6*, 2809.

19. Z. Weng, S. Teo and T. S. A. Hor, *Acc. Chem. Res.* **2007**, *40*, 676.

20. A. K. Diallo, C. Ornelas, L. Salmon, J. R. Aranzaes and D. Astruc, *Angew. Chem. Int. Ed.* **2007**, *46*, 8644.

21. F. X. L. Xamena, A. Abad, A. Corma and H. Garcia, *J. Catal.* **2007**, *250*, 294.

22. S. Jana, S. Haldar and S. Koner, *Tetrahedron Lett.* **2009**, *50*, 4820.

23. K. Okumura, T. Tomiyama, S. Okuda, H. Yoshida and M. Niwa, *J. Catal.* **2010**, *273*, 156.

24. S. Ogasawara and S. Kato, *J. Am. Chem. Soc.* **2010**, *132*, 4608.

25. J. Zhi, D. Song, Z. Li, X. Lei and A. Hu, *Chem. Commun.* **2011**, *47*, 10707.

26. Y. Yu, T. Hu, X. Chen, K. Xu, J. Zhang and J. Huang, *Chem. Commun.* **2011**, *47*, 3592.

27. P. M. Uberman, L. A. Perez, G. I. Lacconi and S. E. Martin, *J. Mol. Catal. A. Chem.* **2012**, *363-364*, 245.

28. Y. M. A. Yamada, S. M. Sarkar and Y. Uozumi, *J. Am. Chem. Soc.* **2012**, *134*, 3190.

29. D. Saha, R. Sen, T. Maity and S. Koner, *Langmuir* **2013**, *29*, 3140.

30. C. Deraedt, L. Salmon, L. Etienne, J. Ruiz and D. Astruc, *Chem. Commun.* **2013**, *49*, 8169.

31. X. Pan, Z. Fan, Z. Chen, Y. Ding, H. Luo and X. Bao, *Nat. Mater.* **2007**, *6*, 507.

32. X. Chen, Y. Hou, H. Wang, Y. Cao and J. He, *J. Phys. Chem. C* **2008**, *112*, 8172.

33. E. Castillejos, P.-J. Debouttiere, L. Roiban, A. Solhy, V. Martinez, Y. Kihn, O. Ersen, K. Philippot, B. Chadret and P. Serp, *Angew. Chem. Int. Ed.* **2009**, *48*, 2529.

34. B. Cornelio, G. A. Rance, M. Laronze-Cochard, A. Fontana, J. Sapi and A. N. Khlobystov, *J. Mater. Chem. A* **2013**, *1*, 8737.

35. B. Yuan, Y. Pan, Y. Li, B. Yin and H. Jiang, *Angew. Chem. Int. Ed.* **2010**, *49*, 4054.

36. J. Huang, W. Wang and H. Li, *ACS Catal.* **2013**, *3*, 1526.

37. A. Corma, H. Garcia and A. Leyva, *Appl. Catal. A: Gen.* **2002**, *236*, 179.

38. S. Mandal, D. Roy, R. V. Chaudhari and M. Sastry, *Chem. Mater.* **2004**, *16*, 3714.

39. M.-J. Jin, A. Taher, H.-J. Kang, M. Choi and R. Ryoo, *Green Chem.* **2009**, *11*, 309.

40. R. Zhang, W. Ding, B. Tu and D. Zhao, *Chem. Mater.* **2007**, *19*, 4379.

41. J. C. Park, E. Heo, A. Kim, M. Kim, K. H. Park and H. Song, *J. Phys. Chem. C* **2011**, *115*, 15772.

42. L. Tan, X. Wu, D. Chen, H. Liu, X. Meng and F. Tang, *J. Mater. Chem. A* **2013**, *1*, 10382.

43. Z. Chen, Z.-M. Cui, F. Niu, L. Jiang and W.-G. Song, *Chem. Commun.* **2010**, *46*, 6524.

44. H. Li, B. Xu, X. Liu, Sigen A., C. He, H. Xia and Y. Mu, *J. Mater. Chem. A* **2013**, *1*, 14108.

45. P. Li, P. –P. Huang, F. –F. Wei, Y. –B. Sun, C. –Y. Cao and W. –G. Song, *J. Mater. Chem. A* **2014**, *2*, 12739.

46. J. Gascon, U. Aktay, M. D. Hernandez-Alonso, G. P. M. van Klink and F. Kapteijn, *J. Catal.* **2009**, *261*, 75.

47. J.-H. Li, W.-J. Liu and Y.-X. Xie, *J. Org. Chem.* **2005**, *70*, 5409.

48. A. Indra, C. S. Gopinath, S. Bhaduri and G. K. Lahiri, *Catal. Sci. Technol.* **2013**, *3*, 1625.

49. K. Nakamoto, in Infrared and Raman spectra of inorganic and coordination compounds Part B, 6th ed., Wiley, New Jersey, **2009**; pp 10-11.

50. P. Brant, L. S. Benner and A. L. Balch, *Inorg. Chem.* **1979**, *18*, 3422.

51. J. M. Tura, P. Regull, L. Victori, and M. Dolors de Castellar, *Surf. Interface Anal.* **1988**, *11*, 447.

52. K. Shimizu, R. Maruyama, S. Komai, T. Kodama and Y. Kitayama, *J. Catal.* **2004**, *227*, 202.

53. K. Mori, K. Yamaguchi, T. Hara, T. Mizugaki, K. Ebitani and K. Kaneda, *J. Am. Chem. Soc.* **2002**, *124*, 11572.

54. N. T. S. Phan, M. V. D. Sluys and C. W. Jones, *Adv. Synth. Catal.* **2006**, *348*, 609.

55. J. M. Richardson and C. W. Jones, *Adv. Synth. Catal.* **2006**, *348*, 1207.

56. J. M. Richardson and C. W. Jones, *J. Catal.* **2007**, *251*, 80

57. S. Bhunia, R. Sen and S. Koner, *Inorg. Chim. Acta* **2010**, *363*, 3993.

58. D. Sengupta, J. Saha, G. De and B. Basu, *J. Mater. Chem. A* **2014**, *2*, 3986.

59. A. Fihri, M. Bouhrara, B. Nekouishahraki, J. –M. Basset and V. Polshettiwar, *Chem. Soc. Rev.* **2011**, *40*, 5181.

60. I. W. Davies, L. Matty, D. L. Hughes and P. J. Reider, *J. Am. Chem. Soc.* **2001**, *123*, 10139.

General Conclusion

1. Conclusions

In the recent decades, the commercial interest in hydrothermal or solvothermal synthesis has increased owing to the possibility of preparation of advanced materials at lower temperatures and pressure values in high purity and excellent reproducibility. In this thesis I have studied the preparation of novel materials using hydrothermal and solvothermal methods and investigated their catalytic properties. Also, a strategy for design of catalyst with the desirable characteristics are explored and illustrated in this thesis.

In **Part I**, a critical discussion on the preparation of novel catalyst for efficient utilization of biomass-resources was done successfully and compiled in three chapters to conclude that the catalytic activity can be tuned by controlling the active species.

Chapter 1 of **Part I** elucidated the preparation of a viable copper catalyst under hydrothermal conditions with surfactants and their remarkable catalytic activities for the production of organic acids from sugars under mild conditions. Use of Cu-CTAB/MgO along with NaOH (2.5M, 1 mL) sustained 70% lactic acid yield from glucose at 393 K for 1 h in water solvent. I also found that Cu-CTAB/MgO catalyst in the presence of aqueous 30% H_2O_2 furnished 65% formic acid (FA) yield from glucose at 393 K after 12 h. The catalysis were observed as a function of metal content and calcination temperature of the catalyst. The characterization of the prepared catalysts revealed the presence of novel catalytic active Cu species and the effect of calcination on the nature of species of the catalyst. Finally, based on the experimental evidences a suitable reaction mechanism was proposed to convincingly explain the observed catalysis by Cu-CTAB/MgO.

In **Chapter 2** of **Part II**, I have successfully developed a convenient and simple surfactant-mediated hydrothermal strategy to control the supported copper oxide species. The analysis of XRD patterns, Raman spectra and H_2-TPR profiles and their correlation with the catalytic activity data suggested Cu_4O_3 (paramelaconite) as the catalytic active species on magnesia. Also, the careful inspection of these data depicted the facile surfactant-mediated approach to control the supported copper oxide species. From the XRD patterns (of the uncalcined catalyst) it was inferred that Cu_2O (cuprite) phase is formed predominantly in the presence of DDAO after hydrothermal treatment which can be selectively converted into CuO (tenorite) on calcination, where the calcination decomposes the capping agent. On the other hand, the catalyst prepared without using surfactant afforded only tenorite phase. The quaternary ammonium salt containing surfactants selectively formed paramelaconite phase and preserved them even after calcination. I was able to clearly sketch the structure-activity relationship for the chemical upgradation of glucose to lactic acid over Cu-surfactant/MgO catalysts and also discuss the facile way to control the supported copper oxide species. Such facile control of copper oxide species using a simple and inexpensive hydrothermal strategy makes this process attractive and promising for applications in advanced materials and devices.

In **Chapter 3** of **Part I**, bimetallic CoPd catalyst were prepared under hydrothermal condition in the presence of three different capping agents without any widely-used reducing agent. I found that CoPd-DDAO/AlOOH catalyst, prepared in the presence of *N,N*-dimethyldodecylamine *N*-oxide (DDAO), emerged as highly active, reusable and active catalyst for the facile hydrogenation of maleic anhydride using FA as a hydrogen source. The TEM, XRD, XPS and XAS analyses suggested the presence of Co-Pd interactions in the bimetallic CoPd catalyst. The alloying of Co with Pd in the presence of DDAO, afforded electron rich Pd and modified the Pd-Pd bond distance

that hastened the hydrogenation reaction. Also, I found that the simultaneous use of CoPd-DDAO/AlOOH in combination with Cu-CTAB/MgO catalyst provides a possibility for the direct utilization of abundant biomass-based glucose as hydrogen source.

The overall summary of Part I can be schematically realized as shown below.
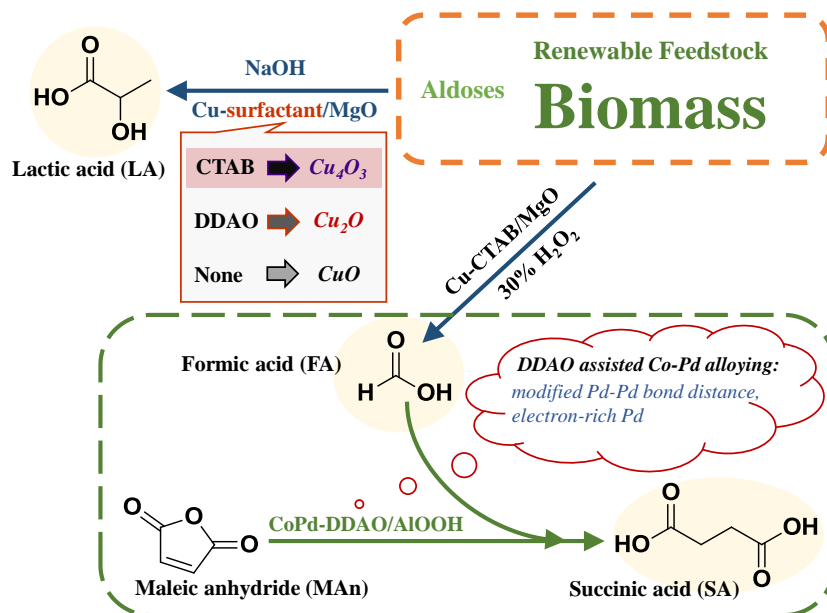
Part II deals with the strategic design of efficacious heterogeneous catalyst for industrially important organic transformations. I designed an easily accessible ionic palladium species grafted on amino-functionalized organozinc coordination polymer (Pd/AZC) as a robust catalyst for the Suzuki-Miyaura coupling reaction of aryl halides. The reusable Pd/AZC demonstrated impressive high turnover numbers (TON= 2,106,720) without any additives under atmospheric conditions. The characterization of the designed catalyst revealed the incorporation of desired characteristics into the prepared material. The Pd/AZC also successfully catalyzed the Mizoroki-Heck coupling, hydrogenation of nitro, and C=C functional groups. The high thermal stability, reflect its high potentials for grafting various metal species as catalytically active centers for wide range of metal-

catalyzed reactions. Overall in Part II, I successsfully developed a highly efficient catalytic material with tunable properties under solvothermal conditions.

2. Original findings

The original findings of the work included in this thesis are mentioned underneath:

a) Preparation of reusable surfactant capped copper catalyst that drastically decreased the energy demand for synthesis of lactic acid (in high yields) from sugars.

b) Paving the path for utilization of biomass as sustainable hydrogen source by producing formic acid from sugars using a heterogeneous copper catalyst.

c) Introduction of a simple approach to control supported copper oxide species.

d) Utilization Co to promote the catalytic activity of Pd for hydrogenation under ambient pressure using formic acid as hydrogen source.

e) Development a one-pot two-step catalytic strategy for the direct applications of sugars as hydrogen source.

f) Introduction of a strategic design to incorporate desirable properties in a catalyst.

g) Design to graft Pd on porous material to achieve stable and ultra-active catalyst for Suzuki-Miyaura coupling reaction.

3. Contribution to current science and technology

In this work, the catalysts are synthesized at T <473 K (and autogeneous pressure) to demonstrate efficacious catalytic activity which in turn results in low energy input for material synthesis in an era of energy crisis. The work included in this thesis also throws light on possible advances in utilization of biomass for some of the current industrial transformations. The use of biomass and biomass derived platform molecules is a research of immense importance in Japan. Japan has 286 biomass towns (as of November 2010), with 6 cities including Nomi being in Ishikawa prefecture, where I have carried out the work for this doctoral dissertation. Moreover, according to Japanese Biomass Policy, Japan have approximately 300 million tons on waste biomass of which approximately 58.7 million tons is unused and forestry residues as well as non-edible parts of farm crops contribute to 22 million tons are also categorized as wasted biomass. The current effort of using abundant biomass in Japan and other parts of world explains the global significance of this research as a high impact contribution to science and technology.

The minimization of energy values from 523 K to 393 K for synthesis of useful organic molecules from renewable and abundant raw-materials like glucose is a major advance in the current science and technology. Not only this, but also decreasing the amount of noble metals by the use of abundant transition metals as a co-catalyst/promoter and creation of new stable and highly-active materials also marks a significant contribution to current science and technology. The development of successful catalytic pathways and design of efficacious catalyst is of tremendous importance recently owing to the concerns of environmental sustainability and depleting resources. Also, in the context of material design for wide range of applications,

[167]

controlled preparation of high-performance heterogeneous catalysts in a simple and facile manner also contribute to the development of current science and technology.

4. Future prospects

The thesis discusses on the preparation of functionalized materials using solvothermal methods. Since preparation of novel materials and rare phases, new catalytic processes for bio-refineries and strategies to design catalysts to incorporate desirable properties were included and illustrated in this thesis, various research topics can be considered which are believed to establish a new research area in materials science. The scope of future research are discussed based on each chapter in details underneath.

In **Chapter 1** of **Part I** of this thesis, a novel synthetic route for the creation of rare phases were explored which had excellent catalytic activity for the synthesis of industrially important organic acids from a range of sugars. However, for the fruitful applications of these catalytic process in industries or for evaluation of greenness of the process, life cycle assessment (LCA) studies are required. Also, the reported catalytic process should be researched upon as a continuation work for the utilization of polysaccharides or real biomass such as bagasse. The knowledge of the catalytic properties of copper oxides can also be investigated with the prepared Cu-CTAB/MgO catalysts, for instance catalytic activities of Cu-CTAB/MgO catalysts can be applied to traditional reactions like CO oxidation or water-gas shift reaction. Also, the achievement of this chapter can be extended to various transition metals to discover novel/rare phases of that particular metal oxide.

Chapter 2 of **Part I** described a new approach for the facile control of supported species (oxidation state of metal in species) as a function of surfactant and treatment conditions. Such research topics are very new in the material sciences research area and can be exploited rigorously for the range of elements in the periodic table. The use of the surfactants as a capping agent were only discussed in this chapter, however, a further scope for the utilization of various organic ligands or polymers and their effect on the oxidation states of metal(s) can be investigated. This study with additional future research can be utilized to make a rule for obtaining a typical metal species by the mere use of the metal and surfactant/organics pair for wide range of applications.

In **Chapter 3** of **Part I**, the concept of preparing novel nanomaterials were extended from monometallic system to bimetallic system. Only one bimetallic pair were prepared and investigated using the current technology. This opens up the scope for the creation of various bimetallic pairs, with a strong focus on noble metal duos. Also, in this chapter, a novel concept of direct utilization of biomass-derived abundant glucose is demonstrated as hydrogen source in hydrogenation reactions that can be realized in future by further chemical and theoretical developments. The scope for the design of highly-active catalysts for the efficient realization of the above mentioned concept is also proposed.

The **Part II** of thesis includes one chapter but introduces a variety of future prospects as discussed here. The Chapter deals with the design of a robust heterogeneous catalyst with easily-accessible active sites for the catalysis of Suzuki-Miyaura coupling reaction. Firstly, from the catalysis aspect, the catalytic activity of the Pd/AZC catalyst could be evaluated for other hetero-atom coupling reactions like C-O, C-N or C-S coupling reactions. Alternatively on the materials context, the crystallinity of the current discussed amorphous material can be controlled in the presence of mineral acids to probably reveal a unique relationship of catalytic activity and the

crystallinity of the easily accessible materials. The functionality of the material can be varied to typically obtain solid acid catalysts possessing Bronsted and/or Lewis acidic sites as a function of preparation conditions.

List of accomplishments

A) *Publications in peer-reviewed scientific journals:*

1. **Hemant Choudhary**, Shun Nishimura and Kohki Ebitani
   "A convenient surfactant-mediated hydrothermal approach to control supported copper oxide species for catalytic upgradation of glucose to lactic acid"
   Submitted.

2. **Hemant Choudhary**, Shun Nishimura and Kohki Ebitani
   "Hydrothermal preparation of robust boehmite-supported *N,N*-dimethyldodecylamine *N*-oxide-capped CoPd catalyst for facile utilization of formic acid as a hydrogen source"
   ChemCatChem, **2015**, *accepted for publication*, DOI: 10.1002/cctc.201500161.

3. **Hemant Choudhary**, Shun Nishimura and Kohki Ebitani
   "Synthesis of high-value organic acids from sugars promoted by hydrothermally loaded Cu oxide species on magnesia"
   Applied Catalysis B: Environmental, **2015**, *162*, 1-10.

4. **Hemant Choudhary**, Shun Nishimura and Kohki Ebitani
   "Tailored design of palladium species grafted on an amino functionalized organozinc coordination polymer as a highly-pertinent heterogeneous catalyst"
   Journal of Materials Chemistry A, **2014**, *2*, 18687-18696.

B) *International conferences (peer-reviewed):*

1. **Hemant Choudhary**, Shun Nishimura and Kohki Ebitani
   "Capped Co-promoted Pd/AlOOH Catalysts in Dehydrogenation of Formic Acid for Hydrogenation of Maleic Anhydride"
   12th European Congress on Catalysis – EuropaCat-XII, Kazan, Russia, September 2, 2015. [Poster]

2. **Hemant Choudhary**, Shun Nishimura and Kohki Ebitani
   "A Robust Palladium Species Grafted on Amino-functionalized Organozinc Coordination Polymer for Efficient Suzuki-Miyaura Coupling Reaction in Open Air"
   7th International Conference on Green and Sustainable Chemistry & 4th JACI/GSC

Symposium, Tokyo, Japan, July 5 –July 8, 2015. [Poster]

3. **Hemant Choudhary**, Shun Nishimura and Kohki Ebitani
"Highly efficient and reusable heterogeneous copper catalyst for the synthesis of value-added organic acids from inedible biomass"
4th International Solvothermal and Hydrothermal Association Conference (ISHA2014), Talence Cedex, Bordeaux, France, October 28, 2014. [Oral]

4. <u>Shun Nishimura</u>, **Hemant Choudhary** and Kohki Ebitani
"Highly-active porous coordination polymer-supported palladium catalyst"
The 44th Peteroleum-Petrochemical Symposium of JPI, Asahikawa, Hokkaido, Japan, October 17, 2014. [Oral-A]

5. **Hemant Choudhary**, Shun Nishimura and Kohki Ebitani
"Catalytic synthesis of organic acids for energy and plastics with biomass resources"
JAIST Japan-India Symposium on Automotive Technologies (Energy, Fuel and Plastics), Nomi, Ishikawa, Japan, August 4, 2014. [Oral]

6. **Hemant Choudhary**, Shun Nishimura and Kohki Ebitani
"Palladium-decorated amino-functionalized organozinc composites as stable and highly-active heterogeneous catalyst for Suzuki-Miyaura coupling"
The Seventh Tokyo Conference on Advanced Catalytic Science and Technology (TOCAT7), Kyoto, Japan, June 2, 2014. [Poster]

7. **Hemant Choudhary**, Shun Nishimura and Kohki Ebitani
"Cooperative catalysis of magnesia loaded copper for selective conversion of sugars into organic acids"
247th ACS National Meeting & Exposition, Dallas, Texas, USA, March 20, 2014. [Oral]

C) *Domestic conferences (peer-reviewed):*

1. **Hemant Choudhary**, Shun Nishimura and Kohki Ebitani
"Green chemistry - Development and practice (Design of heterogeneous catalysts for transformation of inedible-biomass into value-added chemicals)"
JAIST Festival 2013 (JAIST Poster Challenge), JAIST, October 12, 2013. [Poster]
[Faculty members' choice award]

D) *Patent Applications:*

1. Shun Nishimura, Kohki Ebitani and **Hemant Choudhary**
   "Metal-supported catalyst"
   JP Patent Application 2014-096036.

2. Kohki Ebitani, Shun Nishimura and **Hemant Choudhary**
   "Copper catalyst: Synthesis and catalytic activity for lactic and formic acid"
   JP Patent Application 2014-007027.

E) *Awards and Grants:*

1. Awarded 2014 **JAIST Foundation Research Grant** for students for presenting research achievements in an academic conference in Bordeaux, France.

2. Received **JSPS Kakenhi Research Grant** (Grant-in-Aid for JSPS Fellows #26-12396) of 1,900,000 JPY for the financial year 2014-2016.

3. Awarded 2013 **JAIST Foundation Research Grant** for students for presenting research achievements in an academic conference in Dallas, USA.

4. Awarded **JSPS Scholarship 2014 for Doctoral Course** (Financial Support for Research and Life from April 2014- March 2016).

5. Certified as **Best Poster Presenter** (Selected as the faculty members' choice award) in JAIST Poster Challenge, 2013, JAIST, Japan.

Other related achievements not included in this thesis

A) *Publications in peer-reviewed scientific journals:*

1. **Hemant Choudhary**, Shun Nishimura and Kohki Ebitani
   "Supported bimetallic PdPt alloy NPs catalyst for selective aerobic oxidation of HMF to 2,5-furandicarboxylic acid"
   To be submitted.

2. Jaya Tuteja, Shun Nishimura, **Hemant Choudhary** and Kohki Ebitani
   "Selective oxidation of 1,6-hexanediol to 6-hydroxycaproic acid over reusable hydrotalcite supported AuPd bimetallic catalysts in basic aqueous media using H_2O_2 as green oxidant"
   ChemSusChem, **2015**, *accepted for publication*, DOI: 10.1002/cssc.201500255.

3. Ryo Sato, **Hemant Choudhary**, Shun Nishimura and Kohki Ebitani
   "Synthesis of formic acid from monosaccharides using calcined Mg-Al hydrotalcite as reusable catalyst in the presence of aqueous hydrogen peroxide"
   Organic Process Research & Development, **2015**, *19*, 449-453.

4. Jaya Tuteja, **Hemant Choudhary**, Shun Nishimura and Kohki Ebitani
   "Direct synthesis of 1,6-hexanediol from HMF over a heterogeneous Pd/ZrP catalyst using formic acid as hydrogen source"
   ChemSusChem, **2014**, *7*, 96-100.
   [Top 25 Most Accessed Article 11/2013-10/2014]

5. **Hemant Choudhary**, Shun Nishimura and Kohki Ebitani
   "Metal-free oxidative synthesis of succinic acid from biomass-derived furan compounds using a solid acid catalyst with hydrogen peroxide"
   Applied Catalysis A: General, **2013**, *458*, 55-62.

6. **Hemant Choudhary**, Shun Nishimura and Kohki Ebitani
   "Highly efficient aqueous oxidation of furfural to succinic acid using reusable heterogeneous acid catalyst with hydrogen peroxide"
   Chemistry Letters, **2012**, *41*, 409-411.

B) *International conferences (peer-reviewed):*

1. <u>Jixiang Jia</u>, **Hemant Choudhary**, Shun Nishimura and Kohki Ebitani
   "Development of highly active Pd catalysts for the Suzuki-Miyaura coupling reaction of aryl halides with arylboronic acid"
   The 94th Annual Meeting of Chemical Society of Japan, Nagoya, March 30, 2014. [Oral-A]

2. <u>Jaya Tuteja</u>, **Hemant Choudhary**, Shun Nishimura and Kohki Ebitani
   "Ring opening of HMF to produce 1,6-hexanediol over Pd/zirconium phosphate catalyst using formic acid as hydrogenating agent"
   247th ACS National Meeting & Exposition, Dallas, Texas, USA, March 20, 2014. [Oral]

3. <u>Kohki Ebitani</u>, **Hemant Choudhary**, Jaya Tuteja, Pham Anh Son and Shun Nishimura
   "Transformations of biomass-derived compounds into useful chemicals using heterogeneous catalytic systems"
   International Conference on Advances in Biothechnology and Bioinformatics (ICABB 2013), Pune, India, November 25, 2013. [Oral-invited]

4. **Hemant Choudhary**, Shun Nishimura and <u>Kohki Ebitani</u>
   "Synthesis of succinic acid from biomass-derived furans using a reusable solid acid catalyst with hydrogen peroxide under metal-free conditions"
   Word Congress on Petrochemistry and Chemical Engineering (159th OMICS Group Conference), San Antonio, USA, November 18, 2013. [Oral-invited]

5. <u>Jaya Tuteja</u>, **Hemant Choudhary**, Shun Nishimura and Kohki Ebitani
   "Pd/ZrP catalyzed hydrogenolytic ring opening of HMF to 1,6-hexanediol using formic acid as hydrogen donor"
   International Symposium on Advanced Materials 2013, JAIST, October 17, 2013. [Poster]

6. **<u>Hemant Choudhary</u>**, Shun Nishimura and Kohki Ebitani
   "Green oxidation of furan carbonyls over heterogeneous catalyst in aqueous media"
   10th International Congress of Young Chemists (YoungChem 2012), Gdansk, Poland, October 10, 2012. [Oral]

7. **<u>Hemant Choudhary</u>**, Shun Nishimura and Kohki Ebitani
"Green oxidation of furfural to succinic acid using hydrogen peroxide in the presence of heterogeneous catalyst in aqueous medium"
The Asia-Pacific Interdisciplinary Research Conference 2011 (APIRC 2011), Toyohashi University of Technology, Japan, November 17, 2011. [Poster]

C) *<u>Patent Applications:</u>*

1. Kohki Ebitani, Shun Nishimura, Jaya Tuteja and **Hemant Choudhary**
"Metal-supported catalyst, catalyst material and synthesis method of hydroxyl-fatty acids"
JP Patent Application 2015-069723.

2. Kohki Ebitani, Shun Nishimur a, Jaya Tuteja and **Hemant Choudhary**
"Reduction catalyst, synthesis of 1,6-hexanediol, synthesis of amino-benzene compounds"
JP Patent Application 2013-215678.

3. Kohki Ebitani, Shun Nishimura and **Hemant Choudhary**
"Synthesis method of succinic acid"
JP Patent Application 51202100244 (October, 2012).

D) *<u>Awards and Grants:</u>*

1. Awarded 2012 **JAIST Foundation Research Grant** for students for presenting research achievements in an academic conference in Gdansk, Poland.